

**MEASURING THE EFFECTS OF CUTTER SUCTION DREDGE OPERATING
PARAMETERS ON MINOR LOSSES DUE TO FIXED SCREENS INSTALLED
AT THE SUCTION INLET**

A Thesis

by

JOSHUA MARK LEWIS

Submitted to the Office of Graduate and Professional Studies of
Texas A&M University
in partial fulfillment of the requirements for the degree of

MASTER OF SCIENCE

Chair of Committee,	Robert E. Randall
Co-Chair of Committee,	James M. Kaihatu
Committee Member,	Achim Stössel
Head of Department,	Robin Autenrieth

December 2014

Major Subject: Ocean Engineering

Copyright 2014 Joshua Mark Lewis

ABSTRACT

One of the most efficient and versatile types of modern dredges is the cutter suction dredge. Specific regulations mandate the placement of screens over the suction mouth during dredging operations to prevent ordnance, wildlife, and other debris from entering the system; however, these screens change the operational capability of the dredge in the form of an additional minor loss. The goal of this experiment was to determine the effects of different dredge operating parameters – cutter head speed, ladder arm swing speed, flow rate, and screen opening area ratio – on a screen's calculated minor loss coefficient (or k-value). The Haynes Coastal Engineering Laboratory and Center for Dredging Studies at Texas A&M University houses a model cutter suction dredge that is used to test various parameters associated with hydraulic dredging. Testing consisted of 121 test dredge runs, which included water-only runs and slurry runs, at three flow rates, three swing speeds, three cutter head speeds, and three screen configurations. Minor loss coefficients were calculated for each test run and qualitatively and quantitatively analyzed.

The results showed that neither cutter head speed nor swing speed had a significant, direct correlation with the screen's minor loss in the range of selected parameters; however, they did have an indirect effect on k-value through an increased specific gravity in the slurry. The screen opening area ratio (β) showed a direct correlation with the screen's k-value and was quantified for water tests and sand tests in the form of an empirical equation which can be applied to both model and prototype

cutter suction dredges. The k-values for different screen opening shapes showed an upward or downward shift in the overall k-value curves, indicating the possibility of inherent efficiencies for differently-shaped openings. Qualitative observations of the Haynes Laboratory model dredge included sediment spillage at high cutter head speeds and a sand bulldozer effect at low cutter head speeds. Future testing should focus on a wider range of cutter head speeds and swing speeds to determine if any correlation exists beyond the ranges tested in this experiment. Additional testing of screens with more β -values and different screen opening shapes would increase the resolution and precision of the proposed k-value prediction equations.

ACKNOWLEDGEMENTS

I would like to first thank my lovely wife, Jessica for her patience during my working hours during the day and night, especially in the midst of our growing family. The stability she provided at home made it possible for me to focus on academics to complete this work.

My gratitude goes out to Dr. Robert Randall, my academic advisor, who guided me through the steps needed to create and finish this thesis. His willingness to open up laboratory facilities to complete experimental testing was essential for me to successfully complete this research. Additionally, a big thank you to Mr. John Reed, who, through his experience and expertise in all the Haynes Laboratory equipment, taught me how to run a real experiment.

Thanks to the Haynes Laboratory graduate student research assistants, Alex Knoll and Yuanzhe Zhi, and Haynes Laboratory employee Kirk Martin who were always willing to lend a helping hand and advice during this entire process. Thanks to the undergraduate laboratory assistants Chris Williams, Colton Wylie, and David Patterson who provided labor, rapid repairs, and general assistance to successfully complete the experimental testing.

NOMENCLATURE

a	Scaling Term for k-Value Prediction Equation
b	Shape Term for k-Value Prediction Equation
BHP	Brake Horse Power
β	Screen Opening Area Ratio
C_v	Volumetric Sediment Concentration
c	Spread Scaling Term Constant
d	Dredging Depth
D	Pipe Diameter
d_{50}	Median Particle Diameter
d_c	Depth of Cut (or Cutting Thickness)
D_c	Cutter Head Diameter
DE	Dredge-specific Operating Efficiency Factor
Δh_{Ln}	Head Loss Caused by Screen “n”
ΔP_{1n}	Change in Pressure at Point 1 when Screen “n” was in Place
ΔP_{sn}	Change in Pump Suction Pressure from Screen “n”
$\Delta(V_{2n}^2)$	Change in the Squares of Suction Flow Velocities w/ Screen “n”
ΔX	Cutter Head Advance
ΔY	Ladder Arm Swing Distance
ϵ	Absolute Pipe Roughness

η	Pump Efficiency Factor
f	Friction Factor
g	Gravitational Acceleration
γ	Specific Weight
γ_m	Specific Weight of Slurry Mixture
γ_w	Specific Weight of Water
h_f	Frictional Head Loss
h_L	Total Head Loss
h_{Ln}	Total Head Loss with Screen “n” in Place
h_{Ls}	Total Head Loss in Suction Pipe
h_m	Minor Head Loss
h_p	Pump Input Energy
i_m	Head Loss (per unit length) Due to Friction in Slurry Flow
k	Minor Loss Coefficient
k_n	Minor Loss Coefficient of Screen “n”
L	Pipe Length
μ	Dynamic Viscosity
n	Spread Scaling Term Exponent
$NPSHA$	Net Positive Suction Head Available
$NPSHR$	Net Positive Suction Head Required
ν	Kinematic Viscosity
Ω	Cutter Head Speed

P_1	Pressure at Point 1
P_{1n}	Pressure at Point 1 with Screen “n” in Place
P_2	Pressure at Point 2
P_{2n}	Pressure at Point 2 with Screen “n” in Place
P_a	Local Atmospheric Pressure
P_d	Pressure at Centrifugal Pump Discharge
P_s	Pressure at Centrifugal Pump Suction Inlet
P_v	Vapor Pressure
Q	Volumetric Flow Rate
Q_c	Critical Flow Rate
Re	Reynold’s Number
<i>Region A</i>	Suction Region of Haynes Lab Hydraulic Dredge System
<i>Region B</i>	Sensor Region of Haynes Lab Hydraulic Dredge System
<i>Region C</i>	Discharge Region of Haynes Lab Hydraulic Dredge System
ρ	Density
SG	Specific Gravity
$\overline{SG}_{baseline}$	Baseline Specific Gravity for Water from Averaged Tests
$SG_{calibration}$	Specific Gravity Calibration Constant for a Test Series
V_1	Velocity at Point 1
V_{1n}	Velocity at Point 1 with Screen “n” in Place
V_2	Velocity at Point 2
V_{2n}	Velocity at Point 2 with Screen “n” in Place

V_{50}	Central Value Velocity Parameter for Heterogeneous Slurry Flow
V_L	Ladder Arm Swing Speed
V_S	Suction Inlet Velocity
V_t	Terminal Velocity of a Sediment Grain
\hat{V}	Non-Dimensional Suction Velocity
w	Particle-Associated Velocity
w_{k_n}	Uncertainty in the calculated k-value of Screen “n”
w_{SG}	Uncertainty in Specific Gravity Measurement
w_{V_S}	Uncertainty in Calculated Suction Velocity Measurement
$w_{\Delta P_{Sn}}$	Uncertainty in the Calculated Value of ΔP_{Sn}
$w_{\Delta P_{1n}}$	Uncertainty in the Calculated Value of ΔP_{1n}
$w_{\Delta(V_{2n}^2)}$	Uncertainty in the Calculated Value of $\Delta(V_{2n}^2)$
WHP	Water Horse Power
z	Elevation above reference datum

TABLE OF CONTENTS

	Page
ABSTRACT	ii
ACKNOWLEDGEMENTS	iv
NOMENCLATURE.....	v
LIST OF FIGURES.....	xii
LIST OF TABLES	xv
INTRODUCTION.....	1
History	1
Modern Dredges.....	2
BACKGROUND.....	5
Fluid Flow	5
Slurry Flow.....	7
Production Limitations.....	10
Effects of Dredge Operating Parameters.....	15
The Need for Evaluating Minor Losses	21
OBJECTIVES	23
EXPERIMENTAL TEST SETUP	24
Model Scaling	24
Model Dredge.....	31
Screen Configurations.....	33
Calculation of Opening Area Ratio (β).....	35
TEST SETUP	36
SENSORS	40
Nuclear Density Gauge	40
Flow Meter	42

Pressure Transmitter.....	42
Ladder Location Sensors.....	43
TEST PLAN.....	45
DATA COLLECTION.....	49
DATA PROCESSING	51
QUALITATIVE OBSERVATIONS.....	55
The Bulldozer Effect	55
Spillage.....	56
Screen Clogging	58
The Influence of Flow Rate on Specific Gravity	59
The Influence of Cutter Head Speed on Specific Gravity.....	61
The Influence of Swing Speed on Specific Gravity	63
DATA ANALYSIS	65
Procedure for Calculations	65
UNCERTAINTY ANALYSIS.....	68
EVALUATION OF TESTS WITH VARYING CUTTER HEAD SPEED	73
Cutter Head Speed and k-Value for Water Tests	73
Flow Rate and k-Value for Water Tests Varying Cutter Head Speed	74
Cutter Head Speed and k-Value for Sand Tests.....	75
Flow Rate on k-Value for Sand Tests Varying Cutter Head Speed	77
EVALUATION OF TESTS WITH VARYING SWING SPEED.....	79
Swing Speed and k-Value for Water Tests	79
Flow Rate and k-Value for Water Tests Varying Swing Speed.....	80
Swing Speed and k-Value for Sand Tests	81
Flow Rate and k-Value for Sand Tests Varying Swing Speed	83
SCREEN OPENING SHAPE AND K-VALUE.....	85
SCREEN OPENING AREA RATIO AND K-VALUE	87

Fixed Screen Minor Loss Prediction for Water Tests	87
Fixed Screen Minor Loss Prediction for Sand Tests.....	93
CONCLUSIONS.....	100
RECOMMENDATIONS	103
REFERENCES.....	106
APPENDIX A – TEST PLANS	112
APPENDIX B – RAW DATA.....	116
APPENDIX C – PHOTOS.....	138

LIST OF FIGURES

	Page
Figure 1: Simplified schematic of the energy balance in a typical pipe flow problem.....	6
Figure 2: Model cutter head used at the Haynes Coastal Engineering Laboratory.....	8
Figure 3: Diagram of overcutting and undercutting for a cutter suction dredge.....	8
Figure 4: Slurry flow regimes in a pipeline.....	9
Figure 5: Example of energy transfer from an electric motor to a centrifugal pump.	11
Figure 6: (a) Minor loss coefficient of a fixed screen as a function of both specific gravity and flow rate from Girani (2014); (b) Minor loss coefficient of a fixed screen extrapolated to higher specific gravities and flow rates using the prediction equation from Girani (2014).	17
Figure 7: Production at different cutter head speeds and flow velocities (den Burger, et al., 1999).....	18
Figure 8: Solids concentration at different ladder arm swing speeds and cutting thicknesses (Yagi, et al., 1975).	20
Figure 9: Sieve analysis of sand at Haynes Laboratory.	30
Figure 10: Overview of the model dredge at the Haynes Coastal Engineering Laboratory.	30
Figure 11: Screen configurations and calculated opening area ratios.	34
Figure 12: Screenshot of Apollo dredge control interface.	36
Figure 13: Scheme of maneuver for each test run.....	37
Figure 14: Cutting thickness at a 30° ladder angle with the model cutter head.	38
Figure 15: Summary of test plan.	46

Figure 16: Plan view of sand pit (not to scale).....	47
Figure 17: Video recording apparatus.....	50
Figure 18: Example of data selection for a period of relatively steady data.....	51
Figure 19: Histograms of percent error in data Selections for two methods of data processing.....	53
Figure 20: Bulldozer effect at slowest nominal cutter head speed.....	55
Figure 21: Spillage at different cutter head speeds.....	57
Figure 22: Specific gravity and calculated production for all tests.....	60
Figure 23: Maximum specific gravity observations at different cutter head speeds.....	62
Figure 24: Maximum specific gravity observations at different ladder arm swing speeds.....	63
Figure 25: Suction side evaluation of model dredge system using the modified Bernoulli equation.....	65
Figure 26: Minor loss coefficient variation due to cutter head speeds during water tests. Symbol sizes (small to large) indicate nominal flow rates of 250, 325, and 400 GPM, respectively.....	73
Figure 27: Minor loss coefficient variation due to flow rate during water tests. Symbol sizes (small to large) indicate cutter head speeds of 15, 30, and 45 rpm, respectively.....	74
Figure 28: Minor loss coefficient variation due to cutter head speed during sand tests. Symbol sizes (small to large) indicate nominal flow rates of 250, 325, and 400 GPM, respectively.....	76
Figure 29: Minor loss coefficient variation due to flow rate during sand tests. Symbol sizes (small to large) indicate cutter head speeds of 15, 30, and 45 rpm, respectively.....	77
Figure 30: Minor loss coefficient variation due to ladder arm swing speed during water tests. Symbol sizes (small to large) indicate nominal flow rates of 250, 325, and 400 GPM, respectively.....	79

Figure 31: Minor loss coefficient variation due to flow rate during water tests. Symbol sizes (small to large) indicate ladder arm swing speeds of 1, 1.5, and 2 in/s, respectively.	80
Figure 32: Minor loss coefficient variation due to ladder arm swing speed during sand tests. Symbol sizes (small to large) indicate nominal flow rates of 250, 325, and 400 GPM, respectively.	81
Figure 33: Minor loss coefficient variation due to flow rate during sand tests. Symbol sizes (small to large) indicate ladder arm swing speeds of 1, 1.5, and 2 in/s, respectively.	83
Figure 34: Comparison of k-values between Screen 1 and Screen 3 (blue and black markers indicate water and sand tests, respectively). Symbol sizes (small to large) indicate nominal flow rates of 250, 325, and 400 GPM, respectively.	85
Figure 35: Effect of screen opening on fixed screen minor loss coefficients for water tests.	87
Figure 36: Analysis of k-value spread according to non-dimensional flow rate.	89
Figure 37: Fixed screen minor loss prediction equation for water-only tests (plotted with experimental data).	91
Figure 38: Effect of screen opening on k-value for sand tests. Identification of outliers and evaluation of spread.	94
Figure 39: Minor loss prediction equation plotted at the range of flow rate values and specific gravity values observed at the Haynes Laboratory.	97
Figure 40: Fixed screen minor loss prediction curves (with slurry present).	98

LIST OF TABLES

	Page
Table 1: Model and prototype scale relationships for model dredge operating parameters.	24
Table 2: Theoretical model parameters scaled according to three scaling laws.	25
Table 3: Density gauge calibration adjustments for each test series.	41
Table 4: Test runs completed in addition to test plan.	46
Table 5: Uncertainties of independent variables.	71

INTRODUCTION

History

The importance of dredging to the world's economy cannot be understated; it provides clear and safe passage for all vessels through the oceanic channels of the world. It also provides a method for mining precious marine minerals underwater (Herbich, 2000b). Without the use of channels, worldwide shipping would cease to exist (Huston, 1970). Because commercial vessels can hold so much tonnage, they are considered the most efficient means of transporting large quantities of goods around the world to support national and international economies (Herbich, 2000a). It is for this reason that dredging must continue to occur and improve on a widespread scale.

Dredging can be traced back to around 6000 years ago in Egypt, where soldiers, slaves, and prisoners were forced to dredge rivers (e.g. Euphrates, Nile, Indus, and Tigris) under the rule of ancient emperors (Herbich, 2000b). Dredging technology at that time comprised manual labor, shovels, and buckets. The world's first dredge was the spoon and bag dredger; which consisted of a boat or barge with laborers who would excavate material using buckets or bags (Huston, 1970); the material was loaded into the boat, then placed onto the shore. This technology showed very little improvement over the next few thousand years. The next big step in dredging technology occurred in 1400 AD with the conversion of old wooden ships into scraper dredges that used the method of agitation dredging. This method agitated bottom sediment into suspension which was

then carried out to sea by ambient currents (Randall, 2013; Herbich, 2000b); the first of these dredges was called Kraggelaar and was a wind-powered ship used mostly in Holland (Huston, 1970). Next, the Mud Mill dredge was invented around 1600, which was initially human-powered, but later retrofitted to use horse power. The mud mill was a bucket-ladder-type dredge, which used a chain of buckets mounted on a conveyer. The chain of buckets was lowered to depths of 10 to 15 feet (3 to 4.5 meters) where it excavated material and discharged it onto an attached barge or scow (Huston, 1970). Eventually, the world's first hydraulic dredge was invented in 1864 (Huston, 1970) using a steam-powered centrifugal pump to transport a sediment-water mixture (i.e. slurry) through a pipeline.

Modern Dredges

Today, the world uses different types of hydraulic and mechanical dredges, including: cutter suction, trailing suction hopper, dust pan, plain suction, bucket ladder, and clamshell (Randall, 2013) to transport materials like silt, sand, mud, gravel, clay, or reef material (Fusheng, et al., 2007). Of these, the most widely used dredge type is the cutter suction dredge due to its versatility, high production capacity, efficiency, and ability for uninterrupted operations (Fusheng, et al., 2010).

The most important parameter in the evaluation of a cutter suction dredge is its production capacity (Ivanov, 1992; Basco, 1975a) – the amount of dredged material it can produce within a given time frame. As with any highly technical process like dredging, cost is of utmost concern to the modern day dredger; or, more specifically, the cost per unit of in situ dredged material. The amount of money a dredger is paid on a

dredging contract is directly proportional to the amount of in situ bottom sediment that the dredger excavates (measured by bathymetric mapping before and after dredging). The costs associated with a dredging operation are very significant: fixed costs for dredge mobilization/de-mobilization and variable costs for fuel, wages, and dredge leases. In order to minimize costs, a dredger must maximize the dredge pump's efficiency and production capacity, effectively minimizing fuel usage and project duration, respectively. In order to keep dredging profitable, dredgers must operate their equipment at the maximum possible efficiency and production capacity (Tang, et al., 2008).

A hydraulic dredge system experiences head losses in the form of friction between the slurry and the pipe and minor losses from various pipeline components. Due to environmental regulations, existing debris, and safety concerns, dredgers often install a rigid, fixed screen over the suction inlet of the hydraulic dredge system to keep animals, large rocks, debris, and unexploded ordnance from traveling through the pipeline, as these can cause pipeline plugging or damage to the centrifugal pump. These screens cause an additional minor head loss, quantified by the minor loss coefficient, k (or k -value). Previous experiments quantified this k -value as a function of specific gravity (SG) and suction inlet velocity (V_s) for a commonly-used suction inlet screen on a 1:10 model laboratory cutter suction dredge (Girani, 2014). This research conducted a sensitivity analysis on the suction inlet screen k -value at conditions of both water-only and with slurry present when the following dredge operating parameters were changed:

cutter head speed (Ω); ladder arm swing speed (V_L); screen opening area ratio (β); and geometric shape of screen openings.

BACKGROUND

Fluid Flow

Fluid flow through a pipeline is governed by the Conservation of Mass equation and Conservation of Energy (Modified Bernoulli) Equation with the assumptions of: incompressibility, steady flow, and streamline flow (Randall, 2013). Equation (1) is the energy equation, or sometimes called the modified Bernoulli equation, for flow through a pipeline system with a centrifugal pump.

$$\frac{P_1}{\gamma} + \frac{V_1^2}{2g} + z_1 + h_p = \frac{P_2}{\gamma} + \frac{V_2^2}{2g} + z_2 + h_L \quad (1)$$

where P is pressure, V is fluid velocity, z is elevation above a reference datum, and g is the gravitational acceleration. The head loss (h_L) shown comprises energy losses due to friction (h_f) and energy losses due to minor disturbances in the flow (h_m) – i.e. valves, bends, etc. Each term has units of length and is expressed in feet of head (or meters of head).

The subscripts refer to the point at which the measurements are taken. In typical dredging pipe flow problems, Point 1 is taken to be the reference datum where the fluid starts at rest and only a static pressure head is present due to the depth of water. Point 2 may be taken at any point in the pipeline system, depending on what the evaluator seeks to calculate. When evaluating the entire system, Point 2 is typically taken at the end of the discharge pipe. A simplified schematic of this flow problem is shown in Figure 1.

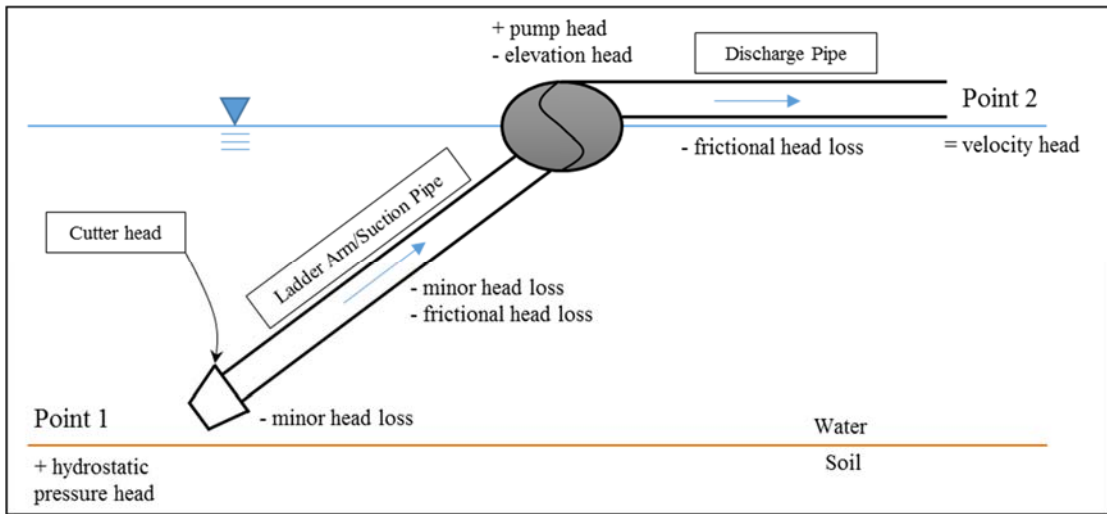


Figure 1: Simplified schematic of the energy balance in a typical pipe flow problem.

For example, if the dredger would like to calculate the pump power required to pump fluid at a certain flow rate through a given pipeline system of specified length, the dredger should choose Point 1 in still water at the dredging depth and Point 2 at the end of the discharge line. The energy equation converts hydrostatic pressure head (at Point 1) into the desired elevation and velocity head (taking into account frictional and minor head losses along the way), leaving the evaluator a solution for the pump head required in the system (h_p).

In order to fully evaluate the energy equation, one must calculate frictional head loss and minor head loss, which are defined by Equations (2) and (3), respectively.

$$h_f = f \frac{L V^2}{D 2g} \quad (2)$$

$$h_m = \sum k \frac{V^2}{2g} \quad (3)$$

where f is the pipe-specific friction factor, whose approximation is defined by Swamee & Jain (1976) in Equation (4).

$$f = \frac{0.25}{\left[\log_{10} \left(\frac{\epsilon}{3.7D} + \frac{5.74}{Re^{0.9}} \right) \right]^2} \quad (4)$$

where ϵ is the material-specific absolute roughness of the pipe that is taken from tabulated values, L is the length of pipe, D is the pipe inside diameter, and Re is the Reynold's number, defined by Equation (5).

$$Re = \frac{VD}{\nu} \quad (5)$$

where ν is the kinematic viscosity of the fluid, and $\sum k$ is the sum of all component-specific minor loss coefficients.

Slurry Flow

In a hydraulic cutter suction dredge, the bottom sediment is first physically suspended by means of a bladed cutter head (such as the one shown in Figure 2) that cuts through the sediment while rotating. Once suspended, the hydraulic suction flow through the pipeline transports the slurry to the desired location.



Figure 2: Model cutter head used at the Haynes Coastal Engineering Laboratory.

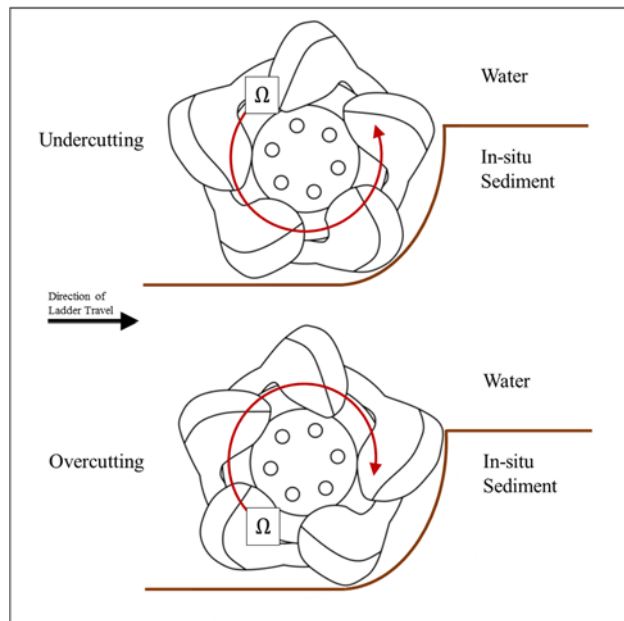


Figure 3: Diagram of overcutting and undercutting for a cutter suction dredge.

There are two different sediment pick-up schemes which are shown in Figure 3: overcutting and undercutting. Greater production is typically realized in the undercutting

scheme, as it is more efficient at suspending sediment and increasing the specific gravity of the slurry.

Once the slurry has reached the pipeline, sediment flow through the pipeline is characterized by three different flow regimes: fixed bed, heterogeneous, and homogeneous (Wilson, et al., 2006). The distribution of sand particles in a cross-section of pipe for the three schemes is shown in Figure 4. The homogeneous case is characterized by a uniform distribution of particles suspended across the pipe cross-section and typically causes excessive pipeline erosion and fuel usage inefficiency (Randall, 2013). The heterogeneous case is characterized by all particles remaining in suspension, but with a greater concentration of particles near the bottom of the pipe cross-section and a lesser concentration near the top (Herbich, 2000b). The fixed bed case is characterized by the particles being supported by the pipe wall itself and can either be moving through the pipeline in or stationary in the pipeline.

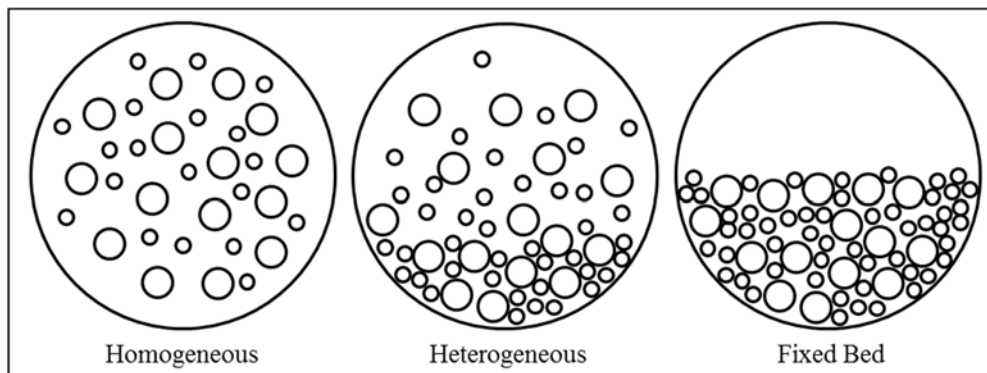


Figure 4: Slurry flow regimes in a pipeline.

The most common and economical flow regime is heterogeneous (Fusheng, et al., 2007) because it allows for an efficient range of pump power usage, minimizes erosion of the pipe walls, and prevents plugging of the dredge pipeline (Randall, 2013).

Production Limitations

There are some limits to cutter suction dredge production, including: pump power, the cavitation limit, storage capacity (for hopper dredges or confined disposal facilities), and the amount of head loss in the system (Basco, 1975a).

Pump Power Limitation

First, the pump head determines the maximum efficient flow rate at which the system can operate. The flow rate is proportional to the dredge production rate (P) according to Equation (6) from (Randall, 2014a),

$$P = QC_vDE \quad (6)$$

where DE is the time-related dredge efficiency factor of the dredge and C_v is the volumetric concentration of dredged material in the mixture defined by Equation (7).

$$C_v = \frac{(SG_m - 1)}{(SG_s - 1)} \quad (7)$$

where SG is specific gravity and subscripts m and s indicate “mixture” and “solids,” respectively. The volumetric flow rate (Q) increases with pump power according to Equation (8) from Randall (2013),

$$Q = \frac{WHP \cdot 550}{\gamma h_p} \quad (8)$$

where γ is the specific weight of the fluid or slurry and h_p is the energy input (in feet of water) from the centrifugal pump, defined by Equation (9),

$$h_p = \frac{P_d - P_s}{\gamma} \quad (9)$$

where P_d is the pressure head measured at the pump discharge, P_s is the pressure head measured at the pump suction inlet, and WHP is the water horse power defined by Equation (10),

$$WHP = BHP \cdot \eta \quad (10)$$

where BHP is the pump brake horse power (i.e. horse power provided by the electric motor) and eta (η) is the pump efficiency factor, expressed as the percent of energy transfer from the motor to the pump, an example of which is illustrated in Figure 5.

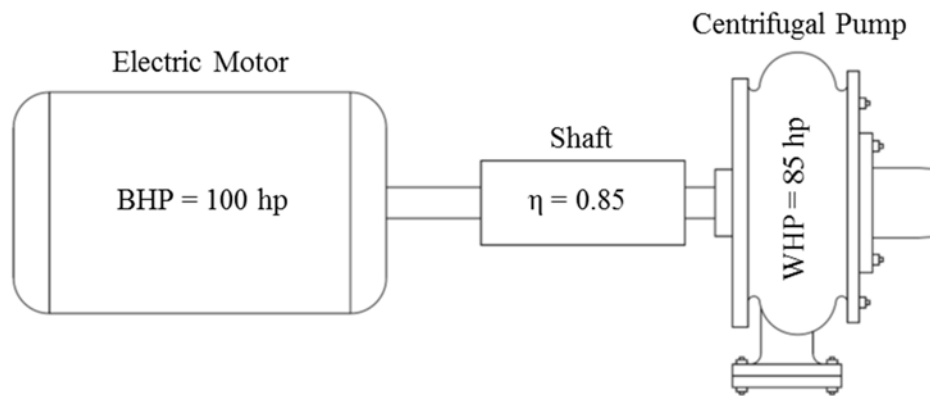


Figure 5: Example of energy transfer from an electric motor to a centrifugal pump.

A typical η value for a system operating at maximum efficiency is around 0.85.

Equations (8) through (10) show that dredge production is limited, at least, by the pump power.

System Head Loss Limitation

To evaluate the production limitation from system head losses Equation (17) must be adjusted from water flow to slurry flow by changing a few parameters. First, the specific weight of the water (γ) must be substituted with the specific weight of the slurry mixture (γ_m), which is defined by Equation (11).

$$\gamma_m = SG_m \cdot \gamma_w \quad (11)$$

where γ_w is the specific weight of water and SG_m is the specific gravity of the mixture, defined by Equation (12).

$$SG_m = \frac{\rho_m}{\rho_w} \quad (12)$$

where ρ_m is the density of the slurry mixture and ρ_w is the density of water.

Second, the measured value for z_1 must be divided by the specific gravity of the mixture in order to change its units into feet of slurry (versus feet of water used in water-only pipe flow), assuming the aforementioned choices for Point 1 and Point 2. To further explain, since z_1 represents a hydrostatic pressure head of pure water at Point 1, it must be adjusted by SG_m to convert it to feet of mixture.

Lastly, the frictional head loss in the pipeline system (h_f) must be increased to account for the presence of sediment in the slurry. To determine the frictional head loss

in heterogeneous slurry transport, Wilson, et al. (2006) developed Equation (13) through experimental methods.

$$h_f = i_m \cdot L \quad (13)$$

where i_m is head loss in units feet or meters per unit length of pipe, and is defined by Equation (14),

$$i_m = f \frac{V^2}{2gD} + 0.22 \cdot (SG_s - 1)V_{50}^{1.7} C_v V^{-1.7} \quad (14)$$

where, SG_s is the specific gravity of the dry solids in the mixture and V_{50} is the velocity at which half of the sediment particles are suspended in the carrier fluid and half are supported by other particles (i.e. a central-value parameter for heterogeneous flow) (Wilson, et al., 2006), defined by Equation (15).

$$V_{50} = w \sqrt{\frac{8}{f} \cosh \left[\frac{60d_{50}}{D} \right]} \quad (15)$$

where d_{50} is the median particle diameter and w is a general particle-associated velocity described by Equation (16).

$$w = 0.9V_t + 2.7 \left[\frac{(\rho_s - \rho_w)g\mu}{\rho_w^2} \right]^{1/3} \quad (16)$$

where ρ_s is the density of dry solids in the mixture and the terminal (or settling) velocity of a sediment grain (V_t) is approximated by Equation (17) (Schiller, 1992):

$$V_t = 134.14(d_{50} - 0.039)^{0.972} \quad (17)$$

with d_{50} measured in millimeters (mm).

Once the curve is generated that relates system head loss to flow rate, it can be superposed on the manufacturer-provided pump operating curve to find the actual

operating point (flow rate, rpm, and efficiency) of the pump. This operating point is limited by the amount of system head loss that the pump needs to overcome. In short, the system head loss and operating point compose another limit of the system flow rate and overall dredged material production.

Cavitation Limitation

Cutter suction dredge production is limited by the point at which pump cavitation occurs. Within a flowing liquid, cavitation is the microscopic formation and immediate collapse of low-pressure vapor cavities; it typically causes damage to the surface on which it occurs (in dredging, the vanes of a centrifugal pump), excessive vibration, and a severe reduction in pump efficiency (Randall, 2013). The onset of cavitation occurs when the Net Positive Suction Head Available (NPSHA) in the system falls below the pump-specific Net Positive Suction Head Required (NPSHR). The NPSHR is manually read off manufacturer-provided pump curves (based on flow rate); however, the NPSHA is specific to the system and must be calculated by Equation (18) (Randall, 2013).

$$NPSHA = \frac{P_a}{\gamma_m} - \frac{P_v}{\gamma_m} + \frac{d}{SG_m} - z_2 - h_{LS} \quad (18)$$

where P_a is the local atmospheric pressure, P_v is the fluid vapor pressure, and d is the digging depth (i.e. the vertical distance between the in situ material and the water surface). In the calculation of NPSHA, Point 1 remains in quiescent water outside the suction mouth at the dredging depth, while Point 2 is located immediately upstream of the entrance to the main centrifugal pump. Therefore, within Equation (18), z_2 is the

vertical distance from the surface of the in situ material to the pump inlet and h_{LS} is the total head loss in the suction pipe.

Once NPSHA (a constant for the system configuration) is known, the maximum flow rate without cavitation is found at the point where NPSHR is equal to NPSHA; therefore, the maximum rate of production according to Equation (6) without cavitation is limited by the maximum flow rate located at the intersection of the NPSHA and NPSHR curves.

Effects of Dredge Operating Parameters

Research has shown that many factors affect both the specific gravity and production of a hydraulic dredge system. Hayes, et al. (2000) state that, among others, the most important dredge operating parameters include: cutter head speed, ladder arm swing speed, sediment size, suction intake slurry velocity, dredging depth, cutting thickness, soil properties, and ambient environmental conditions.

Influence of Flow Rate and Specific Gravity

At relatively low flow rates, the hydrodynamics of the overall flow (i.e. the flow from still water through the rotating cutter head and into the suction entrance) is dominated by effects of the rotating cutter head. Additionally, significant spillage occurs, where sediment thrown out of the cutter head does not enter the suction pipe (Steinbusch, et al., 1999). Conversely, at high flow rates, the overall flow is dominated by the suction flow through the entrance and relatively less spillage occurs (Henriksen, et al., 2011). The amount of this spillage has been estimated to vary from 5 to 40% of the total dredged material based on environmental considerations (Dekker, et al., 2003). The

low spillage at higher flow rates (suction-dominated flow) can increase the production rate of dredging (Henriksen, 2009) because a greater ratio of the total excavated material actually enters the suction pipe (instead of being thrown away from the cutter head). This greater efficiency is in the form of a higher slurry specific gravity or increased production. In test cases at higher flow rates, it is expected that an amplified minor loss on the sediment screen would occur, slightly slowing the flow, and partially offsetting the desired increase in production.

At suction velocities typically seen in dredging (100-160% of the critical velocity), the minor loss coefficient of suction entrance screens changes with both specific gravity and flow rate (Girani, 2014). The calculated minor loss coefficient of a fixed sediment screen increases as the specific gravity increases, as shown in Figure 6 from Girani (2014). However, the influence of flow velocity on the minor loss coefficient is less apparent at the higher specific gravities shown. Indeed, when the Girani (2014) equation from Figure 6(a) is extrapolated up to specific gravity values expected in cutter suction dredging (e.g. 1.3 or 1.4), the new curves show in Figure 6(b) that minor loss coefficient and flow velocity become inversely correlated. The additional curves show that the calculated minor loss coefficient across the full range of typical dredging specific gravities converges toward a mean value at high flow velocities (160% of critical velocity).

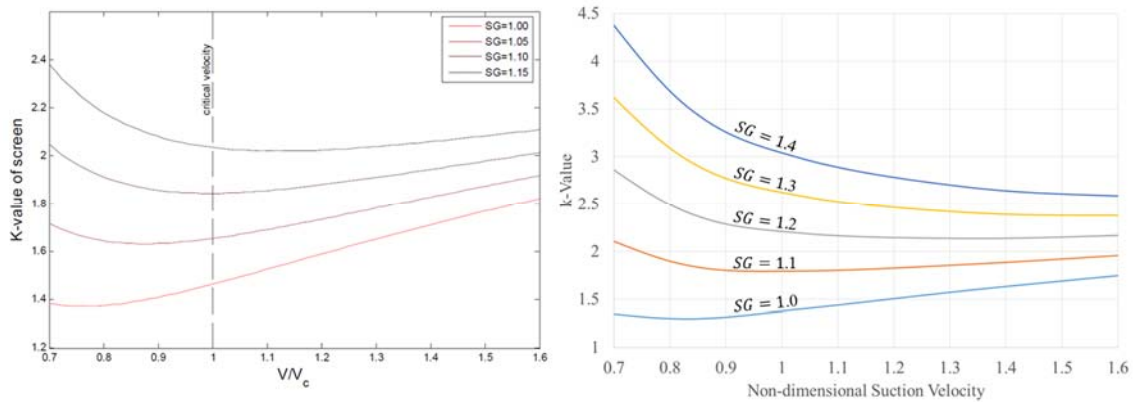


Figure 6: (a) Minor loss coefficient of a fixed screen as a function of both specific gravity and flow rate from Girani (2014); (b) Minor loss coefficient of a fixed screen extrapolated to higher specific gravities and flow rates using the prediction equation from Girani (2014).

The increased k-value at low flow rates and high specific gravity is explained by sedimentation and was mentioned by Girani (2014). When the suction flow rate nears the critical flow rate, more sedimentation is expected to occur near the fixed screen when the slurry has a specific gravity of 1.4 versus that of 1.1, leading to a greater minor loss coefficient.

Influence of Cutter Head Speed

Little data are available relating cutter head speed to sediment spillage or specific gravity of the slurry in the system. Higher values for re-suspended sediment (a result of spillage) have been positively correlated with cutter head speed (Henriksen, et al., 2011), indicating that less of the excavated sediment is going through the system. However, it is unknown if this increased spillage is simply proportional to a cutter-speed-dependent increase in specific gravity, or is an additional loss while specific gravity remains constant. Since specific gravity has a known correlation to sediment screen k-value

(Girani, 2014), it is difficult to determine a relationship between cutter head speed and k -value using re-suspended sediment data.

Den Burger, et al. (1999) conducted an experimental study showing that there exists an optimum cutter head rotational velocity at which the maximum production occurs. Their results are shown in Figure 7. The optimum (production-maximizing) value for cutter head speed at different velocities (n_c in the figure) corresponds to the peaks of the fitted curves.

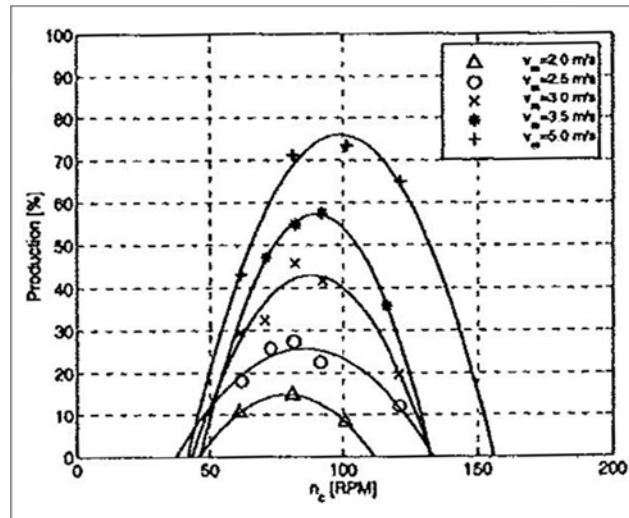


Figure 7: Production at different cutter head speeds and flow velocities (den Burger, et al., 1999).

Video recording of their tests confirmed that the sharp decrease in dredge production on either side of the optimum value is easily explained. When cutter head speed was less than optimum, the gravitational force on the dredged material particles outweighed the centrifugal and drag forces, causing the particles to congregate near the bottom of the cutter head, become poorly mixed, and avoid becoming entrained in the

suction flow. Conversely, when the cutter head rpm was greater than optimum, the centrifugal forces on the particles (caused by the rotating cutter head) outweighed the gravitational and drag forces, causing particles to be thrown out of the cutter head and the suction flow's region of influence.

One problem with using this data to compare with the experiments of this thesis is the sand grain size; den Burger's, et al. (1999) experiments were conducted by cutting into cemented gravel (with a relatively large and unsteady resultant grain size), while the experiments done in this research used relatively fine sand (with a median grain size of 0.275 mm). Gravitational forces play a more significant role in the transport of dredged cemented gravel than of fine sand, resulting in different production curves across the two sets of experiments.

Numerical models based on compiled historical dredging data suggest that the percent of sediment loss (i.e. spillage) increases with cutter head speed (Hayes, et al., 2000), which agrees with the den Burger, et al. (1999) production data when cutter head rpm is greater than optimum. However, limited comparison can be accomplished because most of the historical data used by Hayes, et al. (2000) had sediment characteristics consistent with fine silts, versus den Burger, et al. (1999), who used cemented gravel. While the dimensional and non-dimensional numerical models of Hayes, et al. (2000) admittedly included a very limited range of operating parameters, they both predicted an increase in sediment loss with cutter head rpm. This suggests that a greater cutter head speed would contribute to a lower specific gravity (and, therefore, suction entrance loss); however, sufficient data are not yet available to prove that.

Influence of Ladder Arm Swing Speed

Very little data are available establishing a correlation between ladder arm swing speed and spillage (or specific gravity). Glover (2002) suggested that greater ladder arm swing speeds could result in a greater amount of spillage, implying a lower specific gravity (with constant fluid velocity) and a smaller k-value. Conversely, the dimensional numerical model developed by Hayes, et al. (2000) shows a slight decrease in sediment loss (or spillage) with increasing swing speed, while the non-dimensional model shows a very slight increase. These models suffer from a low correlation coefficient in the range of 0.4 to 0.6, so the data should be considered inconclusive.

Experiments conducted by Yagi, et al. (1975) resulted in a linear relationship between ladder arm swing speed and mud content (i.e. a measure of solids concentration), as shown in Figure 8.

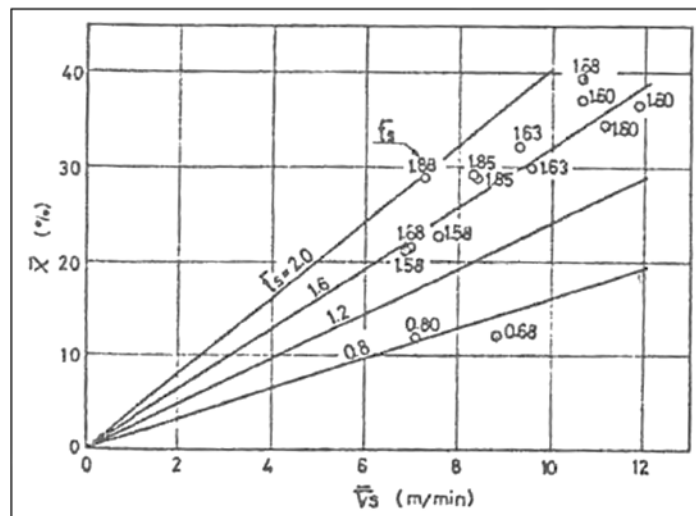


Figure 8: Solids concentration at different ladder arm swing speeds and cutting thicknesses (Yagi, et al., 1975).

These data showed that the average mud content (\bar{X}) increased with average ladder arm swing speed (\bar{V}_S in the figure) for four different average cutting thicknesses (\bar{t}_S in the figure). It is inferred that Yagi's, et al. (1975) non-dimensional values for \bar{X} are proportional to the currently-used measurement of specific gravity; therefore, the data suggest that average specific gravity (and k-value) should increase with ladder arm swing speed. However, a limitation is that the dredged material was classified as silt and clay, which behave quite differently than sand. More experiments in this field are needed to determine the relationship between sediment screen k-values and dredge operating parameters.

The Need for Evaluating Minor Losses

In 1975, the operation of dredges was governed primarily by rules of thumb that were developed by experienced dredgers (Basco, 1975b). Technology and science has continually advanced, but even quite recently greater than 95% of the thousands of operable dredges in the world are operated manually, with significant performance fluctuations across operators (Tang, et al., 2008). The rule-of-thumb mentality has not faded from the dredging world, despite mounting evidence that computer automation of dredges actually increases production and decreases costs. The dynamic nature of dredging implies that full automation will not occur for a long time; however, in order to accelerate the process, more research is needed to quantify the many unknown variables in dredging operations.

In addition to the continual need for technology advancement in the field of dredging, environmental regulations have imposed restrictions on dredging operations in the form of fixed screens to prevent marine life and explosive ordnance from entering the hydraulic dredge system. This mandate introduces considerable uncertainty in the planning and estimating of dredging operations. In order to provide good contract bids and remain profitable, dredgers must be able to quantify the characteristics of the screens they are required to install, especially because it affects their production capacity. This research is needed so that dredgers may become knowledgeable about how the required fixed screens behave under a variety of different operating conditions.

OBJECTIVES

The overall objectives of this research were to qualitatively and quantitatively evaluate the effects of cutter head speed, ladder arm swing speed, screen opening area ratio, and opening shape on the minor losses of fixed sediment screens.

It has already been shown that the minor loss coefficient (k-value) for sediment screens increases with both velocity and specific gravity of the slurry (Girani, 2014). Additionally, past research has shown that operating parameters like swing speed and cutter head speed are correlated with turbidity, sediment spillage, and dredge production, possibly leading to changes in specific gravity.

The specific gravity of slurry being pumped is very dynamic, as it is sensitive to changes in bathymetry and soil characteristics. To the author's knowledge, no published research has identified a correlation between k-value and cutter head speed, ladder arm swing speed, screen opening area ratio, or opening shape. Because of these reasons, the objectives of this research were to conduct independent experiments to evaluate the dependency of the aforementioned parameters. Additionally, any relationship found between dredge operating parameters and minor loss coefficient is to be applied to a prototype-scale cutter suction dredge.

EXPERIMENTAL TEST SETUP

Model Scaling

The model dredge that was used resides in the Reta and Bill Haynes '46 Coastal Engineering Laboratory, located on the campus of Texas A&M University at 600 Discovery Dr., College Station, Texas, 77843, USA. The dredge was designed as a 1:10 scale model of a 30-inch cutter suction dredge (Glover, 2002) and built according to the design parameters which were achievable in the laboratory. The model dredge parameters used for this experiment are outlined in Table 1.

Table 1: Model and prototype scale relationships for model dredge operating parameters.

Operating Parameter	Prototype	Haynes Lab Model Dredge	Model to Prototype Ratio
Cutter Head Rotational Speed	30 RPM	15 to 45 RPM	1:2 to 1: ² / ₃
Cutter Head Diameter	60 in (152 cm)	16 in (40.6 cm)	~1:4
Cutting Thickness	30 in (76 cm)	10 in (25 cm)	1:3
Water Depth	40 ft (12.2 m)	8 ft (2.44 m)	1:5
Grain Size (d_{50})	0.00164 ft (0.5 mm)	0.00090 ft (0.275 mm)	~1:2
Grain Settling Velocity*	0.207 ft/s (63 mm/s)	0.108 ft/s (33 mm/s)	~1:2
Discharge Pipe Diameter	30 in (76 cm)	3 in (0.076 m)	1:10
Ladder Arm Swing Speed	12 in/s (30 cm/s)	1.0 to 3.0 in/s (2.5 to 7.6 cm/s)	1:12 to 1:4
Flow Rate	30,000 GPM (113,550 l/min)	250 to 400 GPM (946 to 1514 l/min)	1:5 to 1:4

*calculated using Equation (17)

Four sets of scaling parameters were initially examined by Glover (2002) to determine the appropriate scales for constructing the Haynes Laboratory model dredge: hydraulic scaling (based on sediment pick-up behavior), kinematic scaling (Froude Number), dynamic scaling (cavitation), and geometric scaling; but, it was impossible to satisfy all sets of scaling laws at the same time. In addition to the 1:10 scale parameter that was set by the dimensions of the existing tank, the hydraulic scaling parameter and kinematic scaling (i.e. sediment pick-up behavior and Froude number scaling, respectively) were determined to be most important scaling parameters because they modeled the dredge according to its primary function: dredged material production. By using hydraulic and kinematic scaling for as many parameters as possible, the behavior of the model dredge could most accurately imitate the behavior of a prototype-sized dredge. Applying the hydraulic, kinematic, and geometric scale laws proposed by Glover (2002) using Equations (19) through (28) resulted in the scaled model parameters in Table 2, and are presented next to the final chosen test parameters for comparison.

Table 2: Theoretical model parameters scaled according to three scaling laws.

Parameter	Scaling Method			Chosen Test Parameters
	Hydraulic	Kinematic	Geometric (1:10)	
Q_{model} (GPM)	1117	1102	30	250 to 400
Ω_{model} (rpm)	21	58	30	15 to 45
$(V_L)_{\text{model}}$ (in/s)	3.2	6.2	1.2	1.0 to 3.0

In order to choose the test parameters shown in Table 2, the three scale laws were evaluated to determine the best scale relationships for the model dredge. If none of the

scaling laws could be satisfied, parameters had to be adjusted to what was achievable in the laboratory setting (e.g. digging depth) or what materials were available for use (e.g. sand grain size). Finally, since much of the laboratory equipment was donated, the scales of some parameters were difficult to control in any case.

Selection of Flow Rates

The range of flow rates used was determined by the slurry critical velocity, hydraulic scaling, kinematic scaling, and the centrifugal pump power. The critical velocity in the 4-inch suction pipe was estimated by Wilson's, et al. (2006) nomograph method as 6.17 ft/s (1.88 m/s), which corresponded to a critical flow rate of 241 GPM (912 l/min). Clearly, the geometrically-scaled flow rate in Table 2 was too low for this experiment. This fact determined the minimum flow rate at which tests would be performed: 250 GPM (946 l/min). The hydraulically- and kinematically-scaled flow rates seemed promising options for maximum model flow rates selection, as they were nearly equal; however, the centrifugal pump installed on the model dredge had a maximum flow rate of 600 GPM (2271 l/min). Additionally, the limit of pump efficiency was at about 80% power, corresponding to about 400 GPM (1514 l/min). This determined the maximum flow rate at which tests would be performed: 400 GPM (1514 l/min). These maximum and minimum testing flow rates corresponded to a cube-root scale ratio of 1:5 to 1:4. The chosen test flow rates were considered acceptable (although not exact) values for the hydraulic and kinematic scale laws shown in Equations (19) and (20), respectively.

$$Q_{model} = Q_{prototype} \left[\frac{(D_c)_{model}}{(D_c)_{prototype}} \right]^2 \left[\frac{(V_t)_{model}}{(V_t)_{prototype}} \right] \quad (19)$$

$$Q_{model} = Q_{prototype} \left[\frac{(D_c)_{model}}{(D_c)_{prototype}} \right]^{5/2} \quad (20)$$

where D_c is the cutter head diameter.

Selection of Cutter Head RPM

The cutter head rpm was scaled to both hydraulic and kinematic scale laws. Past research had kept the cutter head speed at the common prototype value of 30 rpm, so it was desirable to test an rpm at a lesser value and at a greater value. Glover (2002) suggested model design cutter head speed in the range of 100 to 300 rpm; however, later discussion of the underwater video will show that at speeds greater than or equal to 45 rpm, significant sand spillage occurs outside the cutter head, which would lead to inaccurate data. The test range of 15 to 45 rpm was selected and satisfied both the hydraulic and kinematic scale laws shown in Equations (21) and (22), respectively.

$$\Omega_{model} = \Omega_{prototype} \left[\frac{(D_c)_{prototype}}{(D_c)_{model}} \right]^3 \left[\frac{(Q)_{model}}{(Q)_{prototype}} \right] \quad (21)$$

$$\Omega_{model} = \Omega_{prototype} \left[\frac{(D_c)_{prototype}}{(D_c)_{model}} \right]^{1/2} \quad (22)$$

Selection of Ladder Arm Swing Speed

The ladder arm swing speed and discharge pipe diameter followed the intended geometric scaling (1:10), kinematic scaling, and hydraulic scaling. The selected values of 1.0 to 3.0 in/s (2.5 to 7.6 cm/s) were slightly less than the values suggested by

hydraulic and kinematic scaling laws to prevent excessive y-direction forces on the ladder arm and potentially tripping circuit breakers during ladder arm swing movements. The ladder arm swing speed was considered well-scaled and followed the hydraulic and kinematic scaling laws shown in Equations (23) and (24), respectively.

$$(V_L)_{model} = (V_L)_{prototype} \left[\frac{(\Omega D_c)_{model}}{(\Omega D_c)_{prototype}} \right] \quad (23)$$

$$(V_L)_{model} = (V_L)_{prototype} \left[\frac{(D_c)_{model}}{(D_c)_{prototype}} \right]^{1/2} \quad (24)$$

Cutter Head Scaling

The cutter head diameter was limited by the equipment available in the laboratory. The model cutter head had a 16-inch (40-cm) diameter (1:4 scale ratio) and was the only one available for testing; therefore, the desired geometric scale ratio of 1:10 could not be satisfied. It was assumed that a greater cutting thickness resulted in greater dredge production (on average) and, hence, specific gravity of the slurry being transported. In order to achieve a wide range of specific gravity measurements for data analysis, the cutting thickness was maximized at 10 in (25.4 cm), resulting in a model-prototype cutting thickness scale ratio of approximately 1:3. A cutting thickness greater than 10 in (25.4 cm) would have resulted in the cutter head being completely buried and risked causing excessive y-direction forces which could overload the motor used to provide the ladder arm swing movement.

Water Depth Scaling

The water depth scale ratio of was limited by the laboratory tank dimensions and equipment available. For the fully loaded, floating hopper barge to maintain a minimum 12-in (30.5-cm) clearance with the concrete bottom of the tow tank, at least 6 ft (1.82 m) of water was necessary in the tank. The location of the dredge suction mouth at the intended digging depth in the sand pit (shown in Figure 10) was 2 ft (0.61 m) deeper than the bottom of the tow tank, resulting in a total digging depth of approximately 8 ft (2.44 m) and a geometric scale ratio of 1:5.

Sediment Scaling

The scale ratio for sand grain size was limited by the material available at the Haynes Laboratory and the cohesive properties of fine-grained sediment. Since silt and clay with a median grain size less than 0.000328 ft (0.1 mm) exhibit significant cohesive properties, the minimum median grain size that would be usable in a laboratory setting would be 0.000328 ft (0.1 mm), resulting in a grain size ratio of 1:5. With unlimited resources, time, and funds, a median grain size of 0.000328 ft (0.1 mm) would be preferred, as it is the closest to the target 1:10 ratio; however, the sand already available at the Haynes Laboratory was used for this experiment. A sieve analysis was conducted with the sand and is shown in Figure 9 to have a median grain size of 0.0009 ft (0.275 mm), resulting in geometric scale ratio of approximately 1:2. Subsequently, the settling velocity was dependent on the median grain size, so its scale ratio also became 1:2.

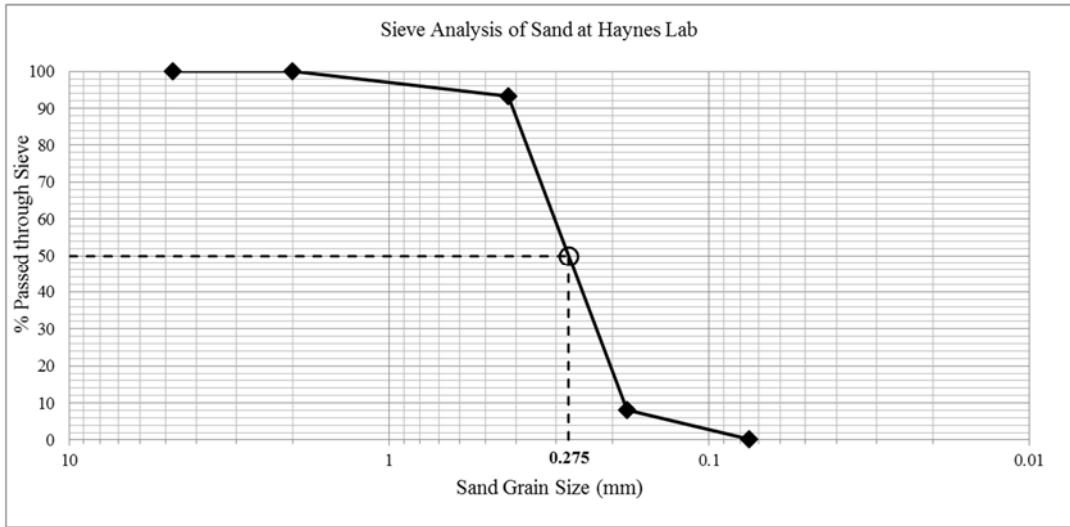


Figure 9: Sieve analysis of sand at Haynes Laboratory.

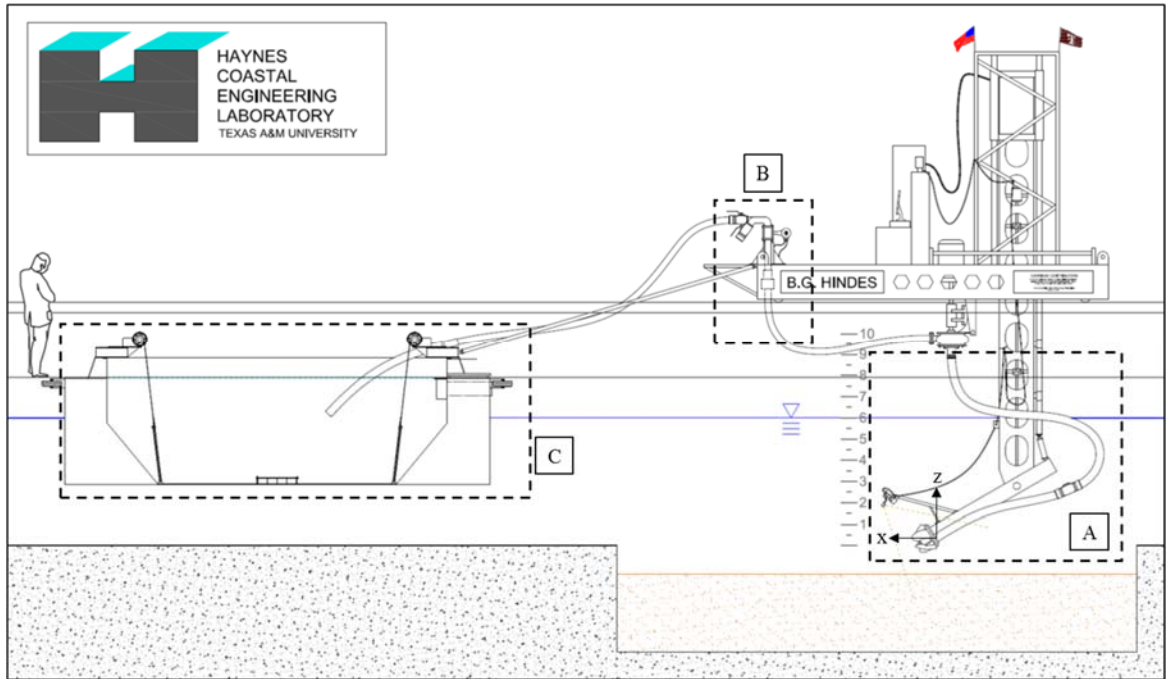


Figure 10: Overview of the model dredge at the Haynes Coastal Engineering Laboratory.

Model Dredge

The model dredge was set up as shown in Figure 10, with different regions specified (A, B, and C) for ease of discussion. For this experiment, the reference datum and coordinate system was chosen as shown in Figure 10 to be consistent with that of the model dredge controls; however, the raw data received from the model dredge displayed data assuming the z-axis is in the opposite direction than shown here. All calculations accomplished in MatLab and Microsoft Excel have accounted for the change in z-axis direction. The y-axis was assumed to point into the page.

Region A

Region A was the suction zone of the hydraulic dredge system and was where all of this experiment's data analysis took place. Region A started with otherwise quiescent water and was where sediment was excavated into suspension by the cutter head. It traveled through the sediment screen (if installed at the suction inlet) and into the 4-in (10-cm) suction pipe. Region A ended at the entrance to the centrifugal pump, with the pressure in the pipe equal to the suction pressure of the pump (P_S) which was measured with a pressure gage. The centrifugal pump was installed just below the level of the dredge carriage and was powered by an electric motor. In general, the pumping capacity of centrifugal pumps is increased by placing the pump as low as possible in the water column (Randall, 2013; Ogorodnikov, et al., 2013); however, the existing setup of the dredge carriage mount limited the location of the centrifugal pump to its current location. For this reason, a priming pump (in Region B) and swing check valve (in

Region A) were necessary to fill the system with water and maintain it there just prior to starting the main pump.

Region B

Region B contained a vertical section of pipe where the Ohmart GEN2000[®] Density Gauge (for specific gravity) and Krohne IFC 090 Electromagnetic Flowmeter sensors were located. This was an optimum location because vertical flow homogenizes the sediment layers in the heterogeneous flow scheme, providing the most accurate sensor measurement (Randall, 2014b). Additionally, Region B contained a T-split in the pipe where the flow could be directed either through the 3-in (7.6-cm) discharge hose to the hopper barge or free-flowing back into the tank.

Region C

Region C contained the end of the discharge line and the hopper barge, which was used to collect the dredged material for each set of tests. The barge had a 6-in by 24-in (15-cm by 61-cm) weir installed on the end nearest the dredge that drained overflow water back into the tank through an 8.125-in (20.6-cm) diameter cylindrical passage in the wall of the barge. The weir ensured that the water level in the barge remained relatively constant throughout each test and that excess water could escape the barge after sediment settled out.

The barge was constructed with two doors on the bottom that were able to swing open via the use of two hand-operated, 7500-lb (33-kN) winches installed with ¼-inch (0.635-cm) wire rope and chain. The discharge line was rigidly mounted onto the edge of the hopper barge and its end was submerged under the static water level. This created

a small, constant back pressure at the end of the discharge pipe, but did not affect any calculations because no data were required from the discharge region.

When the barge was loaded to its full capacity of water and sand, approximately 1 inch of stretch was measured in the wire rope, allowing the barge doors to open slightly and let water and sand leak out onto the floor of the tank. In most cases, the system flow rate of slurry into the barge was greater than the flow rate of leakage (indicated by water flowing through the weir); however, in a few test runs at the smallest flow rate, the inflow of slurry could not keep up with the amount of leakage through the barge doors. The imbalance caused the water in the barge to decrease by a maximum of about 3 in (7.62 cm) during certain tests. While not exactly constant during those tests, the small change in water level was not enough to affect the data. Since the flow rate was manually and continuously adjusted during all test runs at the pump controller, the very minor change in barge water level did not affect the flow rate. Additionally, the final calculations were only conducted within Region A (not including pump head input), so any change in pump power to keep flow rate constant did not affect final calculations. To prevent these problems in future tests and shorten the time required to clean up and re-level the sand bed, the author recommends that the mechanism to open the barge doors be re-designed with higher capacity winches, larger diameter wire rope, and an additional rubber seal between the barge doors.

Screen Configurations

Little research was available evaluating the performance of different fixed screen types on a hydraulic dredge system. An additional minor head loss is always expected

with the installation of a fixed screen, but this thesis sought to quantify the effects of cutter head rpm, ladder arm swing speed, screen opening shape, and screen opening percentage. The three screens shown in Figure 11 were used on the suction entrance for this experiment.

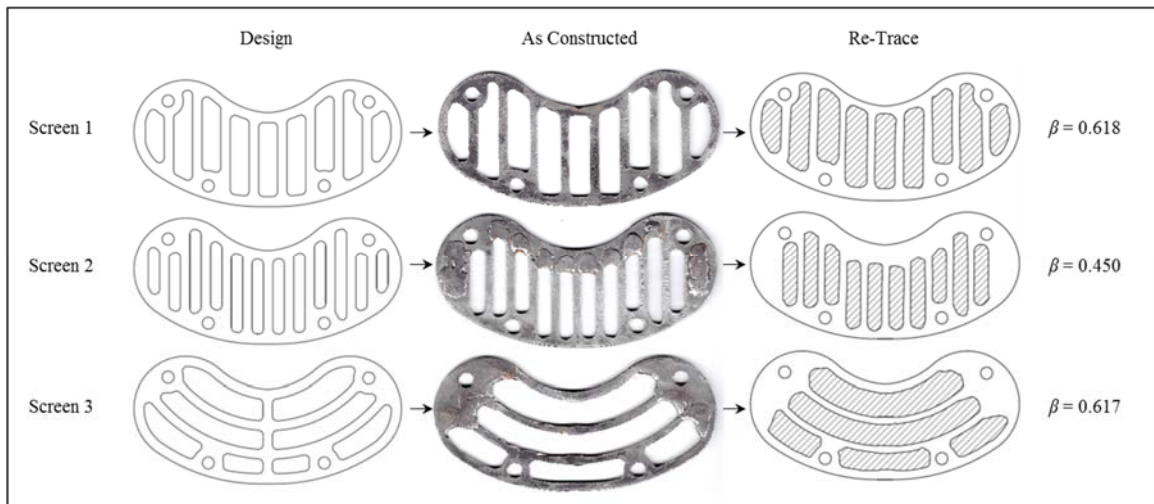


Figure 11: Screen configurations and calculated opening area ratios.

Screen 0 was the configuration with no screen in place. Screen 1 and 2 were designed with significantly different β values to find a correlation between β and k . Screen 3 was designed with the same β value as Screen 1 to show the effects of screen opening shape on minor losses. Subscripts of 0, 1, 2, and 3 on different variable or measurements indicate Screen 0, Screen 1, Screen 2, and Screen 3.

Screen 0 was considered a 100% opening of the suction mouth with a dimensional opening area of 14.00 in² (90.32 cm²). Screens 1, 2, and 3 were cut from 3/16-inch sheet metal to the appropriate shape using a plasma cutter (construction

pictures are found in APPENDIX C – PHOTOS). The plasma cutter had a kerf width of 0.25 in (0.635 cm), which required that the minimum interior curve radius of the screen design was 0.125 in (0.318 cm). After the cutting process was complete, the β values were calculated and were found to be significantly different than the designed β values. This was due to inaccuracies that increased with total length of the plasma cutting path due to the kerf width. In order to adjust β to the desired value, minor welds and cuts were done to Screen 2 and Screen 3. Photos of the screens as constructed and used are shown in Figure 11.

Calculation of Opening Area Ratio (β)

In order to determine the opening percentage of each screen as constructed, an accurate method of measuring the actual openings was necessary. High definition photographs were taken of each screen, imported into AutoCAD 2014[®], and scaled to the correct dimensions based on the measured width of the screen. Once to scale, lines were traced on the image around each opening, creating the digital copies of the screens shown in Figure 11.

The area within the openings was automatically calculated in AutoCAD 2014[®] and entered into Equation (25), yielding β values of 0.618, 0.450, and 0.617 for Screen 1, Screen 2, and Screen 3, respectively.

$$\beta_n = \frac{[\text{Opening Area of Screen "n"}]}{[\text{Opening Area of Suction Entrance}]} \quad (25)$$

TEST SETUP

In accordance with the overall objective of this research, the test plan altered ladder arm swing speed (V_L), cutter head speed (Ω), water only or slurry tests, screen opening area ratio (β), and screen opening shape across three different flow rates: 250 GPM (946 l/min), 325 GPM (1230 l/min), and 400 GPM (1514 l/min).

Each test run comprised an overcutting ladder arm translational movement (ΔY in the positive y-direction) of approximately 79 in (200 cm), a ladder arm advance (in the positive x-direction) of approximately 9 in (23 cm), then an undercutting ladder arm translational movement (ΔY in the negative y-direction) of approximately 79 in (200 cm). This series of movements was executed as an automatic program within the dredge control interface.

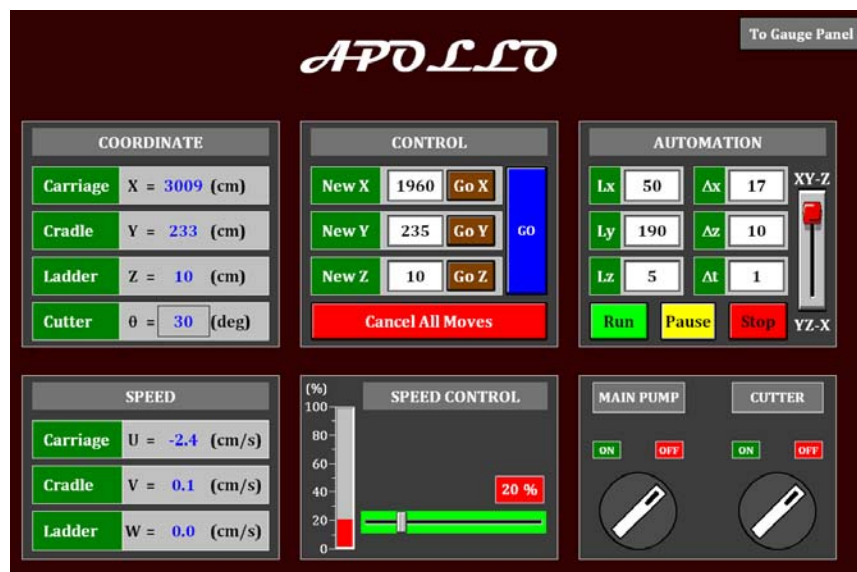


Figure 12: Screenshot of Apollo dredge control interface.

Figure 12 shows the setup that was used, with the automated path indicated by “XY-Z.” The values for ΔY and ΔX are indicated by “ $L_y = 190$ ” and “ $\Delta x = 17$ ”, respectively. The input values had units of centimeters and were slightly less than the planned values of 79 in (200 cm) and 9 in (23 cm), respectively, to account for the overshoot of the dredge carriage and ladder arm. Using the values in Figure 12, the carriage overshoot by an average of 4 in (10 cm) in the y-direction and 2.4 in (6 cm) in the x-direction, making the measured path equal to the desired path for each test run. After completing each test run, the apparatus was readied for the next test run by stopping data collection and advancing the ladder another 9 in (23 in). The scheme of maneuver for each test run is outlined in Figure 13.

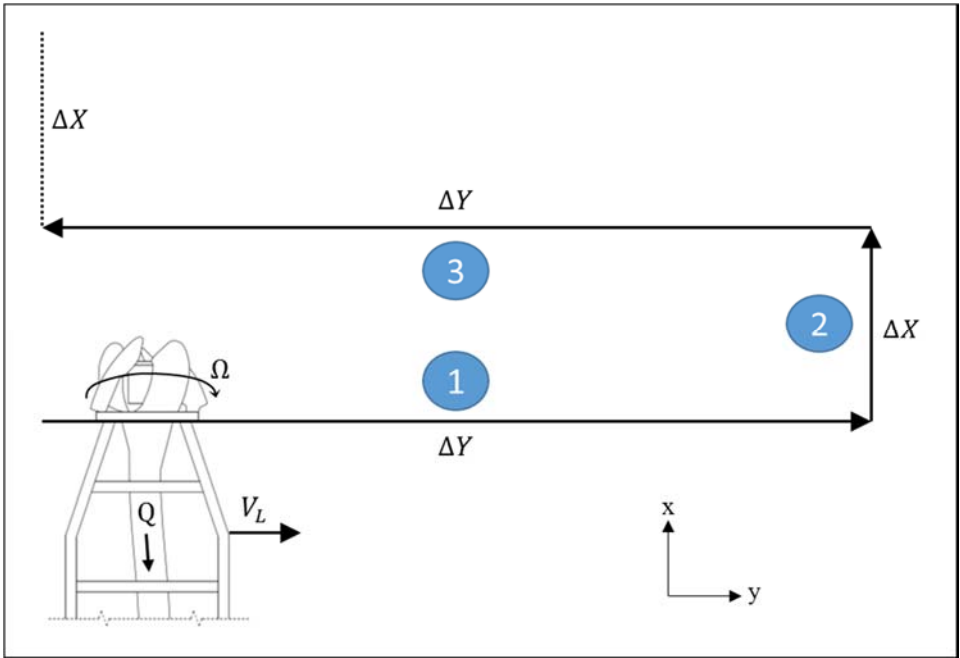


Figure 13: Scheme of maneuver for each test run.

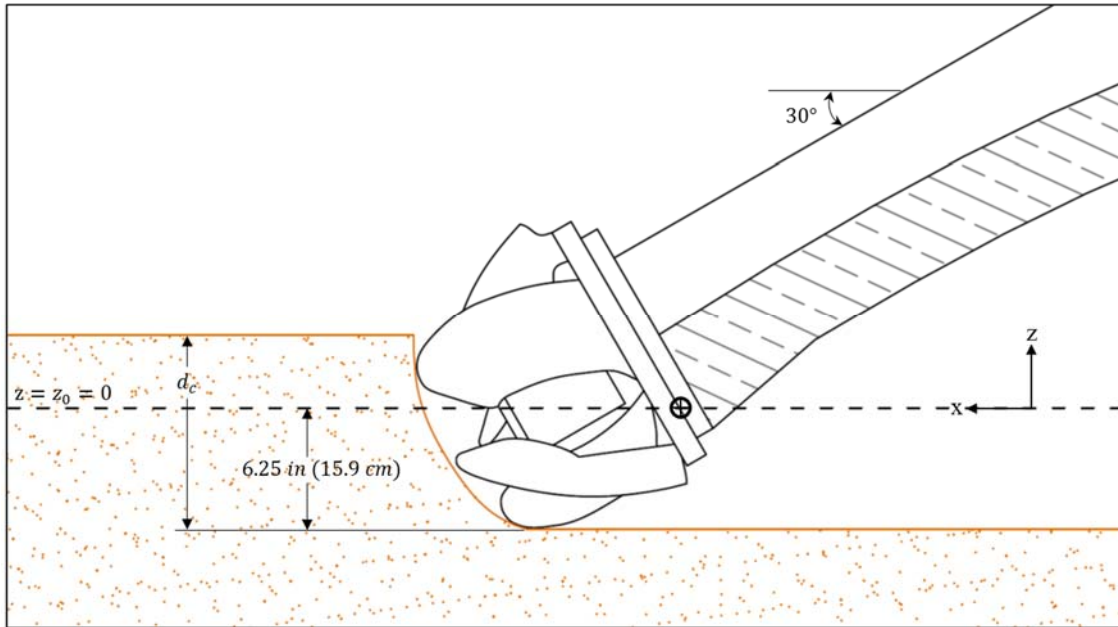


Figure 14: Cutting thickness at a 30° ladder angle with the model cutter head.

The cutting depth (or cutting thickness), shown in Figure 14, is defined by the vertical distance between the bottom-most edge of the cutter head blades and the surface of the sand. It was alternated between 0 inches (water only) and 10 inches (25.4 cm) in order to evaluate the effects of slurry in the system. Past research with the Haynes Laboratory model dredge showed that a maximum-depth cut of 12 in (30.5 cm) produced the least turbidity near the cutter head (Henriksen, 2009), suggesting a decrease in dredged material re-suspension with greater thickness of cut. The cutting thickness of 10 in (25.4 cm) was chosen to maximize the total amount of excavated material without completely burying the cutter head in the sand, which could have led to excessive y-direction forces. Additionally, the hopper barge capacity limited the number

of consecutive test runs to nine, so anything greater than a 10-inch (25.4-cm) cut would either overload the barge or increase the overall duration of project testing.

Prior to each set of test runs, the z-coordinate where the cutter head blades first touch the sand surface (corresponding to a cutting depth of 0 inches) was measured via the use of the existing force sensors on the ladder arm. To accomplish this, the ladder arm was slowly lowered in the negative z-direction (with no cutter head rotation) until the z-direction force measurement started increasing in value. The force sensors typically fluctuated $\pm 1\%$ around a constant value, but when the stationary cutter head entered the sand, the value rapidly increased by greater than 5%, indicating the presence of the sand surface. The sand surface was measured at $z=80$ cm for every set of tests except on Day 4, when it was measured at $z=79$ cm.

SENSORS

Nuclear Density Gauge

Nuclear density gauges on dredges operate on the principle that the gamma radiation emitted by a radioactive isotope is absorbed by both water and sand. The small levels of radiation emitted from an isotope are able to pass through the walls of a pipeline, through slurry, and into a detector on the other side of a pipe (VEGA Americas, Inc., 2014). The detector accurately measures the level of radiation that passed through the slurry (which changes with the density of the slurry) and converts that measurement into a density or specific gravity. Density gauges are typically placed on vertical sections of pipe to allow the slurry flow to reach a homogenous state, which makes the cross-sectional distribution of solids even and precise. If the density gauge were placed on a horizontal section of pipe, the possibility exists that a heterogeneous flow regime would cause a large sand concentration differential across the plane of density measurement, leading to sensor inaccuracies.

In the Haynes Coastal Engineering Laboratory, an Ohmart GEN2000® density gauge is installed on a vertical section of rigid, 3-inch discharge pipe in Region B of Figure 10. The density gauge includes a 1 mCi (37 MBq) radiation source of the Cesium-137 isotope (Ohmart Vega Corp., 2006a) and a detector with an output range of 4-20 mA. The system is factory calibrated to specific gravity measurements of 1.0 to 2.0, and accounts for the presence of the pipe walls. The system accuracy was given as

±0.71% of full scale (Ohmart Vega Corp., 2006b), corresponding to an absolute specific gravity error of ±0.014. The effect of this error, which was mostly in the form of noise in the SG reading, was minimized when the data series were truncated and averaged during data analysis. The Ohmart density gauge was integrated into the dredge user interface and data collection system to record data at a rate of 1 Hz.

In order to calibrate the specific gravity readings from the density gauge, nine water-only tests were conducted during each series of tests according to Figure 15. The data selections from these tests were individually averaged and then averaged across all nine tests, providing one baseline specific gravity value for calibration. Since the fluid going through the system during these tests was known to be water only, the difference between the measured calibration specific gravity and 1.00, as shown in Equation (26), was used as a calibration adjustment and subtracted from all specific gravity values for that test series. The measured calibration adjustments in

Table 3 show that the density gauge overestimated specific gravity by an average of 0.055.

$$SG_{calibration} = \overline{SG}_{baseline} - 1.00 \quad (26)$$

Table 3: Density gauge calibration adjustments for each test series.

Test Series	Day 1	Day 2	Day 3	Day 4	Day 4a	Day 5	Day 6	Day 6a
$SG_{calibration}$	0.053	0.057	0.053	0.056	0.057	0.055	0.053	0.053
<i>Average $SG_{calibration}$</i>	0.055							

Flow Meter

Electromagnetic flowmeters measure the velocity of electrically conductive fluids based on Faraday's law of induction (Krohne, Inc., 1997), which states that the mean flow rate of a fluid is directly proportional to the voltage it induces when passing through a magnetic field perpendicular to its direction of flow. The Krohne IFC 090K electromagnetic flowmeter installed on the model dredge at the Haynes Laboratory is installed on a vertical section of 3-inch diameter pipe in Region B of the hydraulic dredge system. Because the inside diameter of the pipe is known by factory specifications, the mean fluid velocity is easily converted into a mean flow rate by multiplying by the cross-sectional area of the flow. The signal converter attached to the Krohne IFC 090K flowmeter accomplishes this conversion and displays the near instantaneous flow rate in US gallons per minute (GPM).

The installed Krohne flowmeter is characterized by the pipe's nominal diameter of 3 in (76 mm) and has a measurement range of 24 to 956 GPM (91 to 3619 l/min) with a maximum error of $\pm 0.3\%$ of the measured value (Krohne, Inc., 1997). At the maximum nominal flow rate in this experiment of 400 GPM (1514 l/min), the maximum possible error is 1.2 GPM (4.5 l/min); however, Krohne, Inc. (1997) stated that this maximum error was neither typical nor expected.

Pressure Transmitter

Since pump discharge pressure measurements were unnecessary for calculations in this experiment, only the pump inlet pressure gauge will be examined. The model

dredge has a Rosemount 1511AP (Range Code 5) Smart Pressure Transmitter mounted near the centrifugal pump inlet rated up to 27 psi (186 kPa) of vacuum pressure. The gauge is factory calibrated to provide pressure measurements between 0 psi and -14.7 psi (-101.3 kPa) across its range of current output: 20 mA to 4 mA, respectively. It has an accuracy range of $\pm 0.25\%$ of the calibrated span (Rosemount Inc., 2007), which corresponds to ± 0.037 psi (0.25 kPa) of absolute uncertainty in the suction pressure measurement.

The pressure transmitter was mounted 19 in (48 cm) above the measurement location at the centrifugal pump suction inlet and connected with a small leader line. Because of this elevation change, the gauge measurement had to be corrected by a constant of +19 in (+48 cm) of water during data analysis. Because the leader line from the suction pipe to the pressure transmitter had a very small diameter, it was assumed that very little sand intrusion occurred into the leader line; therefore, it was unnecessary to adjust the head pressure correction by the specific gravity of the slurry for when sand was present in the pipeline. For this reason, the head pressure correction was considered constant for both water-only tests and slurry tests.

Ladder Location Sensors

The z-direction distance sensor installed on the Haynes Laboratory model dredge is a ToughSonic® Distance Sensor Model number TS30S1-1V with an operational range of 4 in (10.1 cm) to 14 ft (4.27 m), maximum resolution of 0.003384 in (0.086 mm), and nominal repeatability of 0.1% (Senix Corporation, 2007). It is an ultrasonic distance sensor and transducer which operates in a 4-20 mA current loop and is vertically

installed (pointing downward) at the top of the ladder between the two flags shown in Figure 10. As the ladder arm descends deeper into the water, the distance sensor increases its measurement displayed. The measurement from the z-direction sensor is used to calculate the hydrostatic pressure at Point 1 (P_1). With the water level in the tank kept constant at the 6-ft wall marking, the relationship between z measurement and depth of the suction mouth is quantified by Equation (27).

$$\text{Depth of Suction Mouth [in cm]} = z + 133 \quad (27)$$

The ladder location in the y-direction was also measured by ToughSonic® ultrasonic sensor, while the ladder location in the x-direction was measured by a LaserAce® ILM-series laser distance meter. However, the x- and y-direction measurements were only used for the setup of the dredging path; they were not necessary for data analysis or calculations.

TEST PLAN

First, test runs were conducted varying cutter head speed across three values: 15 rpm, 30 rpm, and 45 rpm, with V_L held constant at 1.5 in/s (3.81 cm/s). That series of tests was conducted with water only and with slurry, corresponding to cutting thicknesses of 0 in and 10 in (25.4 cm), respectively. Then test runs were conducted varying swing speed across three values: 1.0 in/s (2.54 cm/s), 1.5 in/s (3.81 cm/s), and 2.0 in/s (5.08 cm/s) while cutter head speed was held constant at 30 rpm. In the same manner as the last section, test runs were conducted with water only and with slurry. Initially, each test run was to be conducted twice to demonstrate repeatability; however, due to the limited capacity of the hopper barge (equivalent to nine consecutive sand test runs) and number of testing days available in the laboratory, no repeat tests were conducted after Day 1 of testing. The entire procedure was conducted for four screen configurations: Screen 0, Screen 1, Screen 2, and Screen 3, with one exception. Due to the limited time available, Screen 3 tests were only conducted across different swing speeds (i.e. no data was collected for different cutter head speeds with Screen 3 in place). A summary of the overall testing plan is shown in Figure 15.

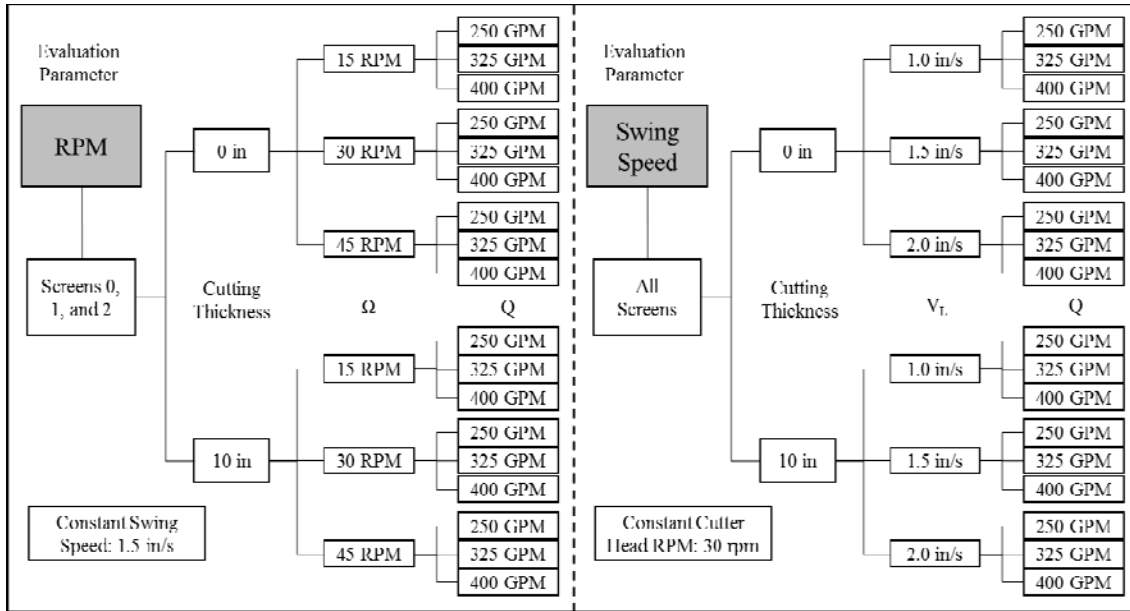


Figure 15: Summary of test plan.

In addition to the test runs outlined in Figure 15, the four tests shown in Table 4 were completed to determine the operating limits and maximum specific gravity possible in the Haynes Laboratory model dredge. In summary, 121 test runs were conducted during the six days of laboratory time allotted for this experiment and are listed in APPENDIX A.

Table 4: Test runs completed in addition to test plan.

Day	Screen No.	Cutter Head Speed (RPM)	Swing Speed (in/s)	Flowrate (GPM)	Cutting Depth (in)
6	2	30	3	250	10
6	2	30	3	325	10
6	2	30	3	400	10
6	2	45	3	250	10

Due to the proximity of the back end of the model dredge to the concrete edge of the sand pit (as shown in Figure 16), only a portion of the sand pit was available for testing within the lateral limits of the ladder arm. During the week prior to testing, the lateral limits of the sediment pit were determined and recorded, yielding the area available to dredge testing shown in Figure 16.

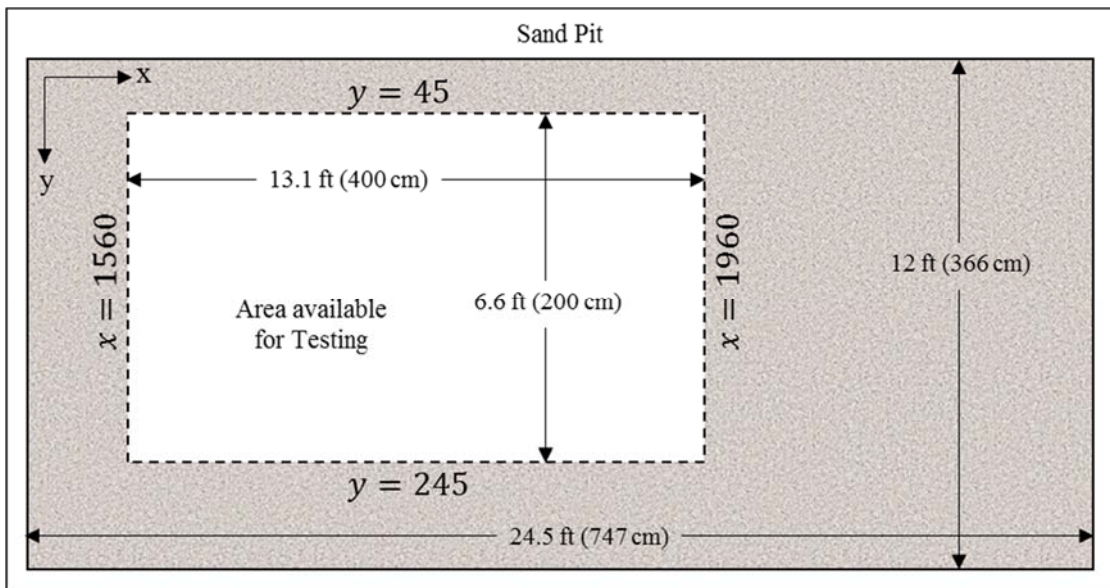


Figure 16: Plan view of sand pit (not to scale).

With the desired scheme of maneuver for each test run and the area available for dredging, nine test runs were possible in each leveled sand pit, which coincided nicely with the loading capacity of the hopper barge. The z-coordinate of the ladder arm was maintained relative to the measured location of the sand surface in order to provide a consistent cutting thickness across all tests. All test runs that pumped only water were conducted at a z-coordinate of 25 cm, which corresponded to the cutter head being 1.8 ft

(55 cm) above the sand surface. The z-coordinate for all 10-in (25.4-cm) cuts was calculated by adding 25.4 cm (10 in) to the measured z-coordinate of the sand surface. For example, when the sand surface was measured at 80 cm, the coordinate at the cutting depth was 105.4 cm.

DATA COLLECTION

The model dredge computer interface was set up to collect data, upon command, at a frequency of 1 Hz. Prior to the commencement of each test run, the data collection was turned on and the test run was started. Depending on the swing speed, the duration of each test run was approximately 80 s, 100 s, or 150 s, corresponding to swing speeds of 1 in/s (2.54 cm/s), 1.5 in/s (3.81 cm/s), and 2 in/s (5.08 cm/s), respectively. Each individual test run was recorded in the form of a comma-separated-values (.csv) file and named according to its test number given in APPENDIX A – TEST PLANS (e.g. Test 51 was named ‘test_51.csv’). The measurements included in the .csv file were: time, centrifugal pump suction and discharge pressure, flow rate, specific gravity, X-, Y-, and Z-coordinates, carriage speed (x-direction), and ladder arm swing speed (y-direction).

In addition to experimental measurements, high definition video was recorded for all slurry tests using a custom apparatus on which a GoPro Hero3+ Black Edition® video camera (with a roll-bar mount) and a DeepSea Multi SeaLite® underwater flood light were mounted. The GoPro® camera was set to record video 1080p, 30 frames per second, 16:9 aspect ratio, and medium field of view. Its battery life (measured prior to testing) was approximately 80 minutes and there was no feasible option to hardwire the camera to a power source. Since the battery life was not long enough to record a full day of tests, the author chose to record only sand tests each day (since the water-only tests would all look the same). Each day, the sand tests took place following the water-only

tests, so in order to start recording video, the author entered the water tank and manually pressed the record button prior to commencing sand tests.

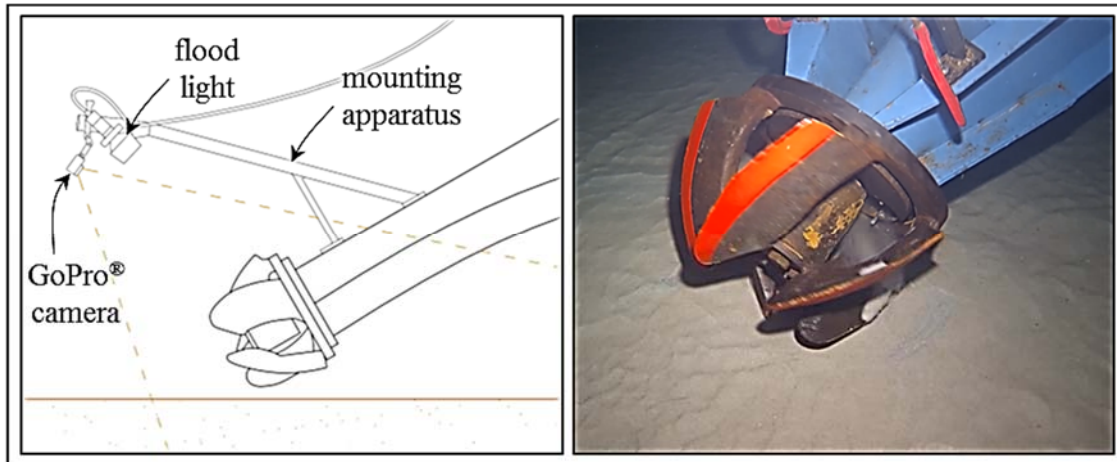


Figure 17: Video recording apparatus.

The DeepSea® underwater halogen flood light was rated for a depth of 3280 ft (1000 m), provided 4,750 lumens of illumination (DeepSea Power & Light, 2014), and was wired to a 110V power source located on the dredge carriage. The mounting apparatus was welded and constructed from scrap metal and provided a video aspect angle of the cutter head in which the sand surface, cutter head rotation, and suction mouth was directly observed; it was connected to the dredge ladder arm using four C-clamps. Figure 17 shows the design of the camera mounting apparatus and the view from the GoPro® video camera.

DATA PROCESSING

During each test run, the model dredge operators continually adjusted the pump power to keep the flow rate as constant as possible in the system; however, the specific gravity and flow velocity measured through the system inevitably changed with time and direction of cutting (overcutting or undercutting). The phenomenon of time-dependent density (specific gravity) has been known to occur in dredging practice (Miedema, 2001) and was experienced by past researchers at the Haynes Laboratory (Girani, 2014). In order to provide more precise data, the full time series for each test's raw data was truncated to include only sections of data where specific gravity, flow rate, suction pressure, and discharge pressure were relatively steady.

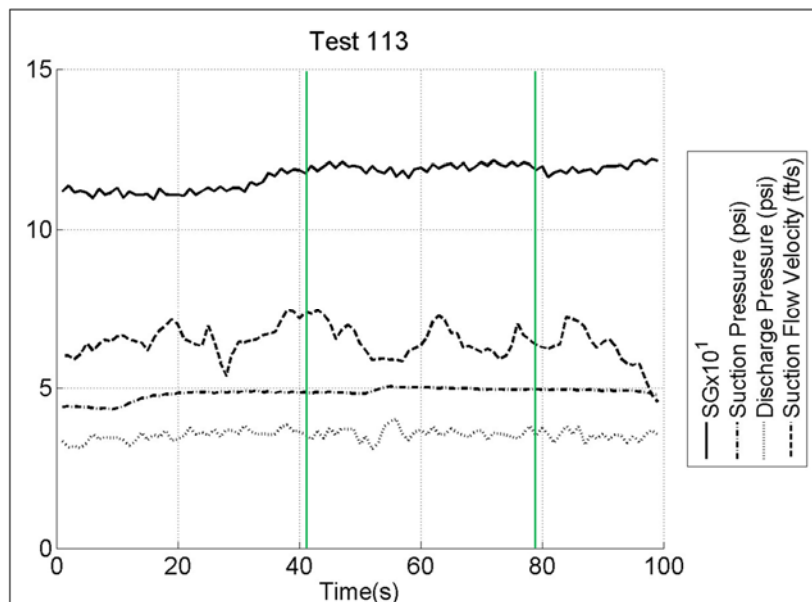


Figure 18: Example of data selection for a period of relatively steady data.

As an example, Figure 18 shows the raw data for Test 113 and a typical data selection (between the green vertical lines). The data in the truncated time series were averaged to provide single values representative of the series which were then used for further analysis. This truncation and averaging process was repeated for every test run via the use of Matlab. The data selections were visually chosen based on the amount of steady data available and varied across all tests in order to target specific values for average flow rate and specific gravity.

Figure 18 shows that the flow rate (i.e. suction flow velocity) and specific gravity fluctuated significantly during any single test. For the calculation of k-values, the Screen 1, 2, and 3 configurations had to be compared against the baseline, Screen 0 configuration. In order to isolate the minor head loss with the screen in place, the values for flow rate and specific gravity had to be matched, leaving suction pressure as the only variable in k-value calculations.

It was near impossible to match both flow rate and specific gravity for two separate test runs at the same time. For this reason, two options were available for data processing: (1) adjust data truncations to make all average measured flow rate close to the three nominal flow rates (while ignoring differences in SG), or (2) adjust data truncations to make average SG measurements of all fixed screen tests match the average SG measurement of the eighteen baseline Screen 0 tests (while ignoring small differences in flow rate). Processing the data using either method introduces error into the calculated k-values, whether by an unmatched flow rate or unmatched SG.

Both data processing methods were completed and errors were measured as a percent difference relative to the Screen 0 values. Figure 19 presents histograms of the percent error in data selections for both processing methods along with a fitted normal distribution curve.

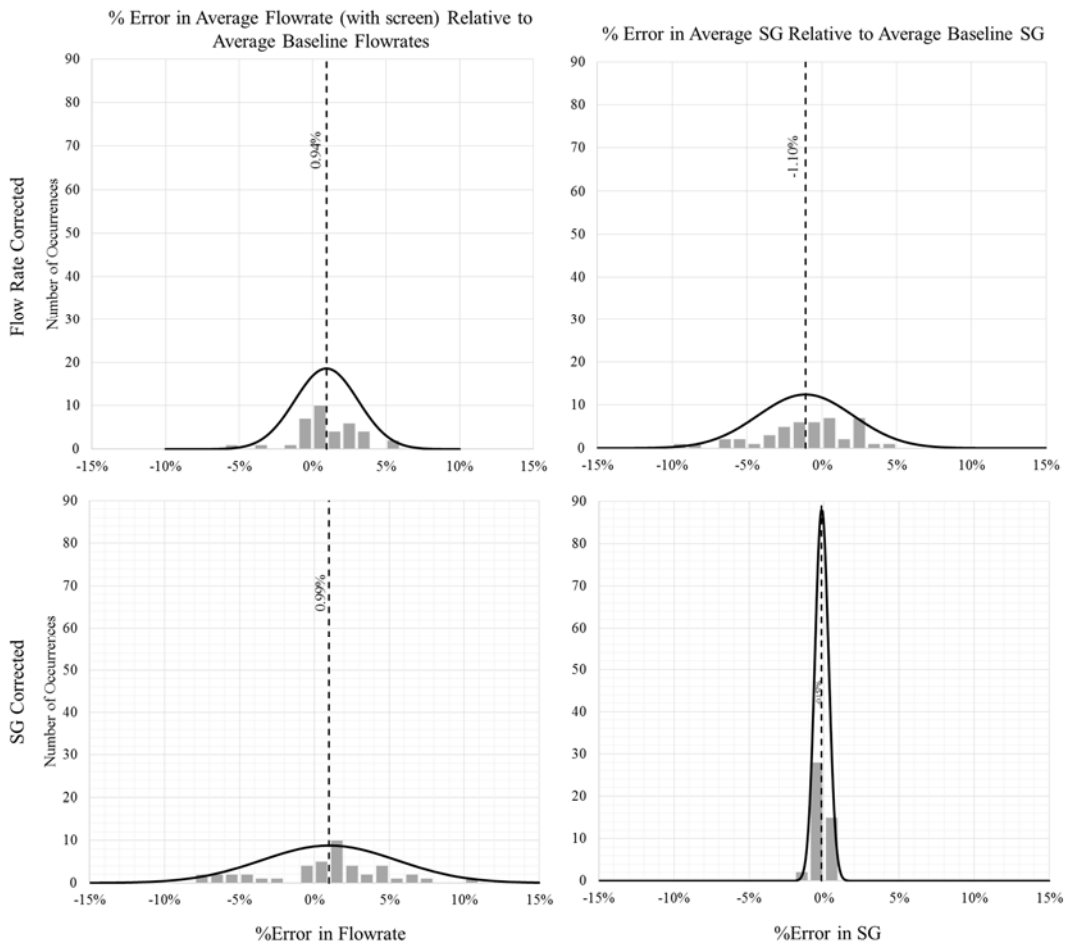


Figure 19: Histograms of percent error in data Selections for two methods of data processing.

The percent error in the data selections was most easily minimized using the SG-correction method of processing. Additionally, qualitative analysis of the raw data plots

in APPENDIX B showed that the suction pressure measurement (which was directly related to head loss and k-value) was more sensitive to changes in SG than changes in flow rate. In fact, within a test run, suction pressure showed little response to flow rate fluctuations. Therefore, to provide more accurate k-values, it was most important to match up average specific gravity values across corresponding test configurations in order to accurately calculate k-values.

QUALITATIVE OBSERVATIONS

The Bulldozer Effect

Miedema (2012) described a bulldozer effect that occurred in the cutting of water-saturated sand at high cutting angles. He determined that if the face of a cutter head blade was oriented perpendicular to the direction of cut, a small wedge of stationary sand forms on the blade's face that acts as a cutting blade of a shallower angle. A similar phenomenon was observed in this research during some of the test cases at the lowest cutter head speed of 15 rpm and is shown in Figure 20.

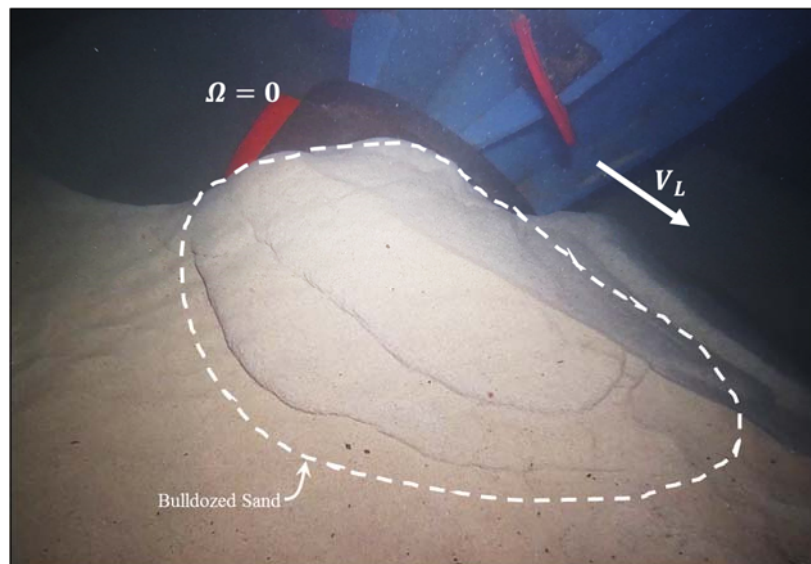


Figure 20: Bulldozer effect at slowest nominal cutter head speed.

In this case, the cutter head rpm did not produce enough rotational force to overcome the sand's gravitational and frictional forces acting on the blades. The cutter head stopped

rotating while the ladder arm continued to traverse at the programmed rate, which caused a bulldozer effect on the exterior surface of the blades. This made the topmost layers of sand shear off, as shown in Figure 20.

In a full-sized dredge, this pseudo-bulldozer effect would risk plugging the suction line; however, in the controlled environment of the laboratory, video evidence showed that slurry was still formed due only to the influence of the suction inlet velocity field (without the need for cutter head-induced mixture formation). It is unlikely that a full-sized dredge would operate at such low cutter head speeds, so this effect is considered to be peculiar to the laboratory setup and not real dredge operating conditions. To prevent this problem in future testing, the cutting thickness should be reduced or the power of the cutter head motor could be increased.

Spillage

In hydraulic dredging, spillage is defined as sediment that is excavated by the cutter head but does not enter the suction pipe (den Burger, et al., 1999). Furthermore, spillage produces both re-suspended sediment (sediment that becomes dispersed and suspended in the water column) and residual sediment (sediment that has been re-suspended and re-deposited onto the sea floor) (Bridges, et al., 2008). During the series of laboratory tests, spillage was observed by reviewing the test video. The amount of spillage was found qualitatively to be positively correlated with the cutter head speed, which is consistent with the observations of den Burger, et al. (1999).

At 45 rpm, significant spillage around the cutter head was observed. Most of this spillage became residual sediment that settled onto the sand surface, while some became

re-suspended or re-entrained in the cutter head. More spillage and re-suspended sediment was observed at shallower cutting thicknesses (i.e. when the cutter head was first being lowered into the sand) than at deeper cuts. This was concurrent with the direct laboratory observations of Henriksen, et al. (2011). The observations in Figure 21 adhered to the positive relationship between spillage and cutter head rpm predicted by the numerical models of Hayes, et al. (2000).

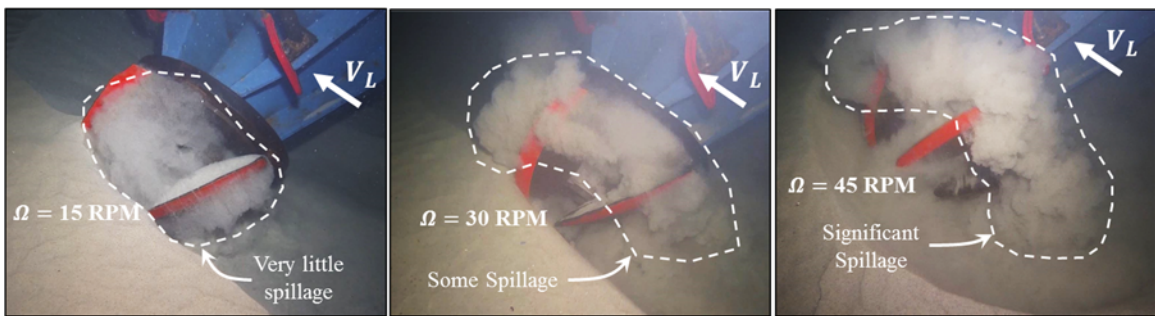


Figure 21: Spillage at different cutter head speeds.

Analysis of the video data showed that the sediment suspended by the cutter head at 15 rpm was nearly all entrained in the suction flow velocity field, resulting in very little spillage. This was initially promising for selection of an optimum cutter head speed; however, the presence of the bulldozer effect at that speed established that it was impractical.

Visual analysis of spillage at 30 rpm showed that some re-suspended sediment was thrown out of the suction flow's region of influence in the form of both residual and re-suspended sediment; although, some fell back into the cutter head and was subsequently entrained in the suction flow. The cutter head speed of 30 rpm was

typically used in prior dredging tests due to its consistency with real dredging operations. It is believed that the use of this median value for cutter head speed is best for the range of flow rates possible at the Haynes Laboratory because it cuts the material most efficiently without encountering any bulldozer effects or excessive spillage.

Screen Clogging

Screen clogging is defined as excessive sediment build-up on the upstream face of the fixed sediment screen that produces an additional minor loss in the system. The research of Girani (2014) showed that when a fixed screen on the Haynes Laboratory model dredge clogs, the suction pressure significantly increases until the clog is removed from the screen. Because the data analysis of this experiment cannot distinguish between head loss due to clogging and head loss due to the fixed screen, the clogging phenomenon produces artificially high calculated fixed screen minor loss coefficients.

In this experiment, screen clogging occurred for two reasons. The first is the opening area ratio. According to data from this thesis and the research of Girani (2014), screen configurations that clogged had opening areas of 0.45 and 0.50, while those that did not clog had opening areas of 0.617, 0.618, and 1.00. The screen opening area ratio is clearly one indicator of the screen's propensity to clog.

The author proposes that another predictor of clogging is the ratio of the sediment's median grain size (d_{50}) to the dimensional screen opening area (e.g. in units of ft^2). Since the sediment grain size was unable to be perfectly scaled, the difference between model and prototype sand is very small. Conversely the difference between model and prototype dimensional screen opening areas is proportional to the square of

the model-to-prototype geometric length scale (i.e. relatively large). The fact that the sediment size is not adequately scaled means that its ratio to screen opening area is artificially high in the model dredge; whereas, at the prototype scale, the ratio to screen opening area is much lower over the range of typical operating parameters.

As a physical explanation of this concept, consider the modeled grain size of 0.275mm and a prototype grain size of 0.275mm (a common sediment found in beaches). At the same time, consider screen opening areas on the order of 5 in² (model) and 100 in² (prototype). It is quite clear that the ratio of grain size to screen opening area is much larger at model scale than prototype. It is believed that the model configuration used in this experiment had an inherently high ratio due to the sand that was available in the laboratory, leading to a greater chance of screen clogging. Conversely, dredges with typical operating parameters which produce lower grain size-to-opening area ratios are expected to be less likely to clog. At constant grain size, the Haynes Laboratory model dredge is expected to experience clogging during consecutive tests at screen opening area ratios (β values) of 0.50 or less. At prototype scale and similar grain size, the threshold of expected screen clogging is expected to be at a much lower β value. However, it would be premature to state a specific β value as the threshold, since there are insufficient data available in this research to make that determination.

The Influence of Flow Rate on Specific Gravity and Production

Conventional dredging engineering says that production increases with flow rate (Randall, 2014a) and that an optimum, production-maximizing flow rate exists (Ogorodnikov, et al., 1987). Production was expected to increase with flow rate,

especially since the smallest tested flow rate of 250 GPM was very close to the critical flow rate at which sedimentation occurs within a horizontal pipeline.

However, Figure 22 shows that specific gravity decreased (on average) with flow rate, resulting in a relatively constant average production. The data points plotted by Girani (2014) were conducted with the same model dredge apparatus and similar test runs. Although not specifically evaluated for a relationship between flow rate and specific gravity or production) the Girani (2014) data points showed that the maximum achievable specific gravity during a single test run occurred most often at the lowest flow rates, which is consistent with the data in this thesis.

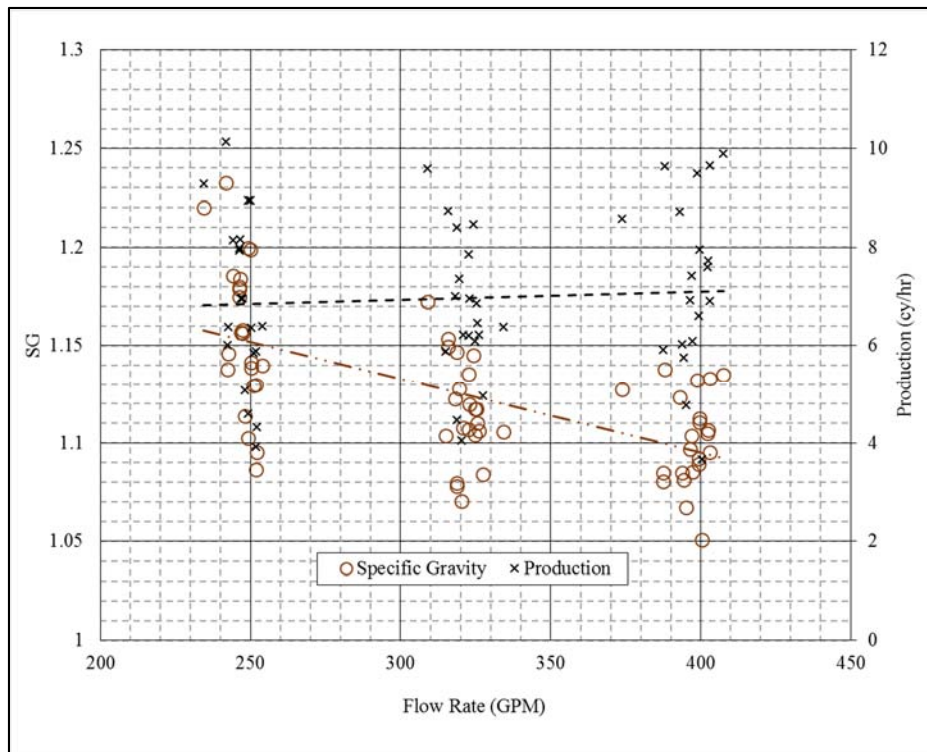


Figure 22: Specific gravity and calculated production for all tests.

The large vertical spread in both specific gravity and production is due to the variations in both cutter head rpm and swing speed across all tests. Aside from these variations, the average decrease in specific gravity with increased flow rate is explained by the ratio of water to solids in the slurry at different flow rates. The volume of dredged material available in a 10-in (25.4-cm) thick cutting path remained constant across all tests; however, as the flow rate increased, more water entered the suction pipe, effectively diluting the solids concentration in the slurry and decreasing the specific gravity. An evaluation of Equation (7) shows that the decrease in specific gravity resulted in a decrease in concentration by volume (C_v), which balanced out the increase in flow rate (Q) in Equation (6). The end result was an almost constant average production across all tests.

The Influence of Cutter Head Speed on Specific Gravity

The relationship between maximum observed specific gravity during a test run and cutter head speed was concurrent with the aforementioned observations of spillage at different cutter head speeds. Since nearly all the maximum SG observations at a given set of dredge parameters occurred at the lowest flow rate of 250 GPM (946 l/min), all the data points shown in Figure 23 were at that lowest flow rate.

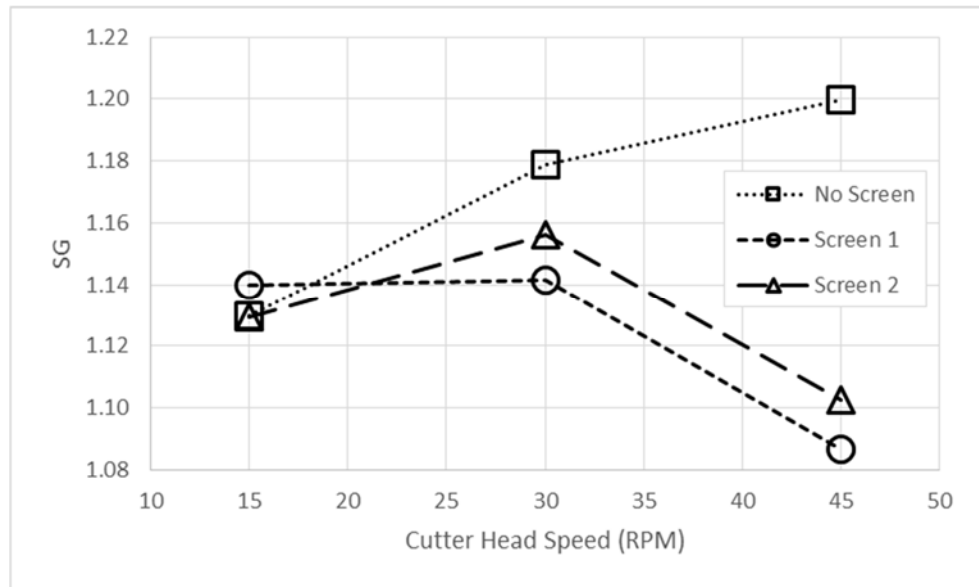


Figure 23: Maximum specific gravity observations at different cutter head speeds.

Figure 23 shows that for Screen 1 and Screen 2, the maximum SG readings increased between cutter speeds of 15 to 30 rpm and decreased at cutter speeds greater than 30 rpm. The value at 30 rpm represents a balance between cutter head speed, flow rate, and swing speed, producing a maximum specific gravity reading. However, at the highest cutter head speed of 45 rpm, the spillage created by high centrifugal forces reduced the maximum specific gravity measured during each test. Additionally, the rate of excavation of material was limited by the constant swing speed of 1.5 in/s (3.81 cm/s). If the swing speed were increased for the points at 45 rpm in Figure 23, the specific gravity would have also increased. This is proven in the Screen 2 test that was run at a swing speed of 3 in/s (7.62 cm/s) and cutter head speed of 45 rpm, which produced an overall experiment maximum specific gravity reading of 1.23.

The Influence of Swing Speed on Specific Gravity

A consistent and positive relationship was observed between the maximum specific gravity achieved during a test run and the ladder arm swing speed. Since the maximum SG occurred at the lowest flow rate, maximum SG observations during the 250 GPM tests were plotted in Figure 24 against their corresponding swing speed.

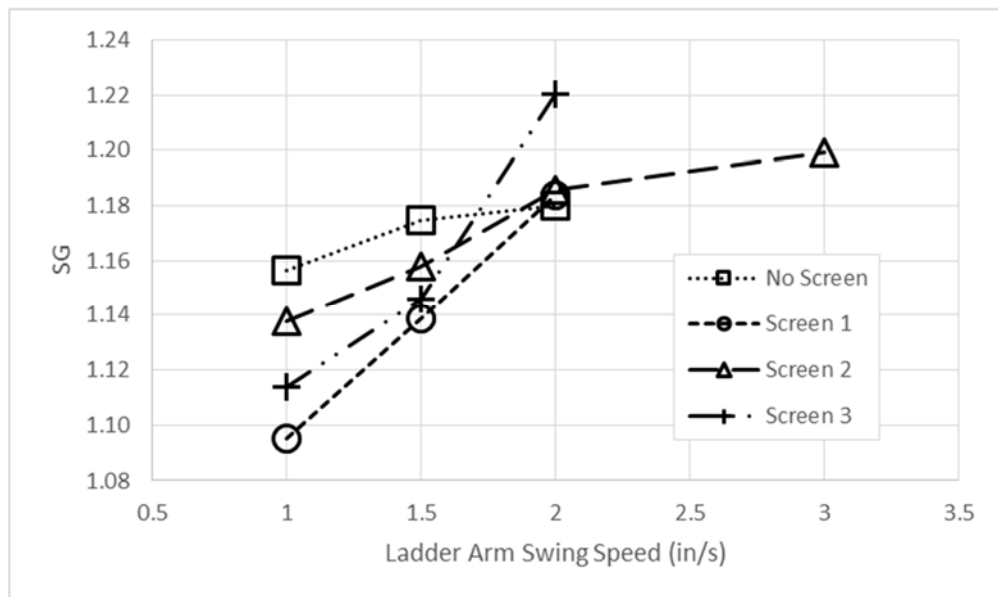


Figure 24: Maximum specific gravity observations at different ladder arm swing speeds.

The positive trend between maximum SG and swing speed was consistent across every screen, and the maximum SG of 1.22 occurred with Screen 3 at 2 in/s (5.08 cm/s). This reading was even greater than the one observed with Screen 2 at 3 in/s (7.62 cm/s) due to the increased opening size (β) of Screen 3 versus Screen 2, despite the slower swing speed. Overall, the Screen 0 configuration had the highest average maximum

specific gravity across the different swing speeds because there was no screen present to hinder the flow of sand into the suction mouth.

It is deduced from qualitative analysis of Figure 23 and Figure 24 that the maximum specific gravity achievable in a given model or prototype dredge configuration is a function of: flow rate, screen configuration, cutter head rpm, and ladder arm swing speed. If the greatest SG reading were sought, one would minimize the flow rate (close to critical flow rate), maximize screen openings (i.e. do not put on a screen), and maximize the balance between swing speed and cutter head speed.

DATA ANALYSIS

Procedure for Calculations

All the information required to analyze minor losses across fixed sediment screens was in the suction section of the system and is shown in Figure 25.

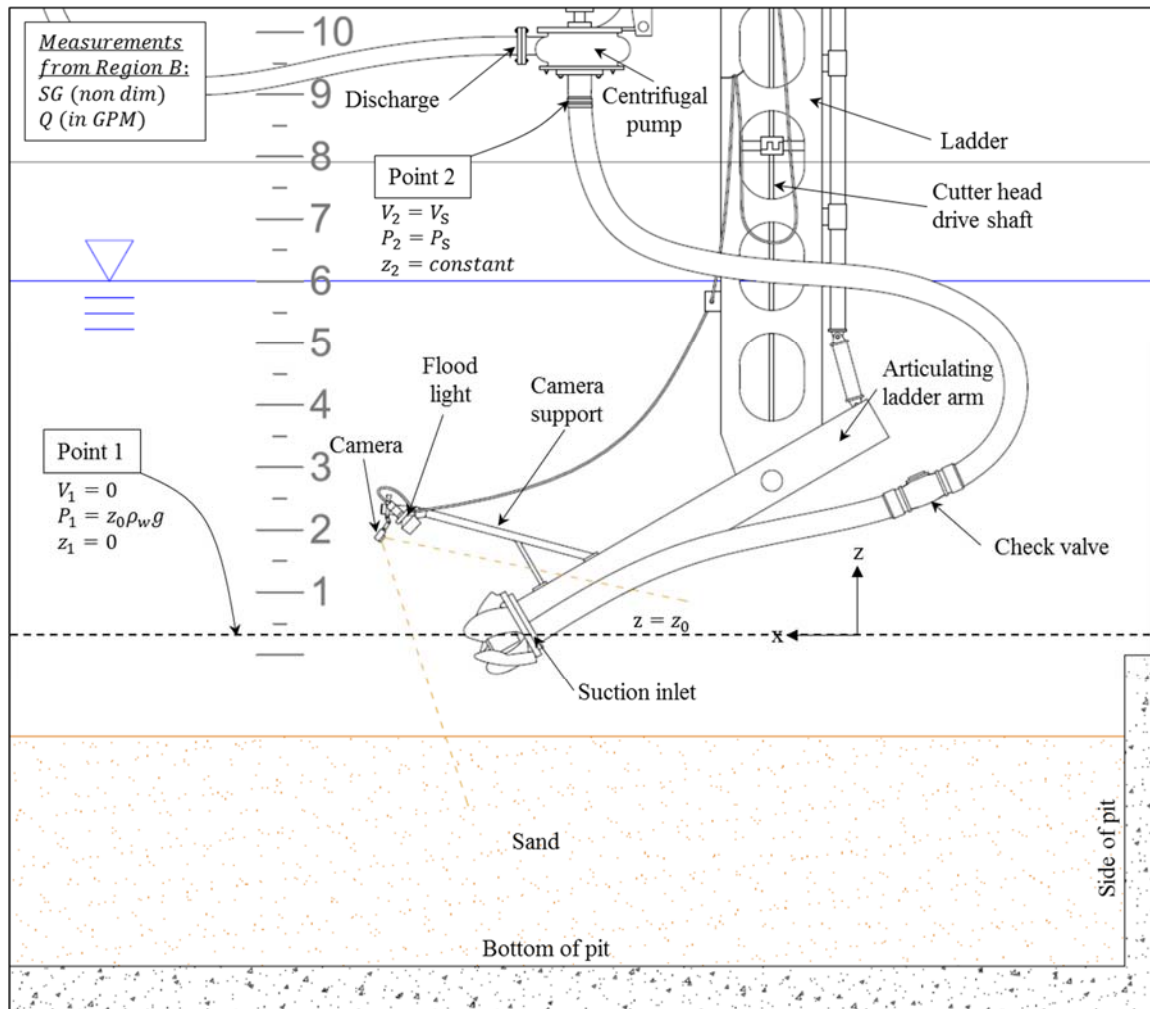


Figure 25: Suction side evaluation of model dredge system using the modified Bernoulli equation.

The method for evaluating suction entrance head loss and fixed screen k-values was similar to the method outlined in Equation (1) and Figure 1; however, the evaluation at Point 2 was different. Point 2 was taken at the location of the centrifugal pump suction pressure gauge. This allowed for direct pressure measurements in the system without requiring pump power (h_p) calculations. Point 1 remained the same: at a still point in the water at the dredging depth.

In general, minor loss coefficients are expressed relative to a baseline state of the system. In this experiment, all k-values of sediment screens were based on the Screen 0 configuration (no screen/open suction intake). Using Equation (1), the k-values of Screen 1 and 2 were calculated by first determining the difference in head loss between a “screen off” test and a “screen on” test. As an example, the additional head loss caused by Screen “n” was calculated via the following process:

First, Equation (1) was evaluated at two conditions: Screen 0 and Screen “n”, yielding Equations (28) and (29), respectively.

$$\frac{P_{10}}{\gamma} = \frac{P_{S0}}{\gamma} + \frac{V_{20}^2}{2g} + z_2 + h_{L0} \quad (28)$$

$$\frac{P_{1n}}{\gamma} = \frac{P_{Sn}}{\gamma} + \frac{V_{2n}^2}{2g} + z_2 + h_{Ln} \quad (29)$$

where, the values P_{10} and V_{2n} indicate “the pressure at Point 1 with Screen 0 in place” and “the slurry velocity at Point 2 with Screen ‘n’ in place,” respectively.

Evaluating the difference between Equations (28) and (29), substituting Equation (11), and rearranging yielded Equation (30):

$$\Delta h_{Ln} = \frac{(P_{Sn} - P_{S0})}{SG \cdot \gamma_w} - \frac{(P_{1n} - P_{10})}{SG \cdot \gamma_w} + \frac{(V_{2n}^2 - V_{20}^2)}{2g} \quad (30)$$

where Δh_{Ln} is the additional head loss caused by Screen “n.” The specific gravities measured in the Screen 0 test and Screen “n” test were matched via data processing and selection in order for this equation to hold true.

Although h_L generally contains terms for both frictional head loss and minor head loss, the frictional terms from Screen 0 tests to Screen “n” tests canceled each other out when calculating Δh_{Ln} (as long as specific gravity remained matched), leaving only the change in head loss due to the addition of Screen “n.” Rearranging Equation (3) using Δh_{Ln} resulted in a solution for k_n (the minor loss coefficient of Screen “n”) using Equation (31).

$$k_n = \Delta h_{Ln} \frac{2g}{V_S^2} \quad (31)$$

UNCERTAINTY ANALYSIS

To comprehensively evaluate the uncertainty of the calculated k_n values, the method presented by Kline and McClintock (1953) and summarized by Holman and Gajda (1989) was used because of its precision and application to experimental results. They proposed that the experimental uncertainty of a calculated, dependent variable is determined when all the uncertainties in the dependent variables are known. This is described by Equation (32)

$$w_R = \left[\left(\frac{\partial R}{\partial x_1} w_1 \right)^2 + \left(\frac{\partial R}{\partial x_2} w_2 \right)^2 + \cdots + \left(\frac{\partial R}{\partial x_n} w_n \right)^2 \right]^{1/2} \quad (32)$$

where R is the dependent variable, w_R is its calculated uncertainty, x_n is an independent variable, and w_n is its uncertainty (expressed as a percentage). In order to apply Equation (32) to the calculations in this thesis, k_n must first be expressed as a function of independent, measured variables; therefore, Equations (30) and (31) were combined, re-arranged, and restated in the form of: $k_n = f(SG, V_s, P_s, \Delta P_1, \Delta V_2)$, as Equation (33).

$$k_n = \frac{1}{V_s^2} \left[\frac{2g}{\gamma_w SG} (\Delta P_{sn} - \Delta P_{1n}) + \Delta(V_{2n}^2) \right] \quad (33)$$

The changes in some variables were re-stated as ΔP_{sn} , ΔP_{1n} , and $\Delta(V_{2n}^2)$ – defined by Equations (34), (35), and (36), respectively – in order to minimize the number of independent variables in subsequent calculations.

$$\Delta P_{sn} = P_{Sn} - P_{S0} \quad (34)$$

$$\Delta P_{1n} = P_{1n} - P_{10} \quad (35)$$

$$\Delta(V_{2n}^2) = V_{2n}^2 - V_{20}^2 \quad (36)$$

Next, experimental variables were substituted into Equation (32) and it was re-written as Equation (37).

$$w_{k_n} = \left[\left(\frac{\partial k_n}{\partial SG} w_{SG} \right)^2 + \left(\frac{\partial k_n}{\partial V_s} w_{V_s} \right)^2 + \left(\frac{\partial k_n}{\partial \Delta P_{sn}} w_{\Delta P_{sn}} \right)^2 + \left(\frac{\partial k_n}{\partial \Delta P_{1n}} w_{\Delta P_{1n}} \right)^2 + \left(\frac{\partial k_n}{\partial \Delta V_{2n}} w_{\Delta(V_{2n}^2)} \right)^2 \right]^{1/2} \quad (37)$$

In order to evaluate Equation (37), the uncertainties of each of the independent variables must be known. In some cases, that is simply the inherent uncertainty in the sensor or gauge itself; but, in others, the overall uncertainty must be calculated. First, the uncertainty in the specific gravity measurement (w_{SG}) is the uncertainty in the gauge itself: 0.71%. The uncertainty in the suction velocity measurement (w_{V_s}) is correlated with the flow rate measurement. The flow meter displays units of GPM and has an uncertainty of 0.3%. The suction velocity differs from the flow rate only by the division of constant factor, the cross-sectional area of the Goodyear Plicord® Con-Ag suction and discharge pipe, which has its own uncertainty based on the inside pipe diameter. The Goodyear pipe specifications do not indicate any error in the pipe's inside diameter measurement, which is listed as 101.6 mm or 4 in (Goodyear Rubber Products Inc., 2010). In the absence of a stated uncertainty, it is assumed that the only viable uncertainty is that of measurement error, which is estimated at the incremental value of the smallest significant figure. In this case, the measurement uncertainty of the inside diameter is 0.1 mm, or 0.098% for the suction pipe, which corresponds to a possible 0.2% error in the cross-sectional area of the pipe. When this uncertainty is considered in

the conversion from GPM to ft/s, the maximum possible uncertainty in the suction velocity measurement is 0.5%.

Next, the value for ΔP_{sn} must be considered. Because the inherent sensor uncertainty in the pressure transmitter is 0.25%, the greatest possible uncertainty when calculating ΔP_{sn} is simply twice that, or 0.50%. The pressure measurements at Point 1 (P_{1n}) are hydrostatic pressure calculations using the depth from Equation (27). Since the uncertainty in the z-direction distance meter is 0.1%, the uncertainty in ΔP_{1n} is twice that, or 0.2%.

Next, the uncertainty in $\Delta(V_{2n}^2)$ was considered, so Equation (36) was evaluated for its own uncertainty (at the sub-level) on a common sense basis. Since the velocity at Point 2 (V_{2n}) was calculated in exactly the same manner as the suction velocity (V_S), the uncertainty for both V_{2n} and V_{20} was 0.5%. Applying the 0.5% uncertainty to each of the variables in Equation (36) resulted in a maximum uncertainty of 0.98% in each of the squared velocities. Further, applying the new uncertainty to Equation (36) resulted in a maximum uncertainty in $\Delta(V_{2n}^2)$ of 1.96%. All the maximum uncertainty values are summarized in Table 5.

Table 5: Uncertainties of independent variables.

	Maximum Uncertainty
w_{SG}	0.71%
w_{V_s}	0.30%
$w_{\Delta P_s}$	0.50%
$w_{\Delta P_1}$	0.20%
$w_{\Delta(V_{2n}^2)}$	1.96%

The next step in evaluating Equation (37) was to find the partial derivatives of Equation (33). These are shown as Equations (38), (39), (40), (41), and (42).

$$\frac{\partial k_n}{\partial SG} = -\frac{1}{SG^2} \frac{2g}{\gamma_w V_s^2} (\Delta P_{sn} - \Delta P_{1n}) \quad (38)$$

$$\frac{\partial k_n}{\partial V_s} = -\frac{2}{V_s^3} \left[\frac{2g}{\gamma_w SG} (\Delta P_{sn} - \Delta P_{1n}) + \Delta(V_{2n}^2) \right] \quad (39)$$

$$\frac{\partial k_n}{\partial \Delta P_{sn}} = \frac{2g}{V_s^2 \gamma_w SG} \quad (40)$$

$$\frac{\partial k_n}{\partial \Delta P_{1n}} = -\frac{2g}{V_s^2 \gamma_w SG} \quad (41)$$

$$\frac{\partial k_n}{\partial \Delta(V_{2n}^2)} = \frac{1}{V_s^2} \quad (42)$$

Finally, the total uncertainty in the k value was considered for each test run by substituting all the uncertainties and partial derivatives into Equation (37). The maximum and minimum k-value uncertainties for all tests runs were 0.066% and 0.019%, respectively. When the maximum uncertainty was applied to the maximum calculated k-value of 7.26, the maximum absolute error in k-value was 0.005.

Further analysis of each term in Equation (37) showed that most of the uncertainty arose from the $\Delta(V_{2n}^2)$ term, which was due to the effect of squaring V_2 . The next largest source of uncertainty was due to the specific gravity measurement. This source of uncertainty was due to the relatively large value of w_{SG} (compared to other sensors' uncertainties) and the previously discussed correlation between specific gravity and minor loss coefficient. The contributions of the remaining independent variables to w_{k_n} were one order of magnitude less than those of SG and $\Delta(V_{2n}^2)$.

EVALUATION OF TESTS WITH VARYING CUTTER HEAD SPEED

Cutter Head Speed and k-Value for Water Tests

Some trends are observed from the plots of minor loss coefficient versus cutter head speed. The relationship between cutter head rpm and k-value must first be examined. Since repeat tests of each configuration of dredge parameters were not possible due to limited laboratory resources and time, there exists only one data point for each configuration. The spread of data across the different cutter head speeds is very small compared to the overall range of values collected, and no definitive trends between k-value and cutter head speed were found. However, qualitative observations using average k-values across all flow rates are useful.

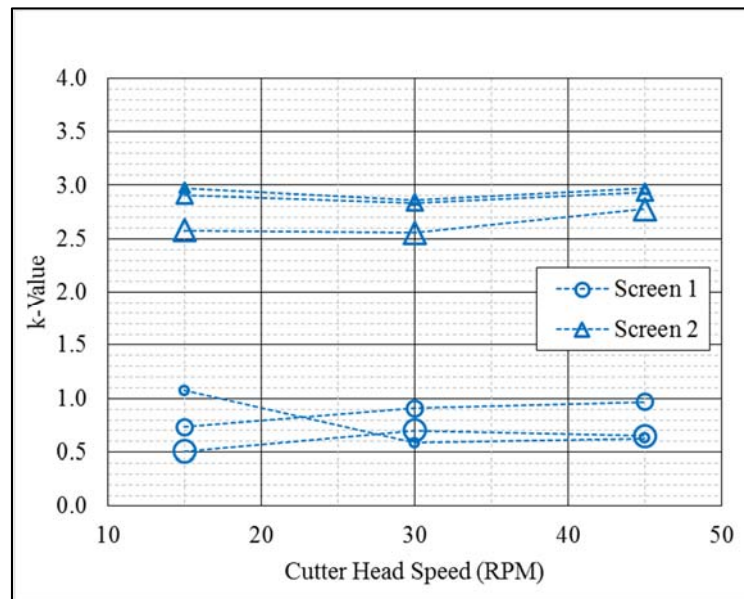


Figure 26: Minor loss coefficient variation due to cutter head speeds during water tests. Symbol sizes (small to large) indicate nominal flow rates of 250, 325, and 400 GPM, respectively.

The data for Screen 1 in Figure 26 show little trend in average k-values with cutter speed across all the flow rates. However, if the values at 15 rpm (considered outliers) are removed, a slight positive k-value trend with increasing cutter head speed becomes apparent. At each flow rate, the total spread in k-values across each of the cutter speeds is very small – roughly 0.2 to 0.3 – so for this reason, a quantitative relationship between k-value and cutter head rpm was not attempted.

Flow Rate and k-Value for Water Tests Varying Cutter Head Speed

Next, the water-only test cases for Screens 1 and 2 (shown in Figure 27) are examined. The first visible trend is that k-value, in general, decreases linearly with flow rate. This trend disagrees with the positive correlation between flow rate and k-value at low specific gravities found by Girani (2014). The differences between the two sets of research were screen type and opening area.

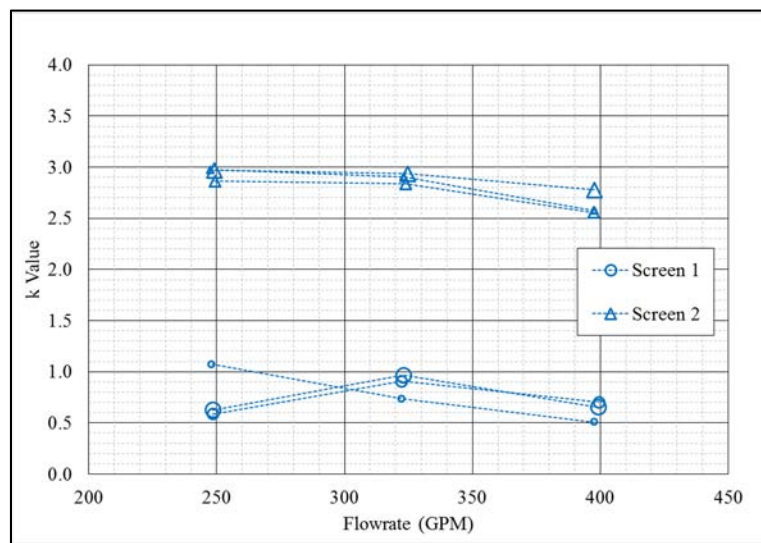


Figure 27: Minor loss coefficient variation due to flow rate during water tests. Symbol sizes (small to large) indicate cutter head speeds of 15, 30, and 45 rpm, respectively.

However, the results of this research show the negative correlation between k-value and flow rate (during water-only tests) across all three screens tested, indicating it was not merely an anomaly characteristic of one screen type. This relationship will later be quantified and expressed in an equation to predict k-value based on β and flow rate.

Cutter Head Speed and k-Value for Sand Tests

According to the data, the k-value of each screen is more sensitive to changes in cutter head speed at low flow rates; while at higher flow rates, the suction velocity dominates the flow field, eclipsing the influence of the cutter head speed. This phenomenon is concurrent with the flow field observations of Steinbusch, et al. (1999) described in the Background section. For Screen 1, the spread of k-values at each flow rate is relatively small, while for Screen 2, the spread is very large (reaching 55% of the total range of k-values).

The large spread brings up the possibility of artificially inflated k-values due to clogging of the screen. Figure 11 showed that Screen 2 had relatively large, flat areas which allowed sand to build up and increase the minor losses. Clogging was not visually observed because of the inability to see the screen on video recordings while at the cutting depth; however, the research of Girani (2014) captured the phenomenon on video and avoided it by temporarily reversing the flow direction in the suction pipe between test runs.

The first iteration of data analysis showed that Tests 213, 214, and 215 were very significant outliers (indicating the screen was clogged). The data from those tests were

disregarded and the tests were re-run on Day 6 and are now circled with a blue-dotted line in Figure 28.

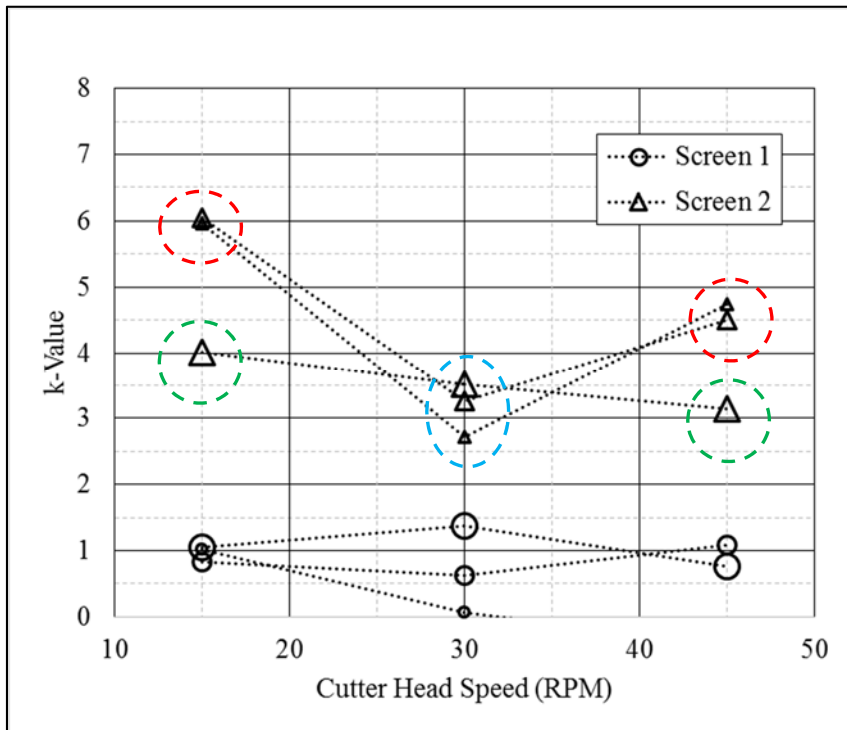


Figure 28: Minor loss coefficient variation due to cutter head speed during sand tests. Symbol sizes (small to large) indicate nominal flow rates of 250, 325, and 400 GPM, respectively.

The two data points circled in green in Figure 28 were the first two slurry tests completed on the afternoon of Day 4 and do not show any signs of screen clogging. For Screen 2, the data show that only two consecutive test runs were accomplished before clogging took place. The remaining four tests (circled in red in Figure 28) experienced clogging, contributing to k-values (i.e. above 4.0) at 15 and 45 rpm. If the remaining Screen 2 tests were re-run while ensuring no clogging was occurring, the author can only

speculate that a tighter spread and clearer relationship between k-value and cutter head speed would be observed.

Flow Rate on k-Value for Sand Tests Varying Cutter Head Speed

The sand tests did not consistently show the same trend as the water tests of decreased k-value with increased flow rate; Screen 1 had an average increase in k-value with flow rate, while Screen 2 had an average decrease, as shown in Figure 29.

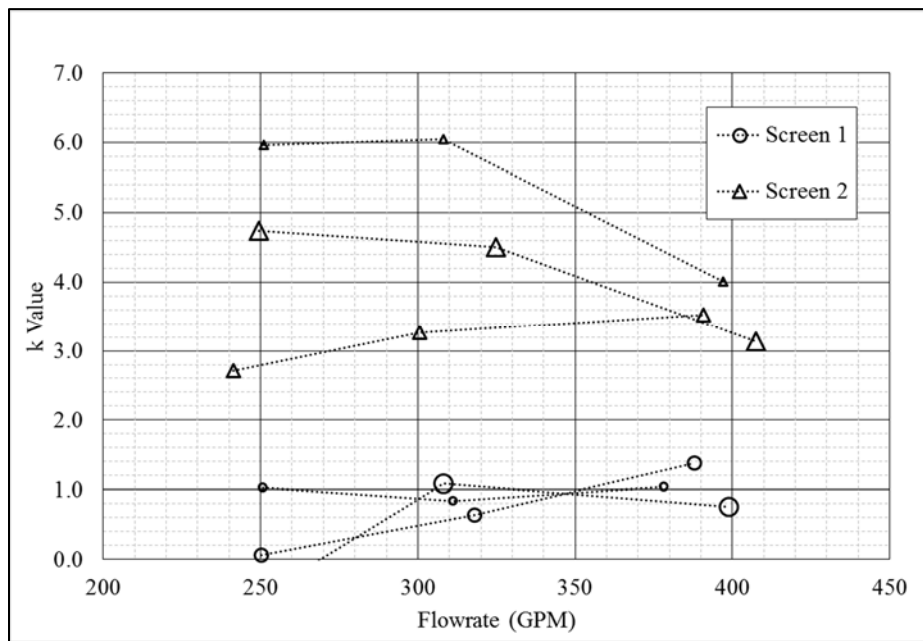


Figure 29: Minor loss coefficient variation due to flow rate during sand tests. Symbol sizes (small to large) indicate cutter head speeds of 15, 30, and 45 rpm, respectively.

This inconsistent relationship between flow rate and minor loss coefficient was also seen in the research of Girani (2014) as the specific gravity of the slurry increased. A more interesting phenomenon consistent with the prediction equation curves proposed by

Girani (2014) was the convergence of the k-values at higher flow rates. In other words, the spread of k-values across different cutter head speeds decreased with flow rate, effectively converging the k-values to near 1.0 and 3.5 for Screen 1 and Screen 2, respectively. If the outlier points shown in Figure 28 were re-run, it is expected that the k-values in Figure 29 would follow a positive relationship with flow rate. This contrasts the flow rate-dependent k-value relationship previously identified in the water tests, indicating that the presence of sand in the suction entrance changes how flow rate affects k-value. However, sufficient evidence is not available in this research to make that determination.

EVALUATION OF TESTS WITH VARYING SWING SPEED

Swing Speed and k-Value for Water Tests

Figure 30 shows very little correlation between swing speed (V_L) and the suction inlet minor loss coefficient (k).

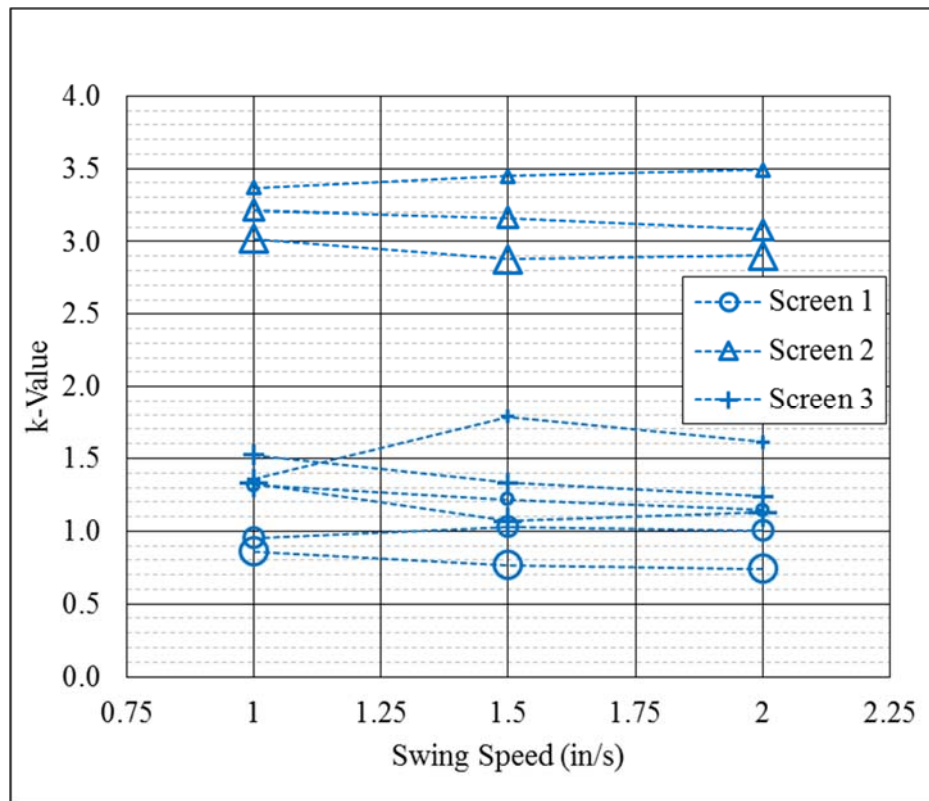


Figure 30: Minor loss coefficient variation due to ladder arm swing speed during water tests. Symbol sizes (small to large) indicate nominal flow rates of 250, 325, and 400 GPM, respectively.

This research has already shown that specific gravity increases with increasing swing speed during sand tests; however, when there was no sand present, it was observed that swing speed, on its own, did not have a significant effect on the k-value.

This phenomenon (or lack thereof) is explained by the scales of the velocity fields involved. The swing speeds themselves correspond to relatively low velocities of 0.083 to 0.166 ft/s (0.025 to 0.076 m/s), while the flow rate produced velocities in the range of 5.68 to 10.43 ft/s (1.73 to 3.18 m/s). This difference of 1 to 2 orders of magnitude ensured that the suction velocity caused by the flow overwhelmed any minor contributions from the swing speed.

Flow Rate and k-Value for Water Tests Varying Swing Speed

Similar to the analysis of previous tests, the k-value linearly decreased with flow rate across the three tested swing speeds, as shown in Figure 30.

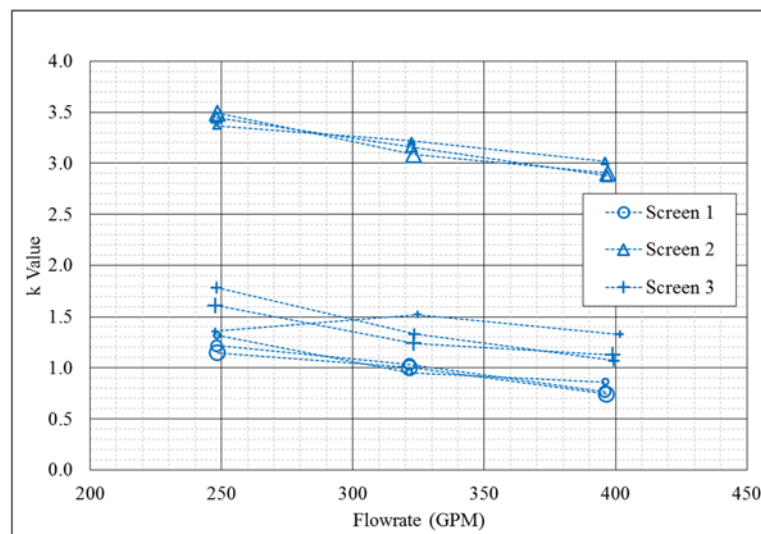


Figure 31: Minor loss coefficient variation due to flow rate during water tests. Symbol sizes (small to large) indicate ladder arm swing speeds of 1, 1.5, and 2 in/s, respectively.

This linear decrease had a relatively constant slope and was similar across all three screen configurations. The calculated spread of k-values across the flow rates ranged from 0.4 to 0.7 and is quantified later in a k-value prediction equation.

Swing Speed and k-Value for Sand Tests

Despite the swing speed showing a good relationship with the maximum achievable SG in a given test run, Figure 32 shows that it did not have a significant correlation with k-value.

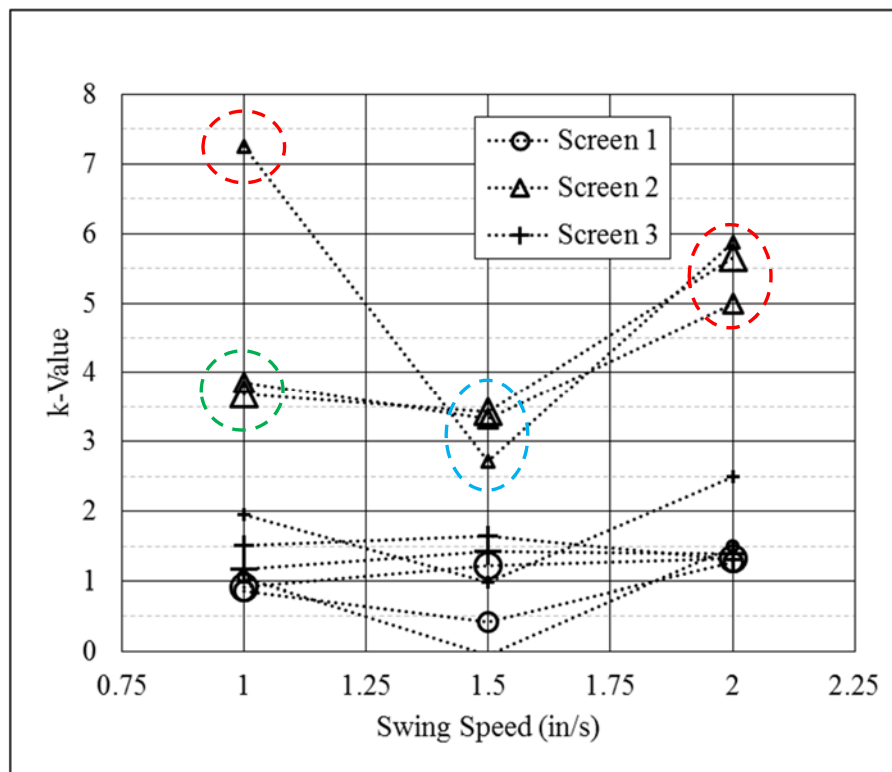


Figure 32: Minor loss coefficient variation due to ladder arm swing speed during sand tests. Symbol sizes (small to large) indicate nominal flow rates of 250, 325, and 400 GPM, respectively.

This is somewhat surprising, since k -value has been shown to increase with specific gravity (Girani, 2014) and in this experiment, it has additionally been shown to increase with swing speed. It logically follows that the k -value would increase with swing speed, albeit through an indirect relationship with specific gravity. Figure 32 shows that the k -value had neither a significant increase nor decrease with swing speed. Not enough good data points were available to establish a prediction equation correlating V_L and k ; therefore, qualitative discussion is the limit of this analysis.

The Screen 2 data in Figure 32 has outliers (circled in a red-dotted line) similar to those found in Figure 28 due to clogging of the screen causing inflated k -values. According to Table A - 6, the first two sand tests on Day 5 of testing were the data points circled in a green dotted line in Figure 32. These two points were considered unaffected by clogging, while the four outliers (circled in a red-dotted line) were completed after the first two good tests. Lastly, the three data points circled in blue represent the original outliers which were re-run on Day 6, resulting in what is considered good data.

The Screen 2 tests in Figure 32 showed that only two consecutive test runs could be completed without screen clogging. The clogging occurred on Screen 2 due to the small β value, large ratio of grain size to dimensional opening area, and the flat screen surfaces upon which sand built up. Because of the outliers, it is impossible to identify any relationship between V_L and k when Screen 2 is in place. It is also difficult to find any consistent pattern in the Screen 1 and Screen 3 data.

Flow Rate and k-Value for Sand Tests Varying Swing Speed

Across the board, the greatest measured specific gravity observed during a test run occurred at the lowest flow rate and the greatest swing speed, which is a possible explanation for the increased minor loss coefficient at low flow rates. However, the clogging effects that occurred in Screen 2 are another explanation and are indicated by k-values greater than 4.0 in Figure 33.

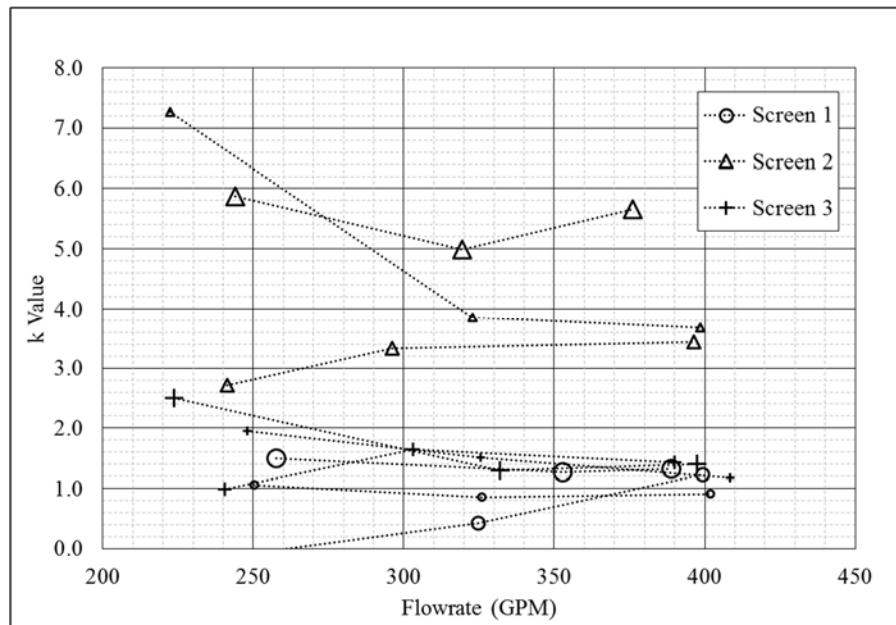


Figure 33: Minor loss coefficient variation due to flow rate during sand tests. Symbol sizes (small to large) indicate ladder arm swing speeds of 1, 1.5, and 2 in/s, respectively.

On average, an increase in k-value with flow rate was observed in the Screen 1 data points and the “good” Screen 2 data points; while the average k-values for Screen 3 decreased with flow rate. In the same manner as the tests with changing cutter speed, the k-values in Figure 33 converged to a single value (approximately 1.2 for Screens 1 and 3

and 3.5 for Screen 2) at the highest tested flow rate. Since it was previously shown that swing speed, on its own, did not change k-value, this convergence is attributed to the balance between the flow dominated by the cutter head rotation and the suction velocity flow field, which was previously discussed. More data is required at a wider range of flow rates, larger swing speeds, steadier specific gravity, and a more careful avoidance of screen clogging in order to effectively describe their influence on k-value.

SCREEN OPENING SHAPE AND K-VALUE

In order to test the effect of screen opening shape on k-value, Screens 1 and 3 were constructed with the same β value, but differently shaped openings. Screen 1 openings were shaped like vertically oriented rectangles and Screen 3 openings were shaped by following the curved contours of the suction mouth. It was anticipated that Screen 3 would have a smaller k-value by more effectively funneling the water or slurry into the suction mouth because of the radial component of its curved openings. However, Figure 34 shows that the average k-value of Screen 3 was greater than that of Screen 1, despite their β values being practically equal.

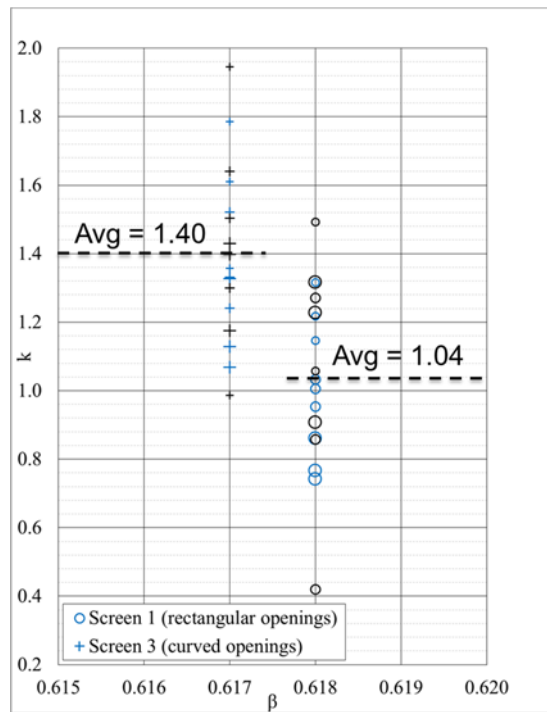


Figure 34: Comparison of k-values between Screen 1 and Screen 3 (blue and black markers indicate water and sand tests, respectively). Symbol sizes (small to large) indicate nominal flow rates of 250, 325, and 400 GPM, respectively.

Since Screen 3 was only tested with varying swing speeds, Figure 34 plots those data points against the swing-speed-varying tests of Screen 1.

It is possible that Screen 3 has a greater average k-value than Screen 1 due to the additional flat, welded surfaces on Screen 3 (shown in Figure 11) which were added to match its β value to Screen 1. As shown in the analysis of Screen 2, the presence of flat surfaces perpendicular to the direction of flow increases the screen's propensity to clog. Conversely, the increased k-value could be an indication of a more energy-intensive flow velocity field through the openings in Screen 3. Future research to more accurately determine the correlation between screen opening shape and k-value should ensure that the so-called flat surfaces on the face of the screen are decreased as much as possible so that screen-clogging effects are minimized. Additionally, computational methods could be used to model the flow fields through each screen to determine the source of the increased minor loss.

SCREEN OPENING AREA RATIO AND K-VALUE

Fixed Screen Minor Loss Prediction for Water Tests

The primary intent of testing Screen 1 and Screen 2 was to quantify the effects of screen opening area ratio (β) on the minor loss coefficient and establish a k-value prediction equation for new screen designs or configurations. As previously discussed, the average k-values of Screen 1 and Screen 2 show an inverse correlation with flow rate, which was quantified because of its fairly constant slope. Additionally, all the k-values for Screen 2 were greater than those of Screen 1, indicating an inverse correlation with β , as shown in Figure 34.

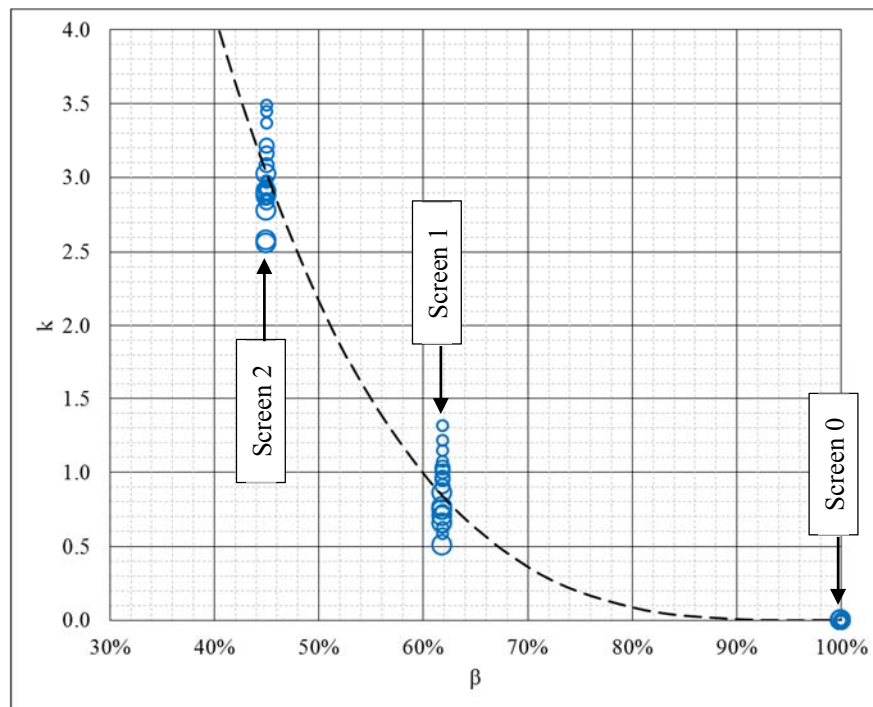


Figure 35: Effect of screen opening on fixed screen minor loss coefficients for water tests.

Figure 34 shows all calculated k-values for water tests (varying both cutter head speed and swing speed) against the β -value of the installed screen and has a curve fitted through the median value of the data points for each screen. The curve was fitted manually and is expressed by Equation (43),

$$k(\beta) = a(1 - \beta)^b \quad (43)$$

where "a" defines the vertical scale of the curve and "b" defines its shape. For the water-only tests shown in Figure 35, $a = 24.5$ and $b = 3.5$.

However, Equation (43) still does not account for the influence of flow rate on k-value. In order to account for that, the data shown in Figure 35 was evaluated for the spread across the three nominal flow rates. First, for a flow-rate-dependent k-value relationship to be general, the flow rates should be made non-dimensional so they can apply in a variety of situations. The flow rate values were non-dimensionalized in the same manner used by Girani (2014): dividing the suction flow velocity by the critical velocity (i.e. the velocity at which sedimentation occurs in a horizontal pipeline). For this research, the critical velocity (V_c), in the suction pipe was used, which is 6.15 ft/s (1.88 m/s). The non-dimensional velocity (\hat{V}), is, therefore, defined by Equation (44),

$$\hat{V} = \frac{V}{V_c} \quad (44)$$

where the three nominal flow rates of 250 GPM (946 l/min), 325 GPM (1230 l/min), and 400 GPM (1514 l/min) correspond to non-dimensional velocities of 1.04, 1.35, and 1.66, respectively.

The k-value spread of data points across the three non-dimensional velocities is quantified for each screen in Figure 36 and a linear relationship is formulated. Because the k-value was not found to be correlated with cutter head speed or swing speed, the highest and lowest k-values in Figure 36 are assumed to correspond to non-dimensional velocities of 1.04 and 1.66, respectively, using a linear flow rate and k-value relationship.

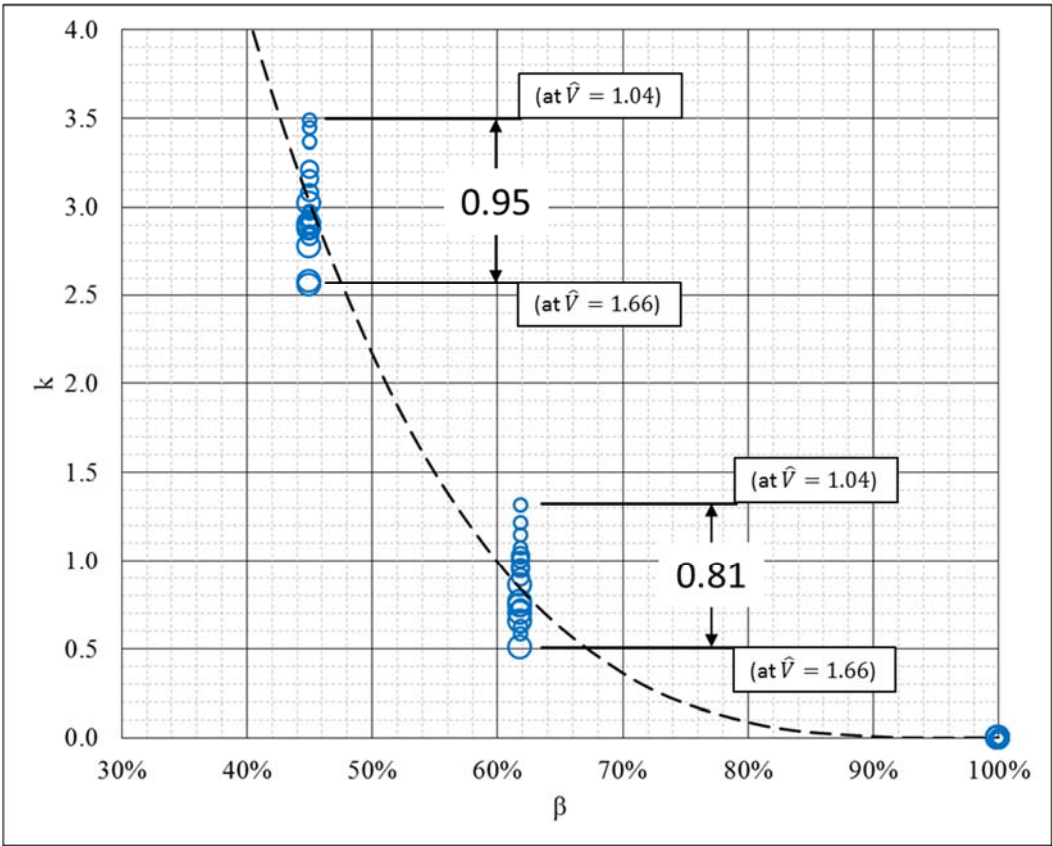


Figure 36: Analysis of k-value spread according to non-dimensional flow rate.

To account for the velocity-induced spread of data points at each screen configuration, a correction term must be added to Equation (43). The average of the two spread values in Figure 36, which is 0.88, must be scaled according to suction velocity. The proposed suction velocity correction term is shown as Equation (45), with explanations of values.

$$\begin{array}{c}
 \text{Average k-value spread} \\
 \text{induced by flow velocity} \\
 \swarrow \\
 \text{Median value for } \hat{V} \\
 \swarrow \\
 \text{Suction Velocity Correction Term} = 0.88 \left(\frac{1.35 - \hat{Q}}{0.62} \right) \quad (45) \\
 \nearrow \\
 \hat{V} \text{ spread across} \\
 \text{tested flow rates}
 \end{array}$$

Next, to account for the slight decrease in k-value spread at greater β values, the suction velocity correction term was multiplied by a scaling term. Through an iterative process, the best fitted scale term was found and is shown as Equation (46).

$$\text{Spread Scaling Term} = \left(\frac{c}{\beta} \right)^n \quad (46)$$

where c is a constant and n is a shaping value. The best fit for the water tests corresponds to $c = 0.66$ and $n = \frac{1}{3}$. Finally, combining Equations (43), (45), and (46) and simplifying results in Equation (47).

$$k(\beta, \hat{V}) = 24.5(1 - \beta)^{3.5} - (1.42\hat{V} - 1.916) \left(\frac{0.66}{\beta} \right)^{1/3} \quad (47)$$

Since Equation (47) uses only non-dimensional arguments, it may be applied to both model- and prototype-scale cutter suction dredging configurations; however, it is

limited to water-only dredging flows. When used as a prediction tool, the k-value should be used as a baseline, as it is expected to increase with any increase in specific gravity. Additionally, the non-dimensional velocity must be calculated using the critical flow velocity in the pipeline. It can also be used to provide a k-value estimate of screens with different opening shapes than those of Screen 1 and Screen 2. Figure 37 shows Equation (47) plotted at the three tested suction velocities and data points from this research. Additionally, three points (at the nominal flow rates) from the $k(SG, \hat{V})$ equation proposed by Girani (2014) are plotted for comparison using a specific gravity of 1.0 and opening area of 0.50.

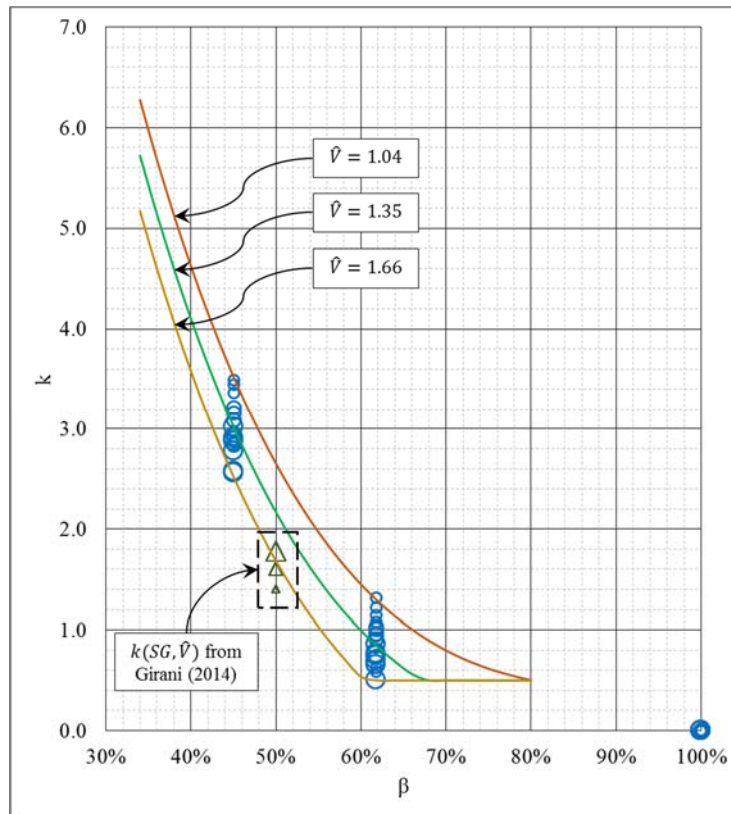


Figure 37: Fixed screen minor loss prediction equation for water-only tests (plotted with experimental data).

The prediction curves corresponding to non-dimensional velocities of 1.35 and 1.66 manually converge to a minor loss coefficient prediction of 0.5 in order to provide an inherent factor of safety and realism in the prediction of k-values for fixed screens. At opening area ratios greater than 0.62, Equation (47) has the possibility of predicting negative k-values, which would be meaningless. In order to prevent those negative predictions, the prediction curves should be visually used – instead of Equation (47) – for extrapolating predictions when the opening area ratio is greater than 0.62. Figure 37 can be interpolated to predict k-values for screens with opening areas from 0.34 to 0.80 and non-dimensional velocities typical of cutter suction dredging.

There are numerous observations to be gleaned from the data presented in Figure 37. First, the Girani (2014) data point at the non-dimensional velocity of 1.66 coincides almost directly with the prediction equation. However, as previously discussed, his equation predicted that k-value scaled up with suction velocity, while Equation (47) predicts the opposite. The median point of the Girani (2014) data lays approximately 0.6 below that of the Equation (47) prediction. This shift is explained by the construction of the screen that was used. The fixed screen used by Girani (2014) was constructed of an expanded metal mesh welded atop a bracket that followed the kidney bean-shaped contour of the suction mouth, while Screens 1 and 2 were constructed using a plasma cutter and 3/16” sheet metal to make large rectangular openings.

It is possible that the Girani (2014) data represents an inherent reduction in k-values due to the shape of the screen openings. However, further investigation into different types and sizes of expanded metal-type screens is required to definitively make

that claim. Figure 34 shows that the average k-value of Screen 3 was 0.3 greater than Screen 1, indicating an upward-shift in the prediction curves in Figure 37. This shift is believed to be representative of the screen shape and construction, but should also be further investigated.

Fixed Screen Minor Loss Prediction for Sand Tests

Since dredging involves the excavation and movement of material, the prediction equation quantifying the relationship between k-value and β when slurry is present is a valuable tool. It has already been established that the data in this thesis cannot provide a quantifiable relationship between k and V_L or k and Ω , which leaves only SG , V , and β as independent variables that affect k . Figure 38 shows the high-value k-value outliers previously identified and, additionally, some low-value outliers whose values do not make sense considering the concentration of most of the data points.

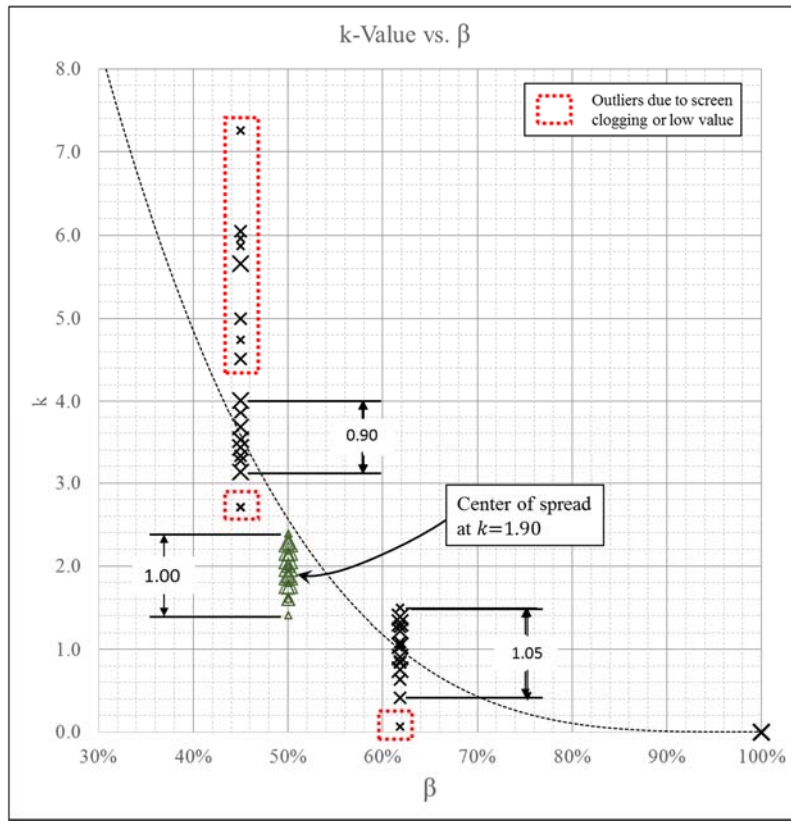


Figure 38: Effect of screen opening on k -value for sand tests. Identification of outliers and evaluation of spread.

Upon removal of the outliers that were caused by screen clogging, the relationship between k and β for sand tests was identified in the same way as the water tests. The plotted curve in Figure 38 was fitted through the good data and is defined by Equation (43), where $a = 29$ and $b = 3.5$, resulting in Equation (48).

$$k(\beta) = 29(1 - \beta)^{3.5} \quad (48)$$

The presence of outliers and the large spread of calculated k -values for sand tests precluded the identification of a consistent relationship between k and V . However, after the removal of outliers, the k -value, if anything, showed a slight increase with flow rate, which would agree with the relationship identified by Girani (2014) for specific gravities

in the range of 1.0 to 1.2; however, sufficient data are not available to quantify that relationship. Additionally, due to model limitations of maximum specific gravity achievable during a test, no data are available to show a relationship between the minor loss coefficient and suction velocity at specific gravities in the range of 1.2 to 1.4. Because of these limitations, Equation (49) from Girani (2014) is used to account for the effects of specific gravity and flow rate,

$$k(V_S, SG) = \frac{2g}{V_S^2} (-0.694 - 0.442 \cdot V_S + 1.302 \cdot SG + 0.0468 \cdot V_S^2 + 0.187 \cdot V_S \cdot SG) \quad (49)$$

where V_S is the suction velocity measured in feet per second. The opening shape of the screen in Girani (2014) was different than that of Screen 1 and Screen 2, causing a downward k-value shift of approximately 0.6. The value of the shift is significant because it is very close to that seen in the water only tests, demonstrating consistency across all tests. Because the two screen shapes cannot be directly compared, it is concluded that only the overall spread of the Girani (2014) data should be used in the k-value prediction equation proposed in this thesis.

To evaluate the spread of the Girani (2014) data, a median value must first be established about which the remaining data converges. Using a velocity range of 6.38 to 10.21 ft/s and specific gravity range of 1.0 to 1.25 (corresponding to the suction flow velocity range at the nominal flow rates and the specific gravity range measured in the Haynes Laboratory model dredge, respectively), the spread of the Girani (2014) data was approximately 1.00 with a central value of 1.90, as shown in Figure 38. This spread value is nearly the same as that of Screen 1 and Screen 2.

To find the distance of each Girani (2014) point from the central value, 1.90 was subtracted from Equation (49), providing the scaling term shown as Equation (50).

$$\text{Spread Scaling Term} = \frac{2g}{V_s^2} \left(\begin{array}{l} -0.694 - 0.442 \cdot V_s + 1.302 \cdot SG \\ + 0.0468 \cdot V_s^2 + 0.187 \cdot V_s \cdot SG \end{array} \right) - 1.90 \quad (50)$$

Combining Equations (48) and (50) resulted in the full, dimensional k-value prediction equation shown as Equation (51).

$$k(\beta, V_s, SG) = 29(1 - \beta)^{3.5} + \frac{2g}{V_s^2} \left(\begin{array}{l} -0.694 - 0.442 \cdot V_s + 1.302 \cdot SG \\ + 0.0468 \cdot V_s^2 + 0.187 \cdot V_s \cdot SG \end{array} \right) - 1.90 \quad (51)$$

where V_s is in feet per second.

Figure 39 shows Equation (51) plotted at the maximum and minimum specific gravity and nominal flow rate values observed during the test runs and matches up accurately with the range of calculated k-values from the experiment. Equation (51) itself cannot be easily non-dimensionalized with respect to suction velocity because of its existing empirical relationship to dimensional values; therefore, it should only be used with the Haynes Laboratory model dredge parameters as inputs.

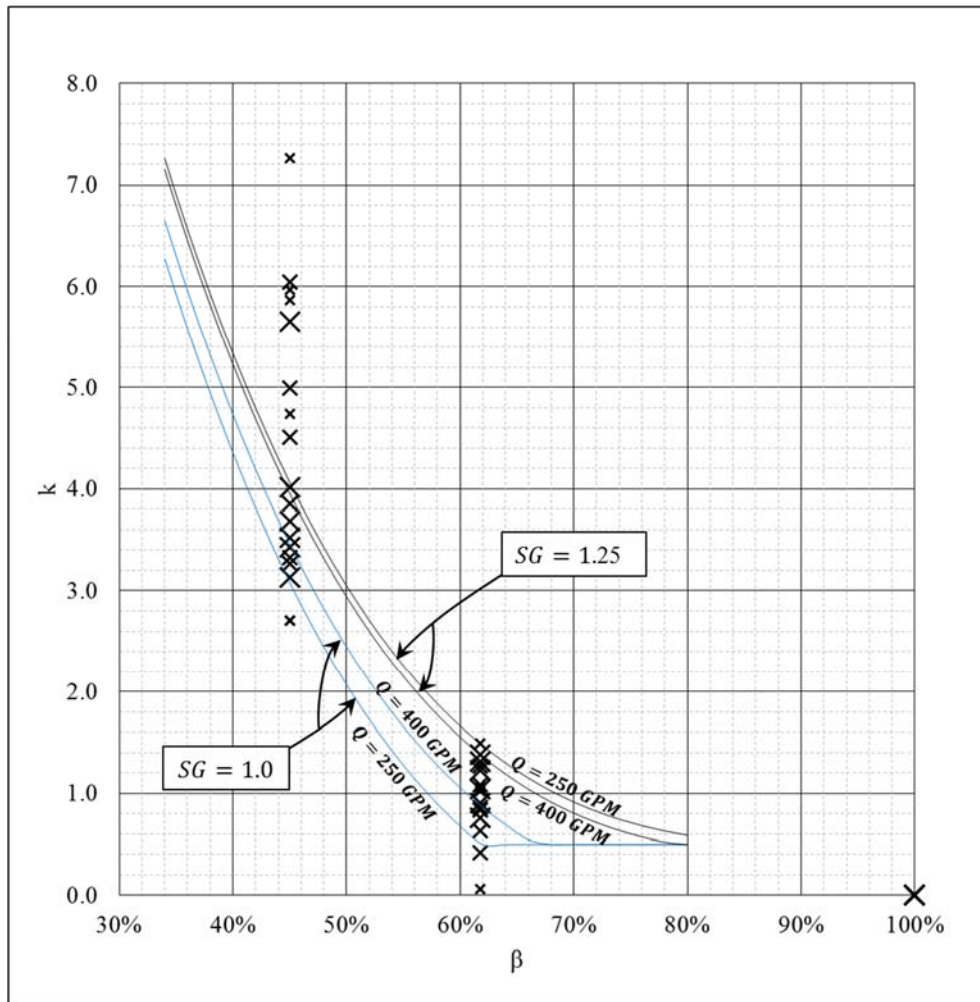


Figure 39: Minor loss prediction equation plotted at the range of flow rate values and specific gravity values observed at the Haynes Laboratory.

However, the resultant plot in Figure 40 uses Equation (51) and is shown with non-dimensional scales, making it applicable to both model and prototype cutter suction dredge configurations. The curves are extrapolated to predict the fixed screen minor loss coefficient using specific gravities up to 1.4 and non-dimensional velocities up to 1.6; they can also be interpolated.

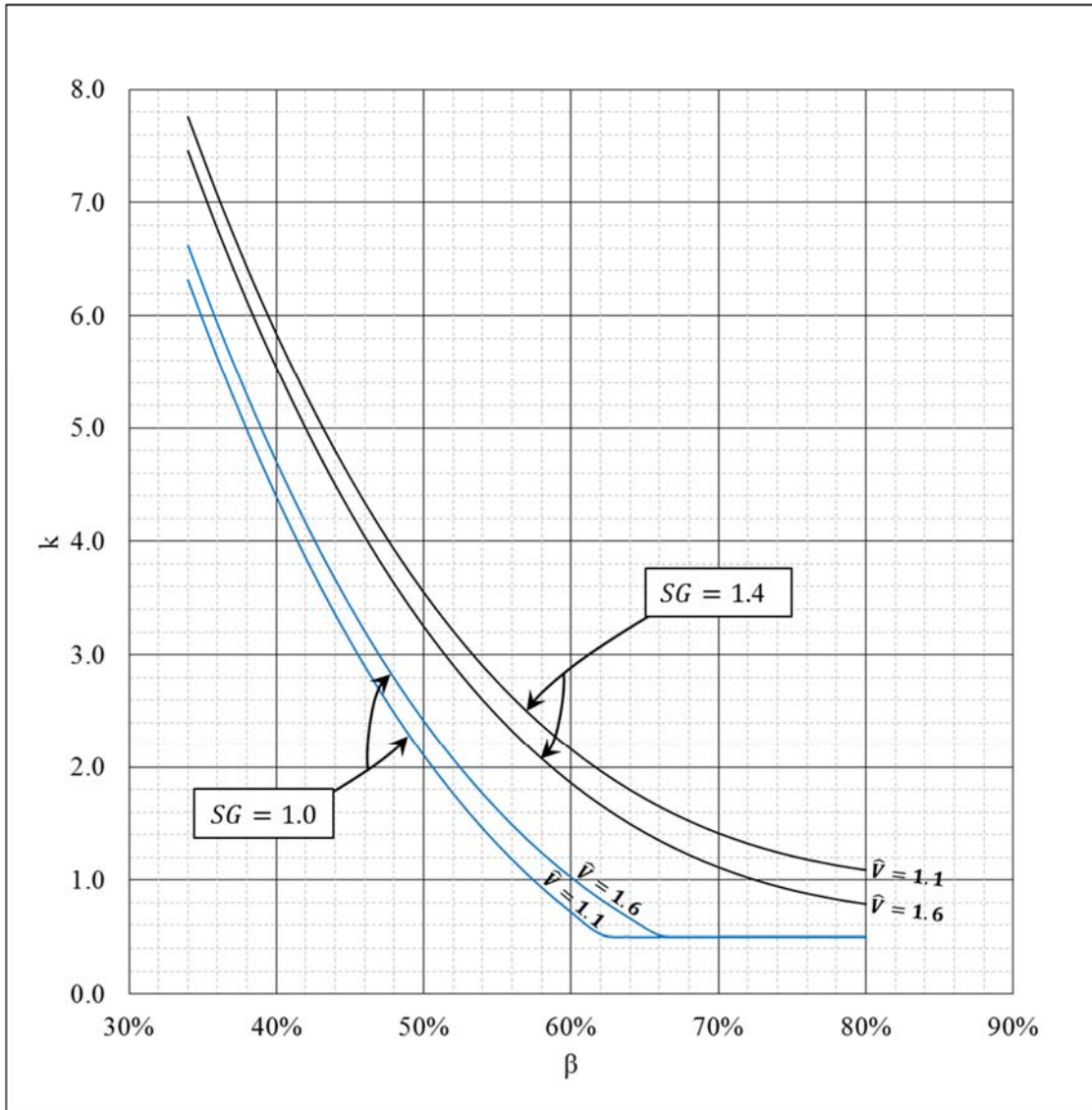


Figure 40: Fixed screen minor loss prediction curves (with slurry present).

Figure 40 can be used for predicting the minor loss coefficient of a fixed screen installed on a prototype dredge using the screen opening sizes, shapes, and operating parameters typically found in cutter suction dredging operations. Although this experiment produced a maximum specific gravity of 1.23, Figure 40 can also be

extrapolated to predict minor loss coefficients at specific gravities of up to 1.4, non-dimensional velocities of up to 2.5, and opening areas from 0.34 to 0.80. Similar to Figure 37, the predicted k-values in Figure 40 reach a minimum of 0.5 near the greater β values in order to provide an inherent factor of safety and prevent negative k-value predictions.

CONCLUSIONS

In the model dredge, significant spillage in the form of re-suspended and residual sediment occurred at the cutter head speed greater of 45 rpm. It was determined qualitatively that the amount of spillage increased with the cutter head rpm. At constant flow rate, it is expected that the amount of spillage would continue to increase at cutter head speeds greater than 45 rpm.

Consistent with the previous experiments of Girani (2014), the specific gravity of the slurry decreased as the flow rate through the system increased, making the average production of the system constant. Because of this phenomenon, the maximum specific gravity measured during each set of tests occurred at the lowest nominal flow rate. At the highest nominal flow rates, the effects of cutter head speed and swing speed were eclipsed, resulting in a convergence of calculated k-values as suction velocity increased. This phenomenon is attributed to the relative influence of the flow field produced by suction flow as compared to the flow field produced by cutter head speed or swing speed. It is consistent with the convergence in the Girani (2014) prediction equation, which shows that the effect of specific gravity on k-value is diminished at high suction flow velocities.

Comparing the maximum specific gravity readings to cutter head speed and swing speed showed two important points. Firstly, it was determined that the specific gravity during a test with a screen in place reached a maximum at the cutter head speed of 30 rpm and that the maximum specific gravity at greater cutter head speeds may have

been limited by slow swing speeds. Secondly, it was shown that the maximum specific gravity increased linearly and consistently with swing speed. These concepts can be applied to both model and prototype scale cutter suction dredges, such that the maximum specific gravity achievable in the system is a function of flow rate, screen configuration, cutter head speed, and swing speed.

Based on the analyzed data, screen clogging during multiple, consecutive test runs is expected to occur in the Haynes Laboratory model dredge at β values of 0.50 or less. The effect of this clogging was an amplified centrifugal pump suction pressure, which led to a very high calculated minor loss coefficient. In this research, minor loss coefficients calculated at values greater than 4.0 were considered to be the product of a clogged screen. Under that definition, two consecutive tests runs with Screen 2 in place could be completed without seeing any effects of screen clogging. Overall, the clogging was attributed to both the small β value of the fixed screen and the large, model-induced ratio of sediment grain size to dimensional opening area (caused by imperfectly scaled model sand). Because of the imperfectly modeled sand, the screen-clogging phenomenon at small β values is expected to be less prevalent at the prototype dredge scale than at the model scale. Clogging was not observed in Screen 1 or Screen 3, which had β values of 0.618 and 0.617, respectively.

Past research showed that the minor loss coefficient of a fixed sediment screen on a cutter suction dredge was a function of both slurry velocity and specific gravity (Girani & Randall, 2014). The data in this experiment was enough to confirm that correlation. Although the specific gravity exhibited good correlation with Ω and V_L , it

was expected that the differences in sediment pickup behavior and suction flow field caused by changes in Ω and V_L would cause k to respond in a way that could be characterized by more than just a different SG. However, the results of this experiment showed that the minor loss coefficient was not significantly correlated with cutter head speed or swing speed at the ranges tested. This research also showed that cutter head speed and ladder arm swing speed had an indirect effect on the minor loss coefficient: they changed the specific gravity of the slurry, which then changed the k-value.

In contrast to the research of Girani (2014), the fixed screen k-values during water tests in this experiment were found to decrease linearly with suction velocity. The fixed screen k-values calculated during sand tests did not show any consistent correlation with suction velocity; however, removal of data points affected by screen clogging revealed data that showed some similarities to the k-value prediction equation proposed by Girani (2014).

An empirical relationship was found between the opening area ratio (β) and minor loss coefficient and was quantified in the form of a k-value prediction equation. The equation quantifying the effects of suction velocity and specific gravity on minor loss coefficient from Girani (2014) was merged with the results of this experiment to re-define the minor loss coefficient as a function of opening area ratio, dimensional suction velocity (in ft/s), and specific gravity, as shown in Equation (51). The dimensional prediction equation was plotted in Figure 40, then shown using non-dimensional scales so that it can be used for both model and prototype scale cutter suction dredges using typical operating parameters.

RECOMMENDATIONS

A few experimental shortfalls were identified that provide opportunities for future testing. First, the limited range of cutter head speeds tested should be discussed. The slowest speed of 15 rpm proved to be unfeasible for large scale testing due to the bulldozer effect caused by the low rotational speed. Conversely, the cutter head at 45 rpm produced significant spillage in the form of both re-suspended and residual sediment, resulting in a small inaccuracy when directly comparing the 15 rpm and 45 rpm tests. However, when both cutter head speed and swing speed were increased, the specific gravity and production increased accordingly. If the upper limit of tested flow rates is increased, it is expected that the spillage phenomenon at high cutter head speeds could be minimized. After minimizing spillage, greater cutter head speeds should be tested in order to provide more data that will either confirm or deny the low correlation between cutter head speed and minor loss coefficient shown in this thesis.

Future testing at the Haynes Laboratory should also focus on a wider range of swing speeds. The selected range of test swing speeds was initially very small – 1.0 to 2.0 in/s (2.54 to 5.08 cm/s) – and was based on the speeds believed to be achievable on the model dredge without overloading the motor moving the ladder across the dredge tank. However, the additional tests at swing speeds of 3 in/s (7.62 cm/s) listed in Table 4 show that the capabilities of the Haynes Laboratory model dredge exceed the selected range of the tested swing speeds. Additional dredge tests at swing speeds greater than 2.0 in/s (5.08 cm/s) may further solidify a linear correlation between swing speed and

specific gravity; or, they may show that some quantifiable correlation between swing speed and minor loss coefficient exists beyond those swing speeds tested in this experiment.

The phenomenon of screen clogging was observed in Screen 2, which had an opening area ratio of 0.45, and in previous research with a screen opening area ratio of 0.50 (Girani, 2014). In order to protect the validity of data, it is recommended that future researchers using screens with β values less than 0.50 be very careful to avoid screen clogging by following the un-clogging technique used by Girani (2014).

The Data Processing section described two methods of truncating each test's time series to find steady data: the first was to truncate data to make the flow rates match up with nominal flow rates, and the second was to match averaged values of specific gravity across corresponding tests using different screens. It was impossible to process the data in such a way to achieve averaged values equal to the nominal flow rates and matched specific gravities, especially given the inherent fluctuations due to the continually adjusted pump. An operator was required to constantly adjust the pump speed to maintain the flow rate near a nominal value. Overall, the data showed that the flow rate fluctuated (sometimes in a sinusoidal fashion) around the nominal flow rates. However, some fluctuations were large, which could have led to data inaccuracies.

Kharin, et al. (1992) claims that the computer-aided automation of a cutter suction dredge (i.e. the elimination of human influence) stabilizes the operation of a system – and even increases production. A more recent study using prototype-scale dredging experiments showed that the slurry concentration, production, and suction and

discharge pressures were more steady when operated by an automated computer system than when operated by an experienced dredger (Tang, et al., 2008). It stands to reason that the automation of the main centrifugal pump at the Haynes Laboratory to stabilize the flow rate fluctuations would lead to overall data quality improvement. A feasibility study is recommended on the development and installation of a system to automate some of the functions of the Haynes Laboratory model dredge.

The three screens tested in this research showed a promising correlation between k and β ; however, the k -value prediction equation proposed in this thesis admittedly suffers from a limited amount of data: specifically regarding the number of different β values tested. Future research should focus on testing more screens using screen opening values from 0.45 to 0.62. Conducting similar tests on those screens would effectively fill the gaps in the experimental data presented in Figure 37 and Figure 40.

Similarly, future testing on dredge screens should focus on different opening shapes. The data from this thesis suggest that, relative to screens with rectangular openings, those with curved or expanded metal openings (Girani, 2014) represent shifts in the prediction curves of +0.3 and -0.6, respectively. Since these shifts were only observed for a limited amount of data, further testing of screens with different opening shapes should be performed at the full range of opening area ratios. This will result in more confident k -value prediction curves, from which the k -value shift across different opening shapes would be more accurately quantified.

REFERENCES

- Basco, D. (1975a). Analytical Model of Hydraulic Pipeline Dredge. *Journal of the Waterways Harbors and Coastal Engineering Division*, 101(1), 33-48.
- Basco, D. (1975b). The Relative Influence of Some Variables on the Performance of a Hydraulic Pipeline Dredge Model. *Proceedings of the First International Symposium on Dredging Technology*. Cranfield, Bedford, England: BHRA Fluid Engineering.
- Bridges, T., Ells, S., Hayes, D., Mount, D., Nadeau, S., Palermo, M., . . . Schroeder, P. (2008). The Four Rs of Environmental Dredging: Resuspension, Release, Residual, and Risk. Vicksburg, MS, USA: Engineer Research and Development Center.
- DeepSea Power & Light. (2014). *Multi SeaLite Family: The Workhorse of All Halogen Lights*. Retrieved June 26, 2014, from http://www.deepsea.com/wp-content/uploads/spec-multi_sealite.pdf
- Dekker, M. A., Kruyt, N. P., den Burger, M., & Vlasblom, W. (2003). Experimental and Numerical Investigation of Cutter Head Dredging Flows. *Journal of Waterway, Port, Coastal, and Ocean Engineering*, 129(5), 203-209.
- den Burger, M., Vlasblom, W., & Talmon, A. (1999). Influence of Operational Parameters on Dredge Cutterhead Spillage. *Proceedings of CEDA Dredging Days 1999*. Amsterdam, The Netherlands.

- Fusheng, N., Li-juan, Z., Lei, G., Shuang, J., Li-na, Q., Li-qun, X., & Kun-jin, H. (2010). Simulation of Dredging Processes of a Cutter Suction Dredger. *2010 International Conference on Audio Language and Image Processing (ICALIP)* (pp. 628-632). IEEE.
- Fusheng, N., Lijuan, Z., Liqun, X., & Vlasblom, W. (2007). A Model Calculation for Flow Resistance in the Hydraulic Transport of Sand. *Proceedings of the 18th World Dredging Congress*. Orlando, Florida, USA.
- Girani, J. (2014). *Experimental Measurement of a Model Pipeline Dredge Entrance Loss Coefficient and Modification of a Spreadsheet for Estimating Model Dredge Performance*. Thesis, Texas A&M University, College Station, TX, USA.
- Girani, J., & Randall, R. (2014). Experimental Measurement of a Model Pipeline Dredge Entrance Loss Coefficient. *Proceedings of the Western Dredging Association (WEDA XXXIV) Technical Conference and Texas A&M University (TAMU 45) Dredging Seminar*. Toronto, Canada.
- Glover, G. (2002). *Laboratory Modeling of Hydraulic Dredges and Design of Dredge Carriage for Laboratory Facility*. Master's Thesis, Texas A&M University, College Station, TX, USA.
- Goodyear Rubber Products Inc. (2010). Goodyear Plicord(R) Con-AG(TM) Water Suction and Discharge Hose Specifications.
- Hayes, D. F., Crockett, T. R., Ward, T. J., & Averett, D. (2000). Sediment Resuspension During Cutterhead Dredging Operations. *Journal of Waterway, Port, Coastal, and Ocean Engineering*, 126(3), 153-161.

- Henriksen, J. (2009). Investigation of Turbulence Characteristics for Model Cutter Suction Dredging Operation. *Bulletin of the Permanent International Association of Navigation Congresses*, 136, p. 17.
- Henriksen, J., Randall, R., & Socolofsky, S. (2011). Near-Field Resuspension Model for a Cutter Suction Dredge. *Journal of Waterway, Port, Coastal, and Ocean Engineering*, 138(3), 181-191.
- Herbich, J. (2000a). *Handbook of Coastal Engineering*. New York, NY, USA: McGraw-Hill.
- Herbich, J. (2000b). *Handbook of Dredging Engineering, 2nd Ed.* New York, NY, USA: McGraw-Hill.
- Holman, J., & Gajda, W. (1989). *Experimental Methods for Engineers, 5th Ed.* New York, NY, USA: McGraw-Hill Book Company.
- Huston, J. (1970). *Hydraulic Dredging: Theoretical and Applied*. Cambridge, MD, USA: Cornell Maritime Press, Inc.
- Ivanov, A. (1992). Output of Suction Dredges with Respect to Solids. *Hydrotechnical Construction*, 26(10), 677-680.
- Kharin, A. I., Spantsireti, A. N., & Fedorov, O. V. (1992). Automation of Control of the Intake on a Suction-Cutter Dredge. *Power Technology and Engineering (formerly Hydrotechnical Construction)*, 26(5), 314-316.
- Kline, A., & McClintock, F. (1953). Describing Uncertainties in Single-Sample Experiments. *Mechanical Engineering*, 75, 3-8.

- Krohne, Inc. (1997). IFC 090 Installation and Operating Instructions. *Signal Converters for Electromagnetic Flowmeters*.
- Miedema, S. (2001). Automation of a Cutter Suction Dredge. *Proceedings of WODCON XVI*. Kuala Lumpur, Malaysia.
- Miedema, S. (2012). The Bulldozer Effect when Cutting Water Saturated Sand. *Proceedings of the ASME 2012 31st International Conference on Ocean, Offshore, and Arctic Engineering* (pp. 143-152). Rio de Janeiro, Brazil: American Society of Mechanical Engineers.
- Ogorodnikov, S. P., Mikheev, I. I., & Kulakov, A. E. (1987). Optimization of the Mud Intakes of Dredges with Submersible Pumps. *Power Technology and Engineering (formerly Hydrotechnical Construction)*, 21(7), 432-436.
- Ohmart Vega Corp. (2006a). Haynes Laboratory Quote No. 6071665. Cincinnati, OH, USA.
- Ohmart Vega Corp. (2006b). Application Sizing Sheet - Gamma Density Gauge.
- Randall, R. (2013). OCEN688 Course Notes: Dredging and Dredged Material Placement. College Station, TX, USA.
- Randall, R. (2014a). Chapter 6: Dredge Production. *OCEN 688 Presentation Notes*. College Station, TX, USA.
- Randall, R. (2014b). Chapter 12: Dredge Instrumentation. *OCEN688 Presentation Notes*. College Station, TX, USA.

- Rosemount Inc. (2007). Rosemount 1151 Smart Pressure Transmitter. *Reference Manual 00809-0100-4593, Rev CA, June 2007*. Chanhassen, MN: Emerson Process Management.
- Schiller, R. (1992). Sediment Transport in Pipes. In J. Herbich (Ed.), *Handbook of Dredging Engineering, 2nd Ed.* (p. 7.54). New York, NY, USA: McGraw-Hill.
- Senix Corporation. (2007). ToughSonic Distance Sensors: TS-30S Series. *Technical Specifications*.
- Steinbusch, P., Vlasblom, W., den Burger, M., & Kruyt, N. (1999). Numerical Simulation of the Flow Generated by Cutter Heads. *Proceedings of the 14th International Conference, Hydrotransport* (pp. 435-443). BHR Group.
- Swamee, P., & Jain, A. (1976). Explicit Equations for Pipe-Flow Problems. *Journal of the Hydraulics Division, 102*(5), 657-664.
- Tang, J., Wang, Q., & Bi, Z. (2008). Expert System for Operation Optimization and Control of Cutter Suction Dredger. *Expert Systems with Applications, 34*(3), 2180-2192.
- VEGA Americas, Inc. (2014). Technologies, Solutions, and Applications. *Radiation-based Density with GEN2000*. Cincinnati, OH, USA. Retrieved July 1, 2014, from [http://www.vega.com/downloads/ohmart/\(CPB\)%20Customer%20Product%20Brochures/31413-US.pdf](http://www.vega.com/downloads/ohmart/(CPB)%20Customer%20Product%20Brochures/31413-US.pdf)
- Wilson, K., Addie, G., Sellgren, A., & Clift, R. (2006). *Slurry Transport Using Centrifugal Pumps, 3rd Ed.* Springer.

Yagi, T., Miyazaki, S., Okayama, Y., Koreishi, A., Sato, Y., Saito, M., . . . Kikuya, T.

(1975). *Effect of Operating Conditions of Hydraulic Dredges on Dredging*

Capacity and Turbidity. Port and Harbor Research Institute, Ministry of

Transport, Japan. Glen Ridge, NJ: Translation by Associated Technical Services,

Inc.

APPENDIX A – TEST PLANS

Table A - 1: Test plan for day 1 – 02 June 2014.

Day	Test No.	Screen No.	Cutter Head Speed (RPM)	Swing Speed (in/s)	Flowrate (GPM)	Cutting Depth (in)	x1	x2	y1	y2	z
1	1	0	15	1.5	250	0			45	245	25
1	2	0	15	1.5	325	0			45	245	25
1	3	0	15	1.5	400	0			45	245	25
1	4	0	30	1.5	250	0			45	245	25
1	5	0	30	1.5	325	0			45	245	25
1	6	0	30	1.5	400	0			45	245	25
1	7	0	45	1.5	250	0			45	245	25
1	8	0	45	1.5	325	0			45	245	25
1	9	0	45	1.5	400	0			45	245	25
1	10	0	15	1.5	250	10	1960	1937	45	245	105.4
1	11	0	15	1.5	325	10	1914	1891	45	245	105.4
1	12	0	15	1.5	400	10	1868	1845	45	245	105.4
1	16	0	45	1.5	250	10	1960	1937	45	245	130.8
1	17	0	45	1.5	325	10	1914	1891	45	245	130.8
1	18	0	45	1.5	400	10	1868	1845	45	245	130.8

Table A - 2: Test plan for day 2 – 03 June 2014.

Day	Test No.	Screen No.	Cutter Head Speed (RPM)	Swing Speed (in/s)	Flowrate (GPM)	Cutting Depth (in)	x1	x2	y1	y2	z
2	51	0	30	1	250	0			45	245	25
2	52	0	30	1	325	0			45	245	25
2	53	0	30	1	400	0			45	245	25
2	56	0	30	1.5	400	0			45	245	25
2	55	0	30	1.5	325	0			45	245	25
2	54	0	30	1.5	250	0			45	245	25
2	57	0	30	2	250	0			45	245	25
2	58	0	30	2	325	0			45	245	25
2	59	0	30	2	400	0			45	245	25
2	60	0	30	1	250	10	1960	1937	45	245	105
2	61	0	30	1	325	10	1914	1891	45	245	105
2	62	0	30	1	400	10	1868	1845	45	245	105
2	65	0	30	1.5	400	10	1822	1799	45	245	105
2	64	0	30	1.5	325	10	1776	1753	45	245	105
2	63	0	30	1.5	250	10	1730	1707	45	245	105
2	66	0	30	2	250	10	1684	1661	45	245	105
2	67	0	30	2	325	10	1638	1615	45	245	105
2	68	0	30	2	400	10	1592	1569	45	245	105

Table A - 3: Test plan for day 3 – 04 June 2014.

Day	Test No.	Screen No.	Cutter Head Speed (RPM)	Swing Speed (in/s)	Flowrate (GPM)	Cutting Depth (in)	x1	x2	y1	y2	z
3	101	1	15	1.5	250	0			45	245	25
3	102	1	15	1.5	325	0			45	245	25
3	103	1	15	1.5	400	0			45	245	25
3	106	1	30	1.5	400	0			45	245	25
3	105	1	30	1.5	325	0			45	245	25
3	104	1	30	1.5	250	0			45	245	25
3	107	1	45	1.5	250	0			45	245	25
3	108	1	45	1.5	325	0			45	245	25
3	109	1	45	1.5	400	0			45	245	25
3	118	1	45	1.5	400	10	1960	1937	45	245	105
3	112	1	15	1.5	400	10	1914	1891	45	245	105
3	111	1	15	1.5	325	10	1868	1845	60	245	105
3	110	1	15	1.5	250	10	1822	1799	60	245	105
3	113	1	30	1.5	250	10	1776	1753	60	245	105
3	114	1	30	1.5	325	10	1730	1707	60	245	105
3	115	1	30	1.5	400	10	1684	1661	60	245	105

Table A - 4: Test plan for day 4 – 05 June 2014 (morning).

Day	Test No.	Screen No.	Cutter Head Speed (RPM)	Swing Speed (in/s)	Flowrate (GPM)	Cutting Depth (in)	x1	x2	y1	y2	z
4	154	1	30	1.5	250	0			60	245	25
4	155	1	30	1.5	325	0			60	245	25
4	156	1	30	1.5	400	0			60	245	25
4	159	1	30	2	400	0			60	245	25
4	158	1	30	2	325	0			60	245	25
4	157	1	30	2	250	0			60	245	25
4	151	1	30	1	250	0			60	245	25
4	152	1	30	1	325	0			60	245	25
4	153	1	30	1	400	0			60	245	25
4	162	1	30	1	400	10	1960	1937	60	245	104
4	161	1	30	1	325	10	1914	1891	60	245	104
4	160	1	30	1	250	10	1868	1845	60	245	104
4	166	1	30	2	250	10	1822	1799	60	245	104
4	167	1	30	2	325	10	1776	1753	60	245	104
4	168	1	30	2	400	10	1730	1707	60	245	104
4	116	1	45	1.5	250	10	1638	1615	60	245	104
4	117	1	45	1.5	325	10	1684	1661	60	245	104

Table A - 5: Test plan for day 4 – 05 June 2014 (afternoon).

Day	Test No.	Screen No.	Cutter Head Speed (RPM)	Swing Speed (in/s)	Flowrate (GPM)	Cutting Depth (in)	x1	x2	y1	y2	z
4a	201	2	15	1.5	250	0			60	245	25
4a	202	2	15	1.5	325	0			60	245	25
4a	203	2	15	1.5	400	0			60	245	25
4a	206	2	30	1.5	400	0			60	245	25
4a	205	2	30	1.5	325	0			60	245	25
4a	204	2	30	1.5	250	0			60	245	25
4a	207	2	45	1.5	250	0			60	245	25
4a	208	2	45	1.5	325	0			60	245	25
4a	209	2	45	1.5	400	0			60	245	25
4a	218	2	45	1.5	400	10	1960	1937	60	245	105
4a	212	2	15	1.5	400	10	1914	1891	60	245	105
4a	211	2	15	1.5	325	10	1868	1845	60	245	105
4a	210	2	15	1.5	250	10	1822	1799	60	245	105
4a	213	2	30	1.5	250	10	1776	1753	60	245	105
4a	214	2	30	1.5	325	10	1730	1707	60	245	105
4a	215	2	30	1.5	400	10	1684	1661	60	245	105

Table A - 6: Test plan for day 5 – 06 June 2014.

Day	Test No.	Screen No.	Cutter Head Speed (RPM)	Swing Speed (in/s)	Flowrate (GPM)	Cutting Depth (in)	x1	x2	y1	y2	z
5	254	2	30	1.5	250	0			60	245	25
5	255	2	30	1.5	325	0			60	245	25
5	256	2	30	1.5	400	0			60	245	25
5	259	2	30	2	400	0			60	245	25
5	258	2	30	2	325	0			60	245	25
5	257	2	30	2	250	0			60	245	25
5	251	2	30	1	250	0			60	245	25
5	252	2	30	1	325	0			60	245	25
5	253	2	30	1	400	0			60	245	25
5	262	2	30	1	400	10	1960	1937	60	245	105
5	261	2	30	1	325	10	1914	1891	60	245	105
5	260	2	30	1	250	10	1868	1845	60	245	105
5	266	2	30	2	250	10	1822	1799	60	245	105
5	267	2	30	2	325	10	1776	1753	60	245	105
5	268	2	30	2	400	10	1730	1707	60	245	105
5	217	2	45	1.5	325	10	1684	1661	60	245	105
5	216	2	45	1.5	250	10	1638	1615	60	245	105

Table A - 7: Test plan for day 6 – 09 June 2014 (morning).

Day	Test No.	Screen No.	Cutter Head Speed (RPM)	Swing Speed (in/s)	Flowrate (GPM)	Cutting Depth (in)	x1	x2	y1	y2	z
6	213	2	30	1.5	250	10	1960	1937	60	245	105
6	214	2	30	1.5	325	10	1914	1891	60	245	105
6	215	2	30	1.5	400	10	1868	1845	60	245	105
6	297	2	30	3	250	10	1822	1799	60	245	105
6	298	2	30	3	325	10	1776	1753	60	245	105
6	299	2	30	3	400	10	1730	1707	60	245	105
6	283	2	45	3	250	10	1684	1661	60	245	105

Table A - 8: Test plan for day 6 – 09 June 2014 (afternoon).

Day	Test No.	Screen No.	Cutter Head Speed (RPM)	Swing Speed (in/s)	Flowrate (GPM)	Cutting Depth (in)	x1	x2	y1	y2	z
6a	357	3	30	2	250	0			60	245	25
6a	358	3	30	2	325	0			60	245	25
6a	359	3	30	2	400	0			60	245	25
6a	356	3	30	1.5	400	0			60	245	25
6a	355	3	30	1.5	325	0			60	245	25
6a	354	3	30	1.5	250	0			60	245	25
6a	351	3	30	1	250	0			60	245	25
6a	352	3	30	1	325	0			60	245	25
6a	353	3	30	1	400	0			60	245	25
6a	362	3	30	1	400	10	1960	1937	60	245	25
6a	361	3	30	1	325	10	1914	1891	60	245	25
6a	360	3	30	1	250	10	1868	1845	60	245	25
6a	366	3	30	2	250	10	1822	1799	60	245	105
6a	367	3	30	2	325	10	1776	1753	60	245	105
6a	368	3	30	2	400	10	1730	1707	60	245	105
6a	365	3	30	1.5	400	10	1684	1661	60	245	105
6a	364	3	30	1.5	325	10	1638	1615	60	245	105
6a	363	3	30	1.5	250	10	1592	1569	60	245	105

APPENDIX B – RAW DATA

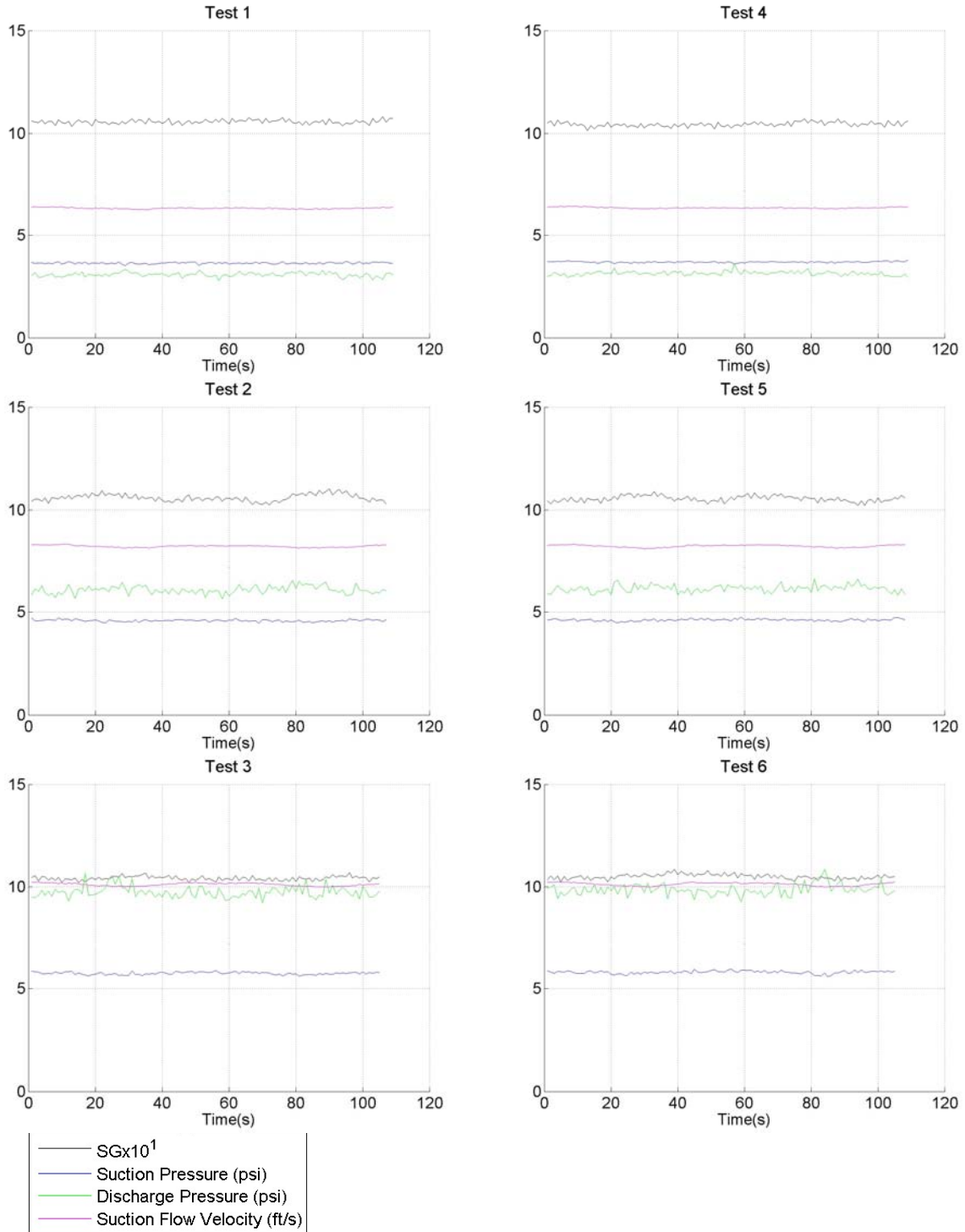


Figure B - 1: Tests 1-7.

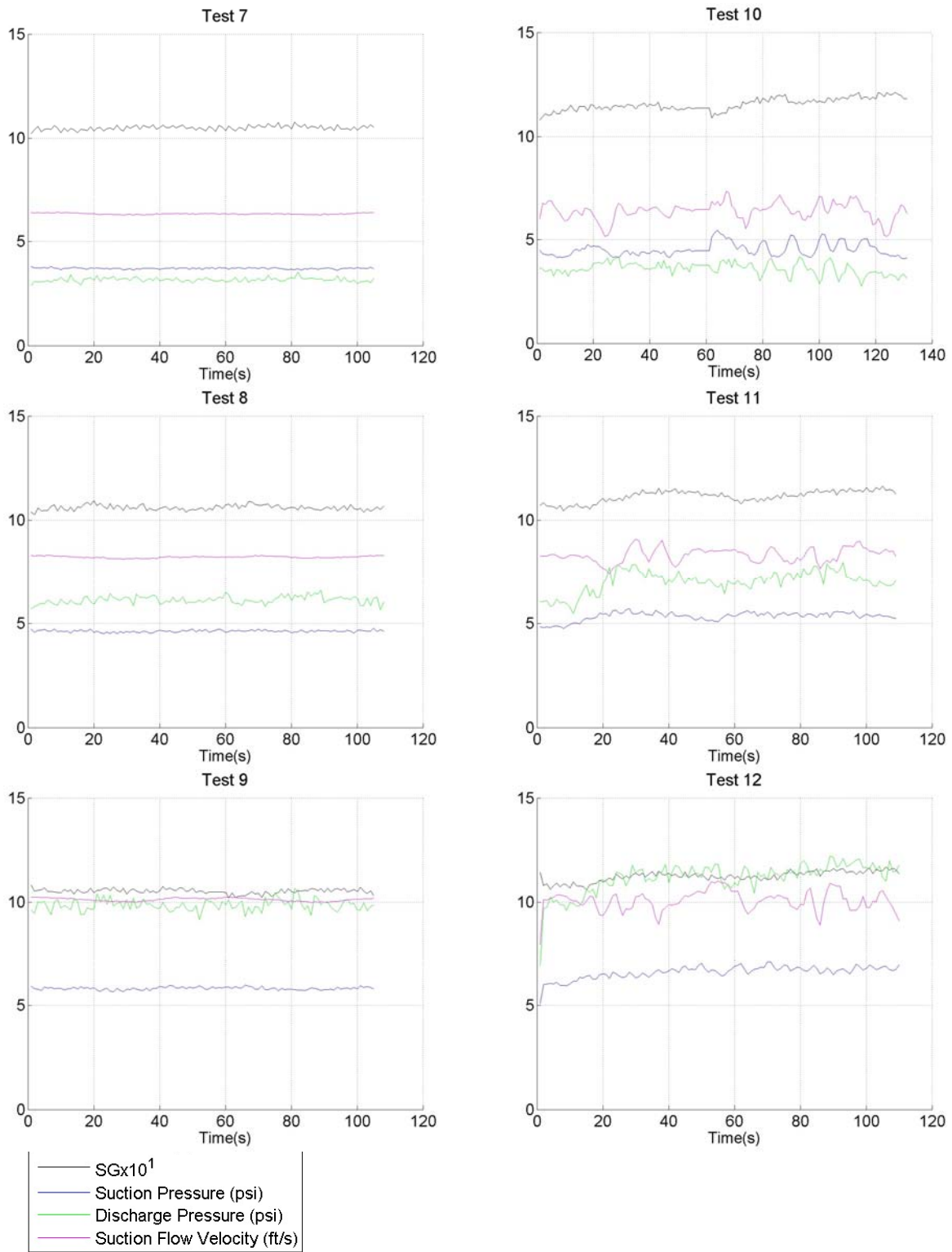


Figure B - 2: Tests 7-12.

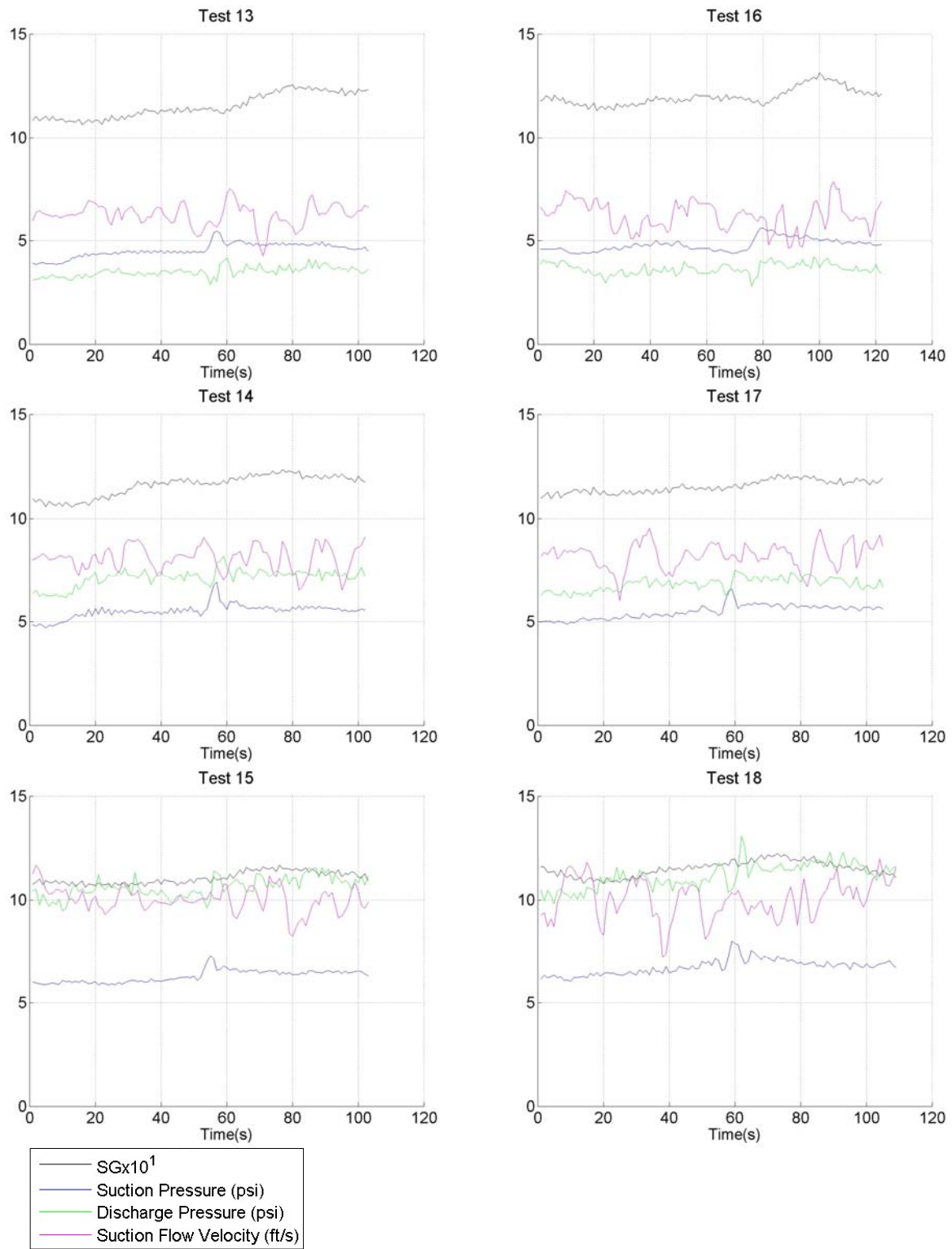


Figure B - 3: Tests 13-18.

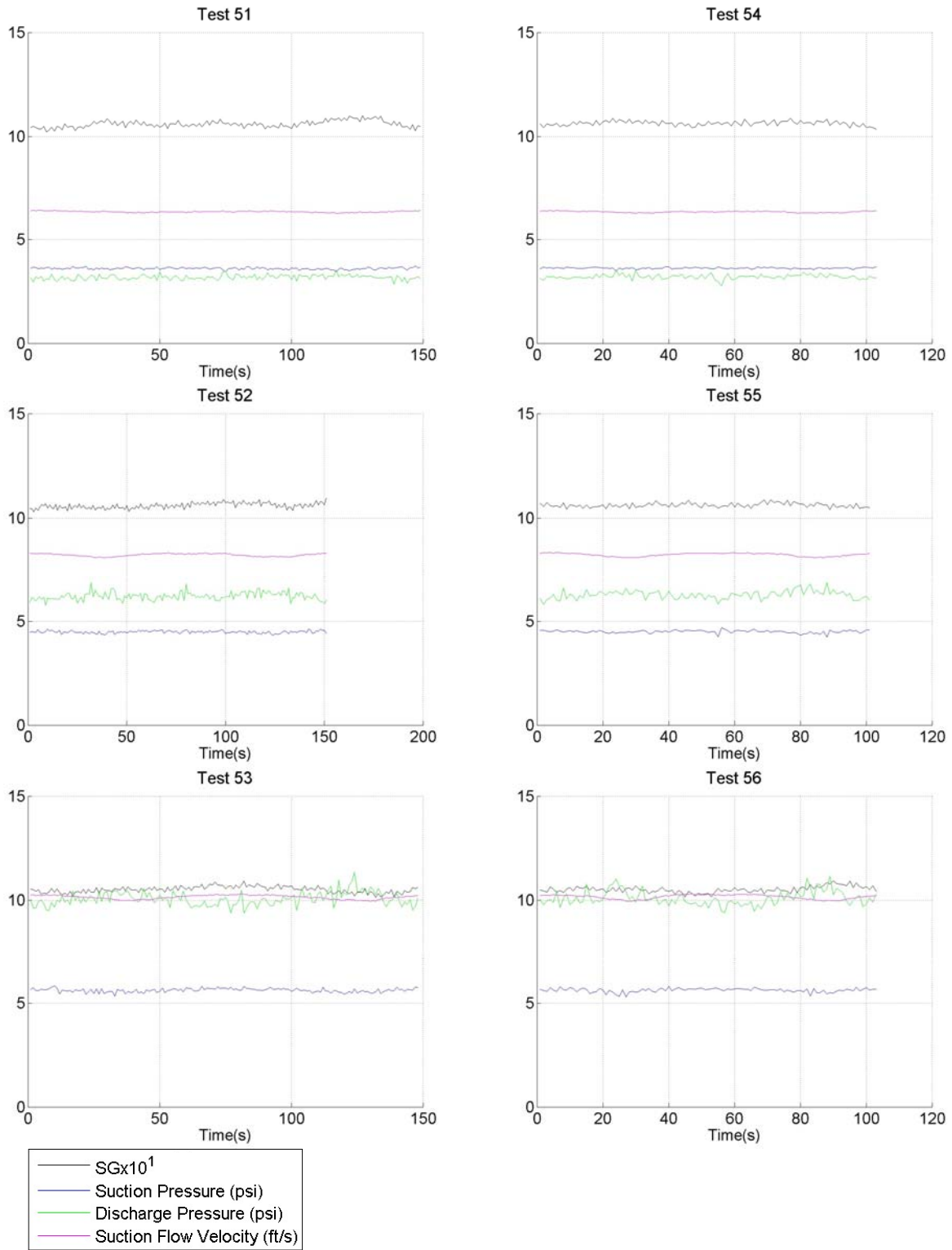


Figure B - 4: Tests 51-56.

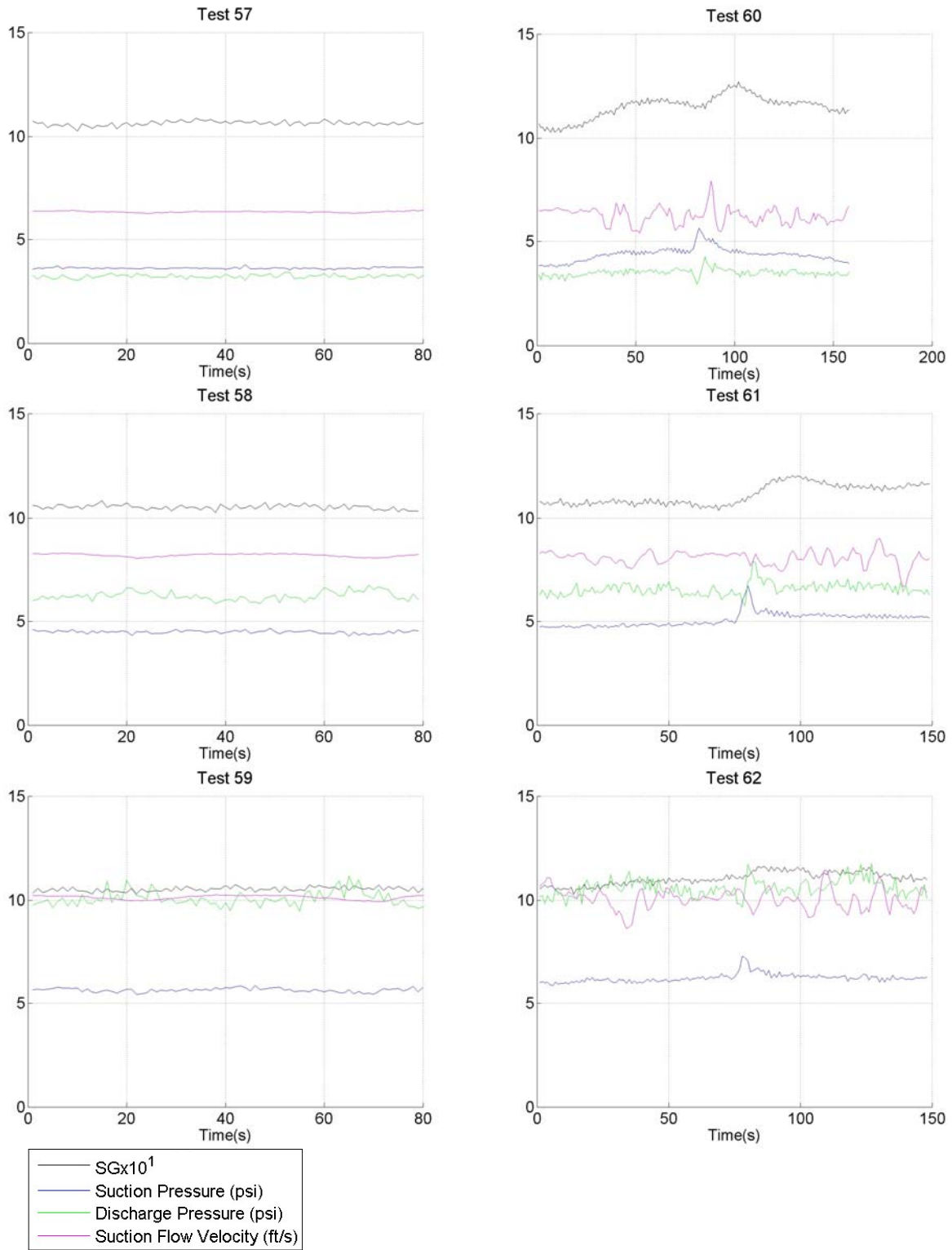


Figure B - 5: Tests 57-62.

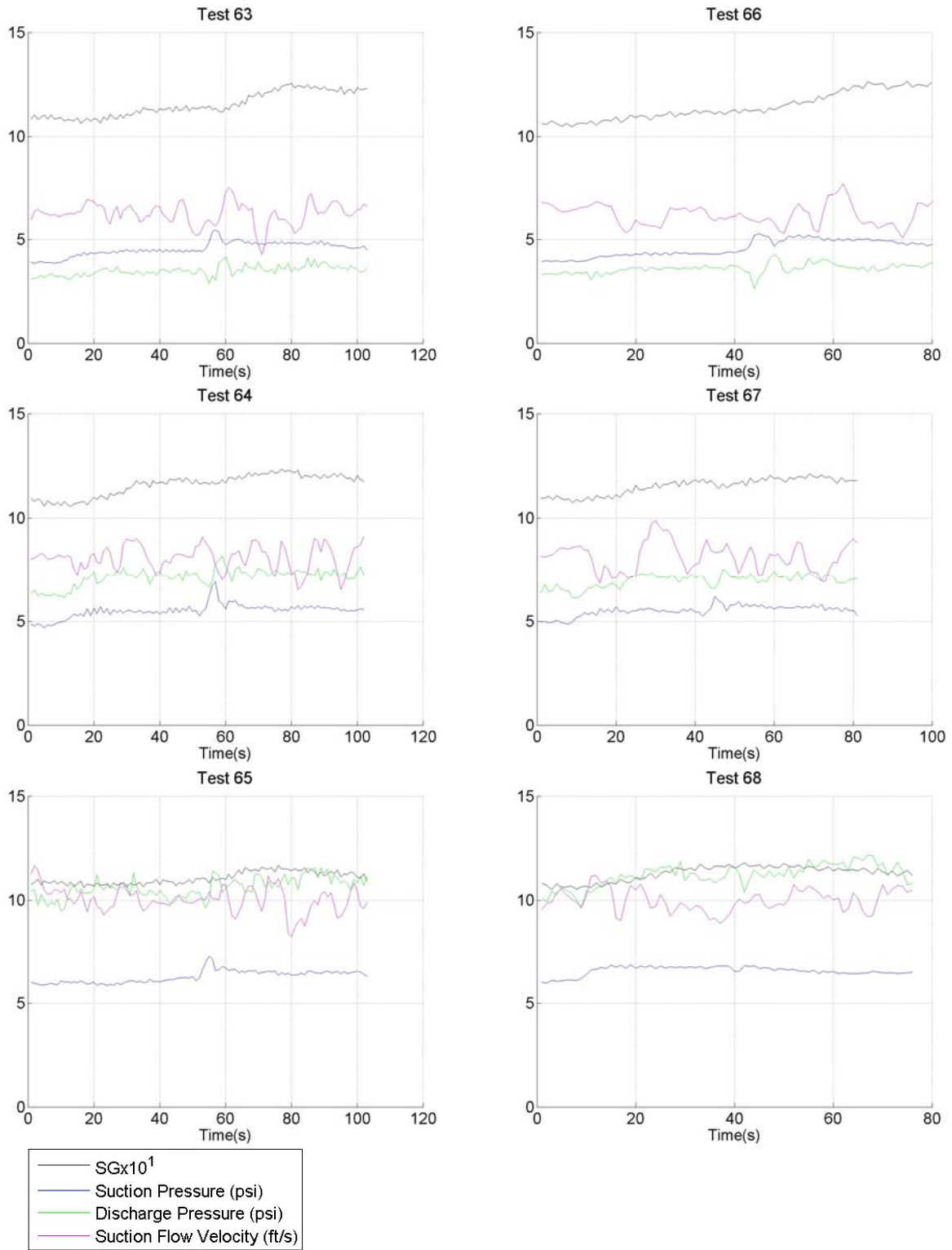


Figure B - 6: Tests 63-68.

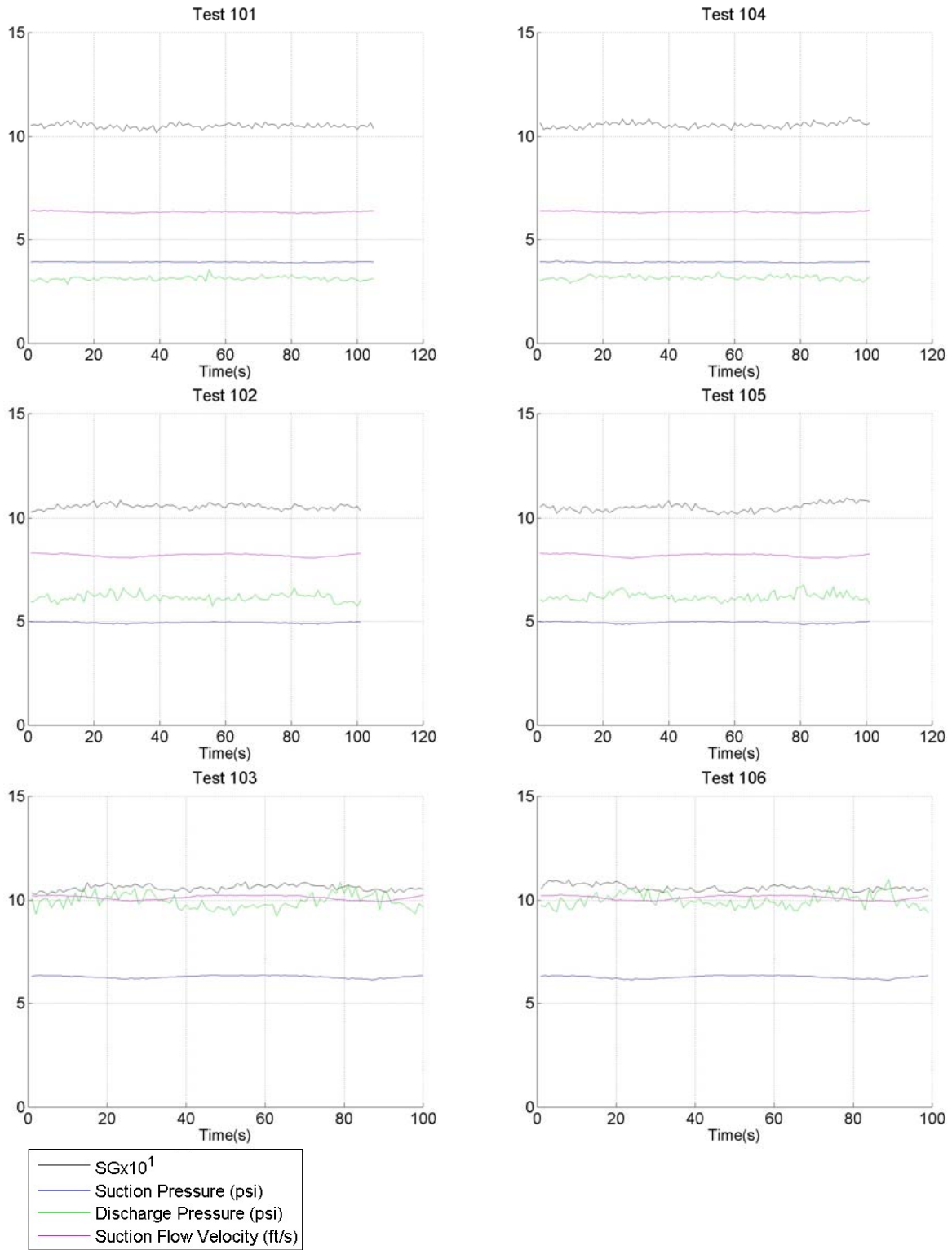


Figure B - 7: Tests 101-106.

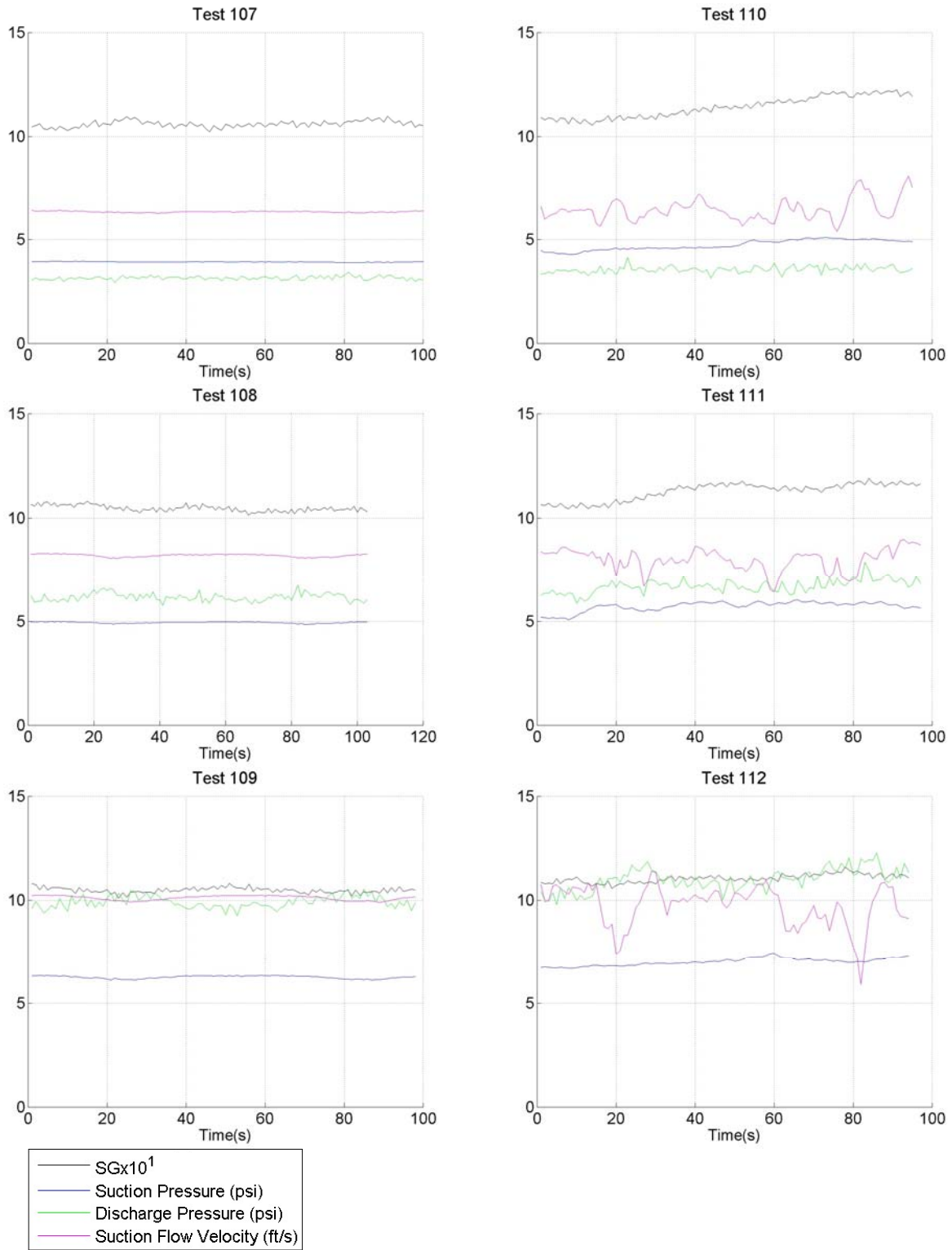


Figure B - 8: Tests 107-112.

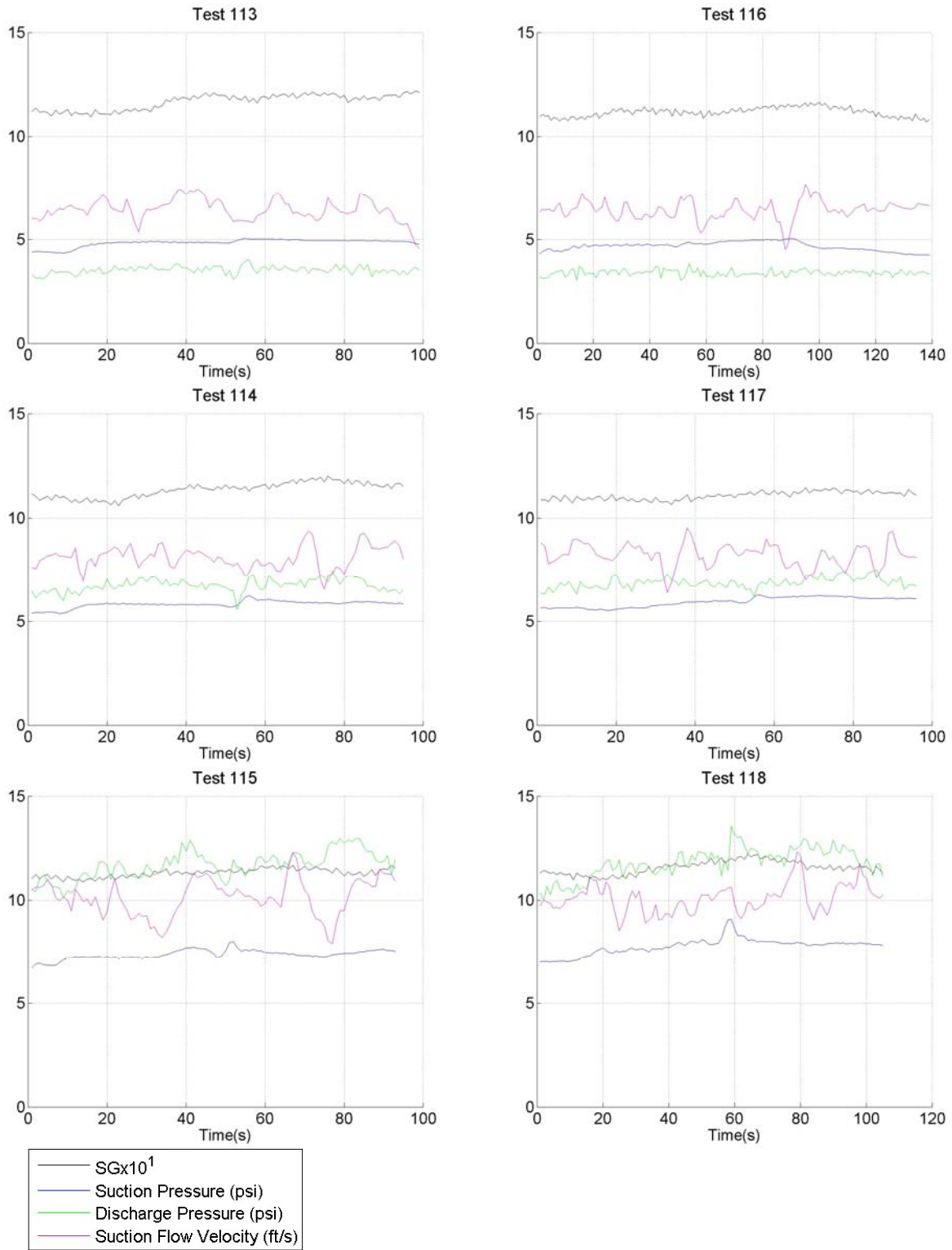


Figure B - 9: Tests 113-118.

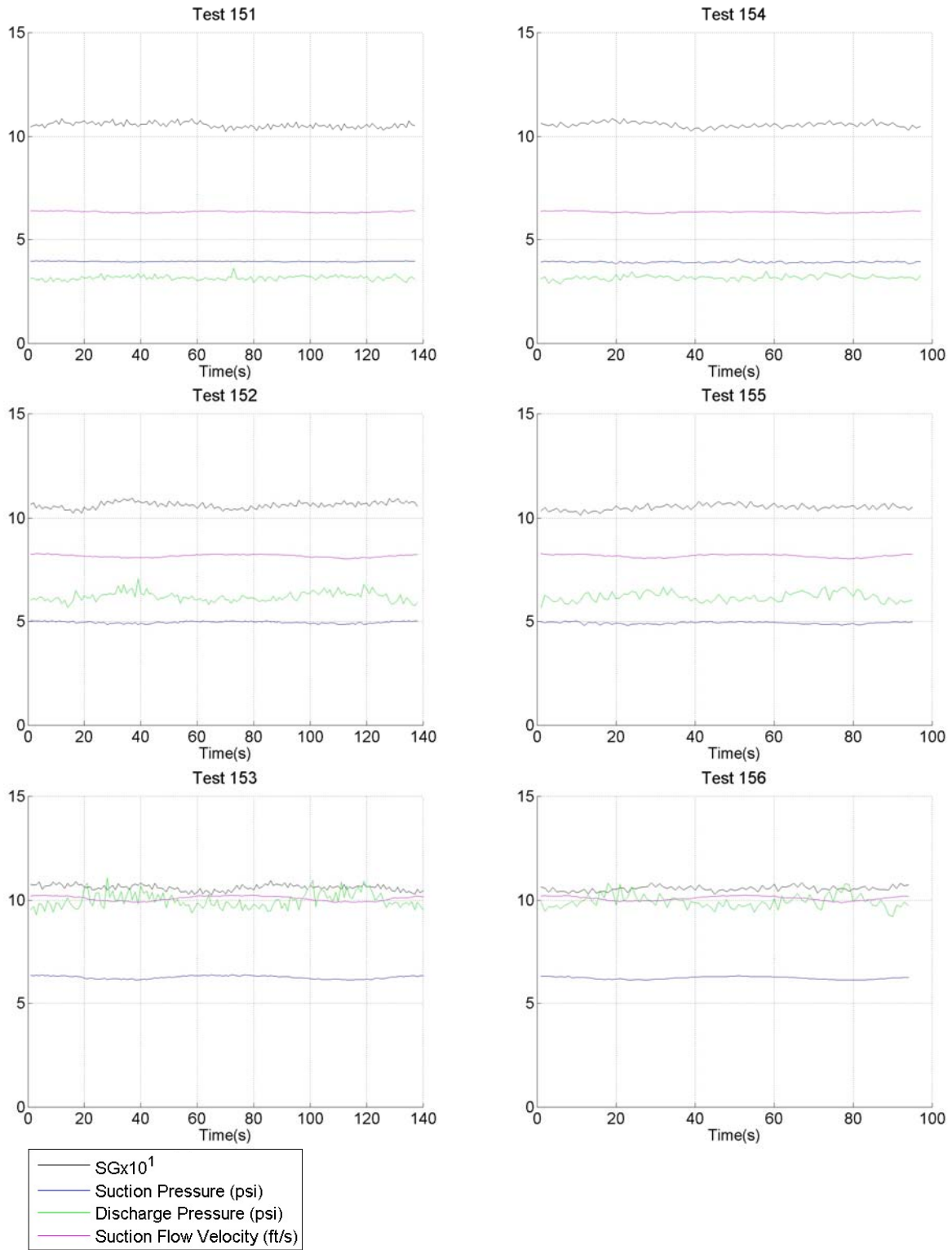


Figure B - 10: Tests 151-156.

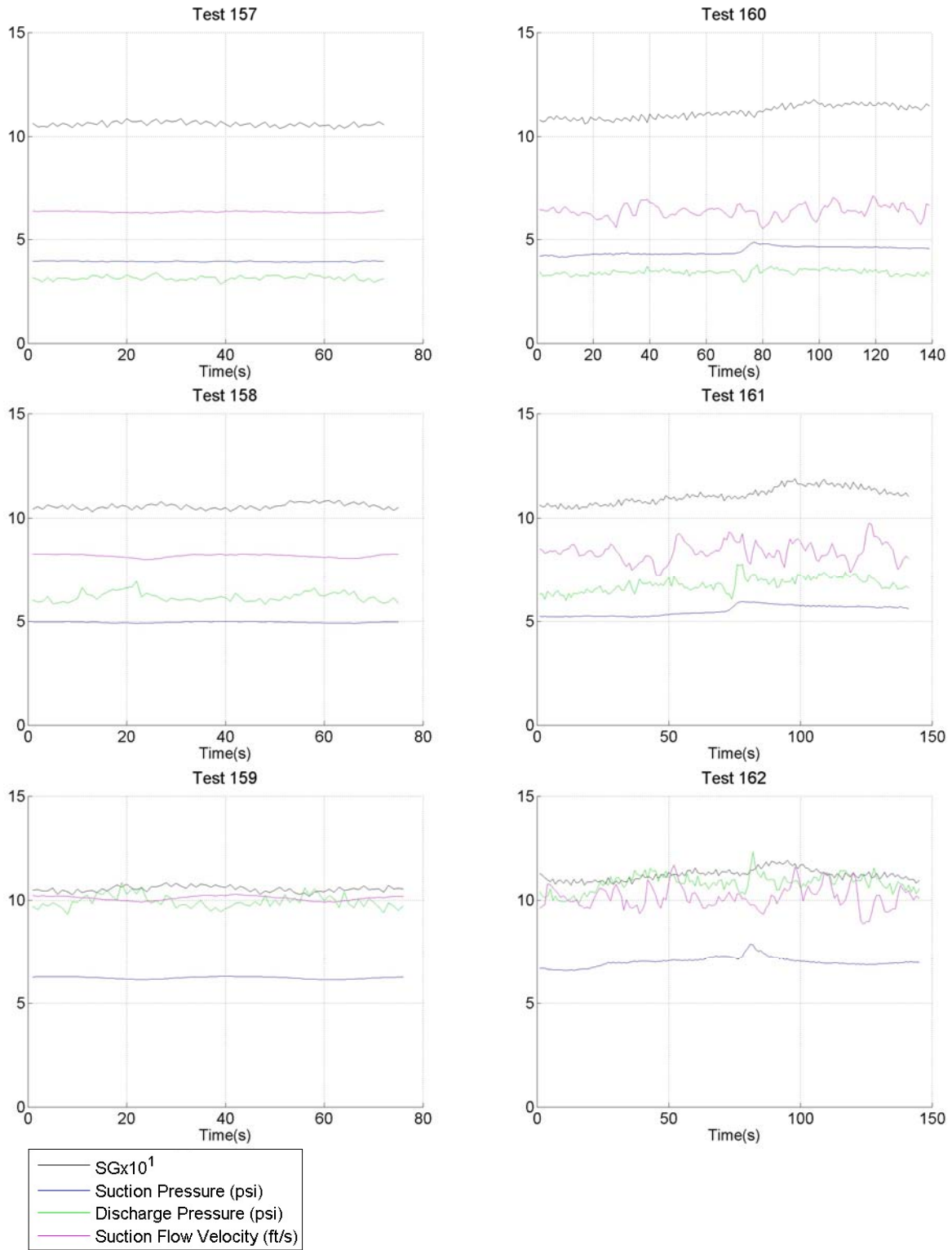


Figure B - 11: Tests 157-162.

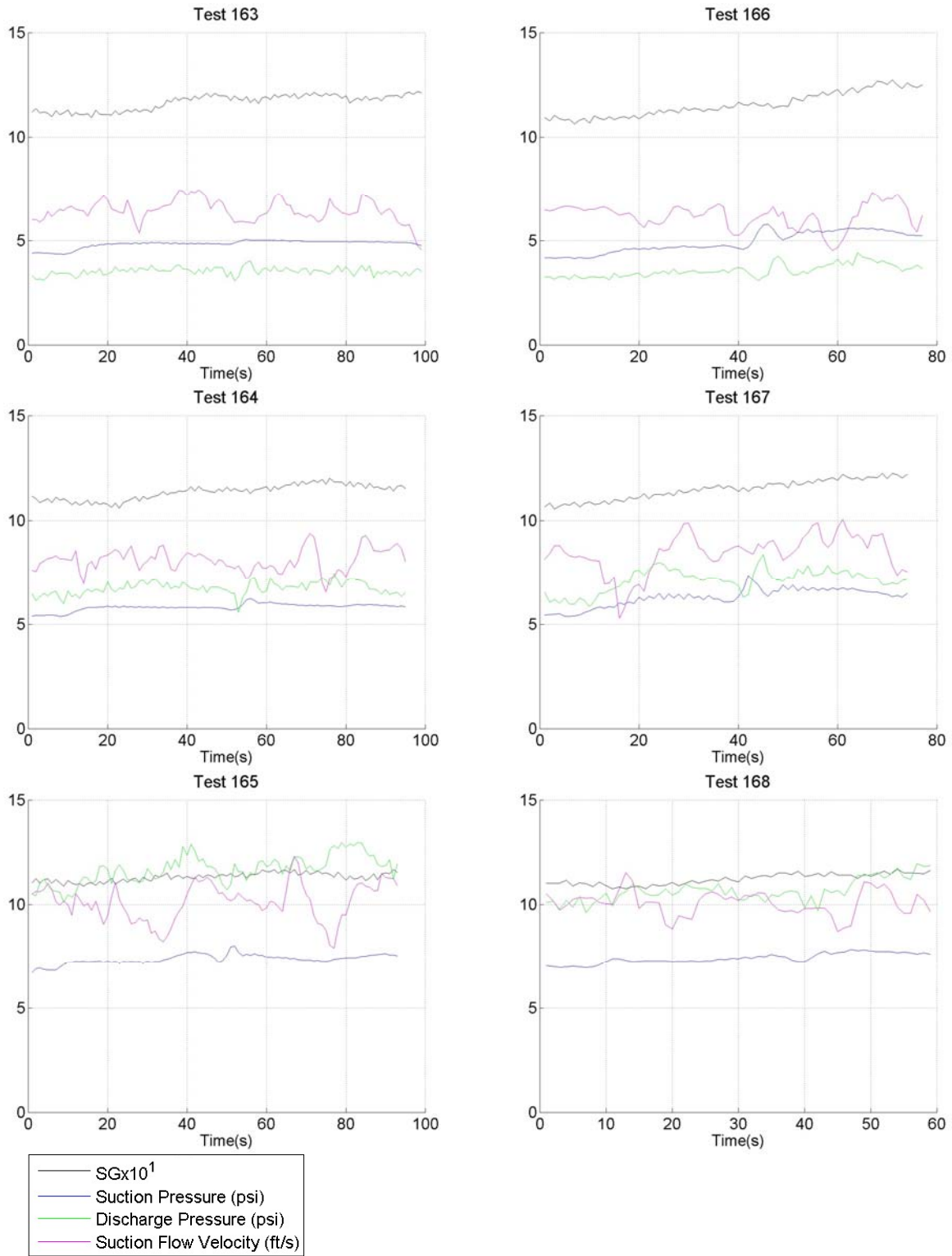


Figure B - 12: Tests 163-168.

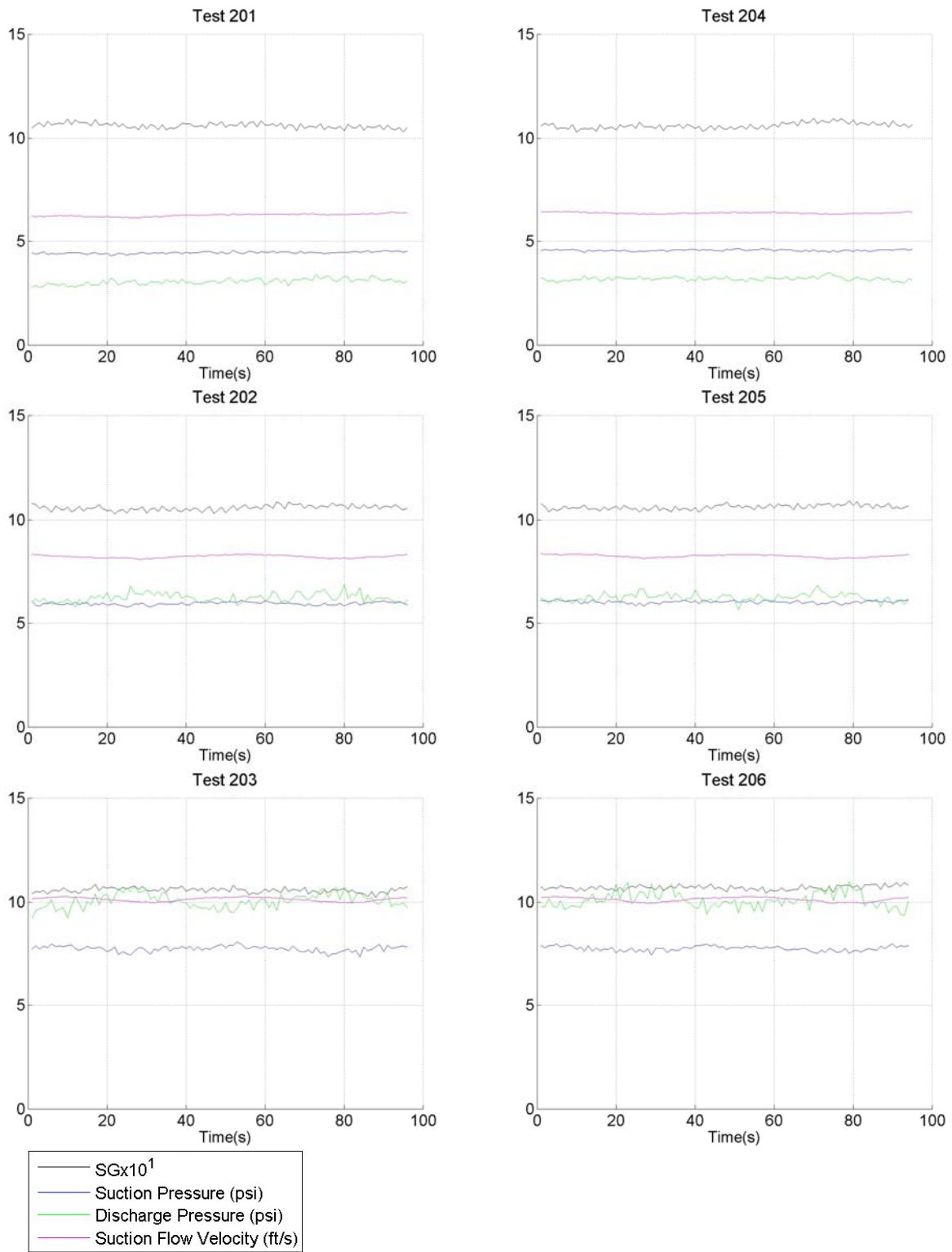


Figure B - 13: Tests 201-206.

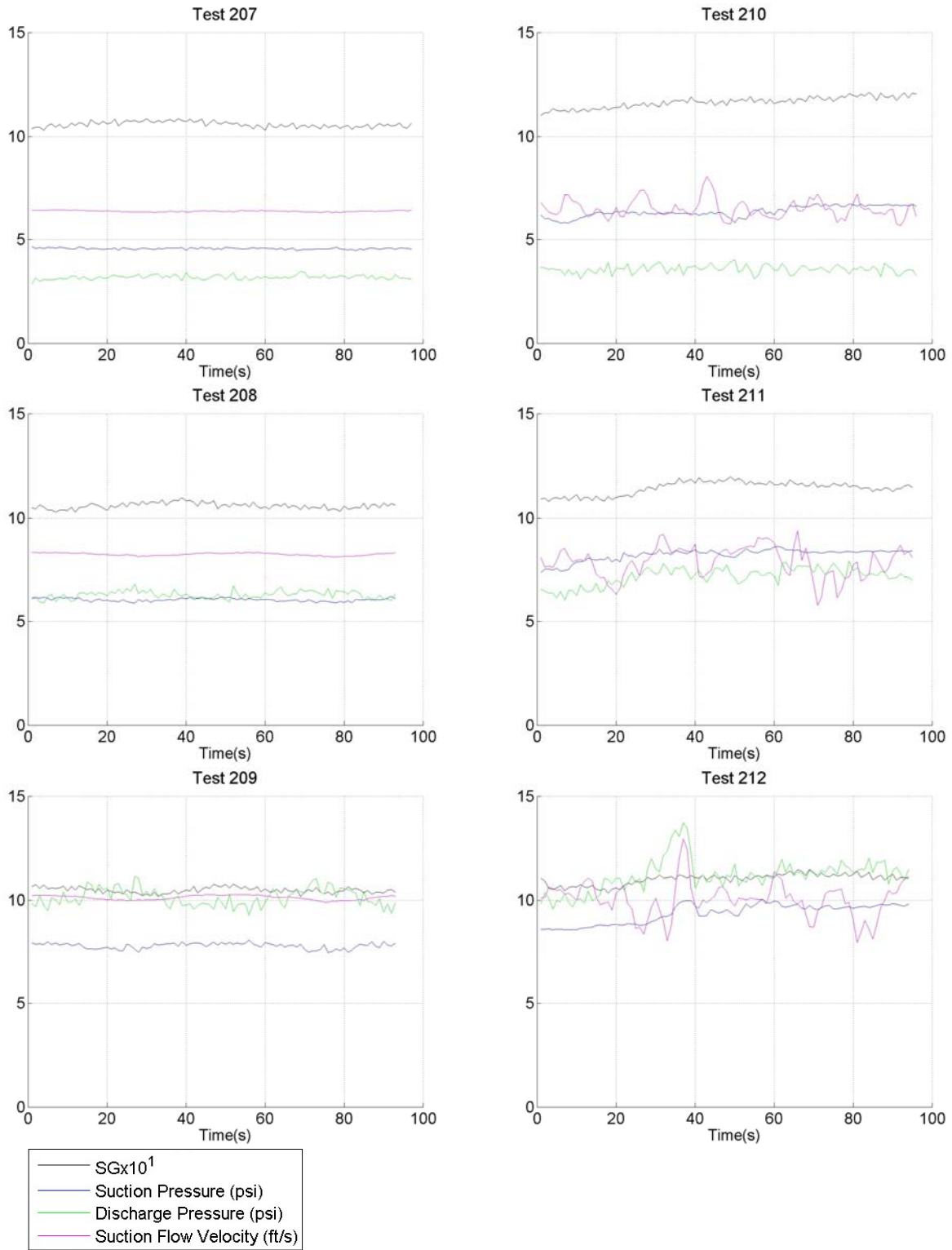


Figure B - 14: Tests 207-212.

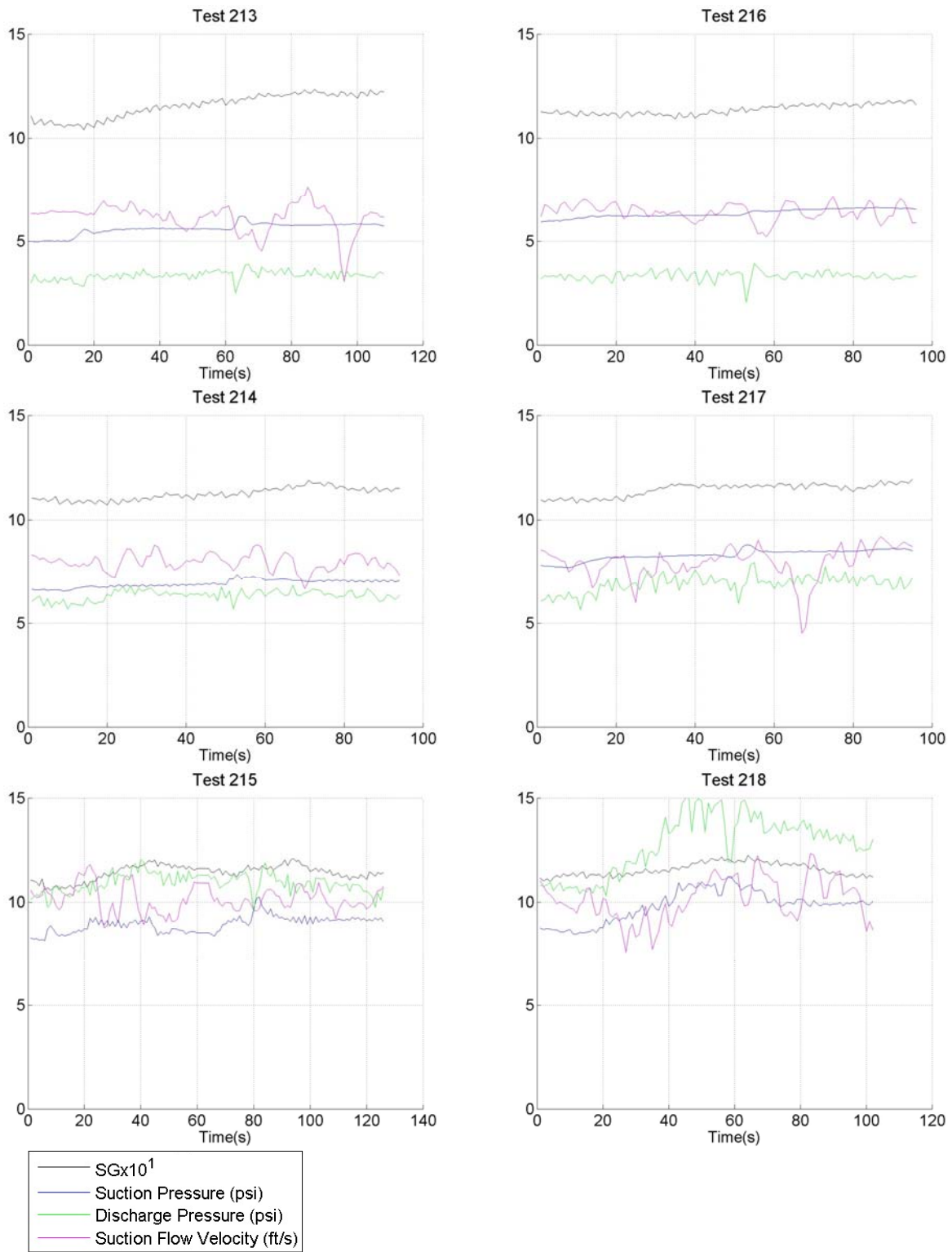


Figure B - 15: Tests 213-218.

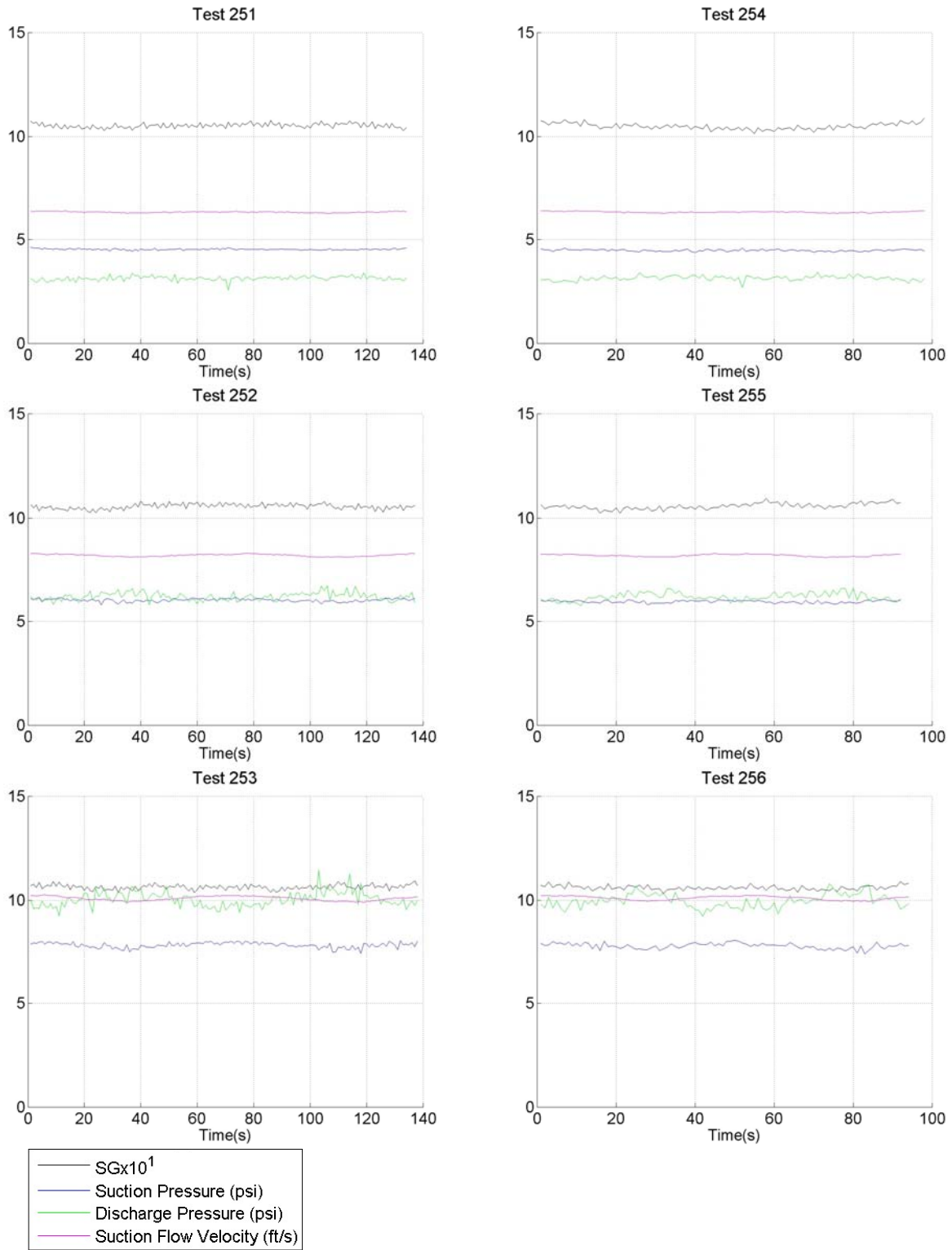


Figure B - 16: Tests 251-256.

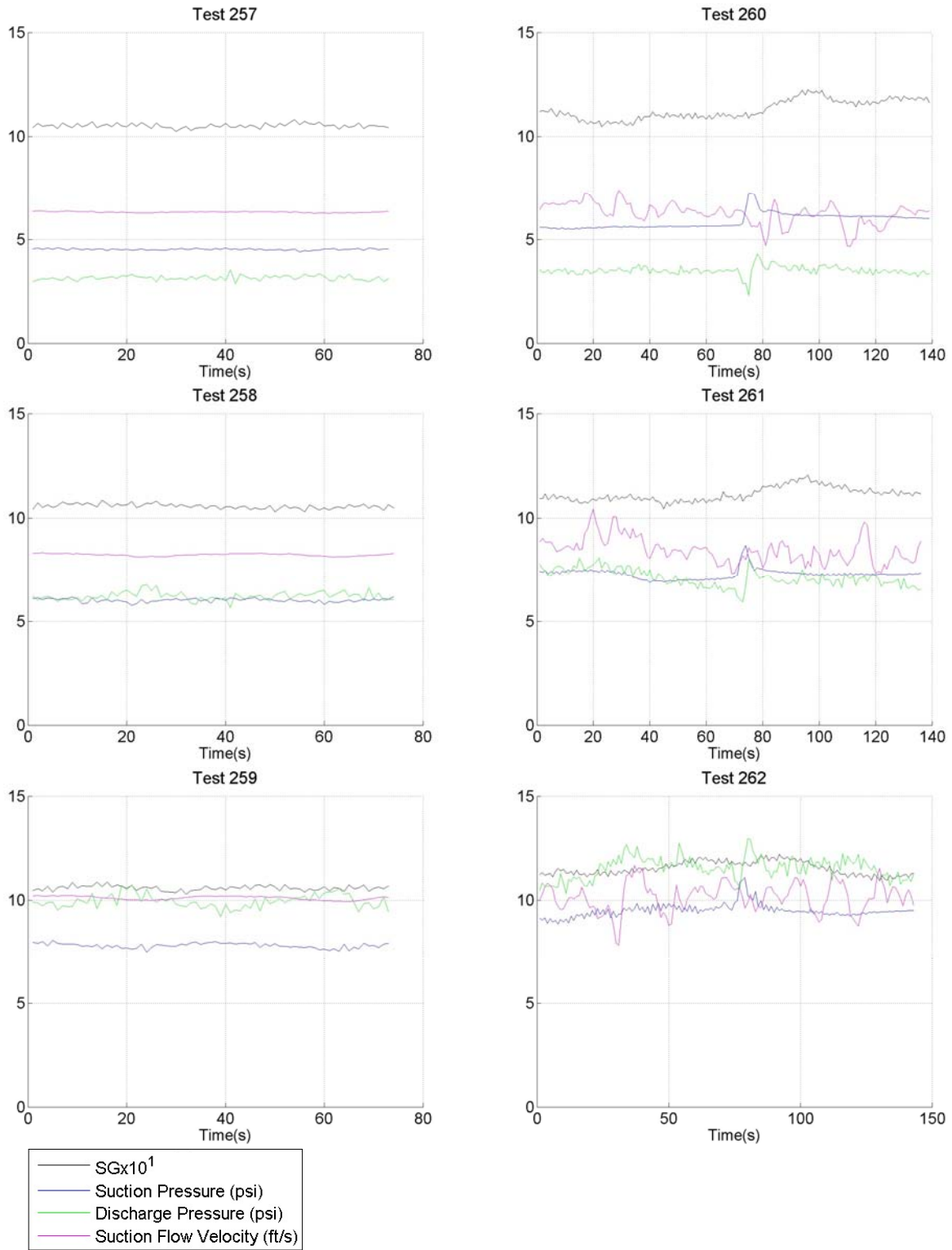


Figure B - 17: Tests 257-262.

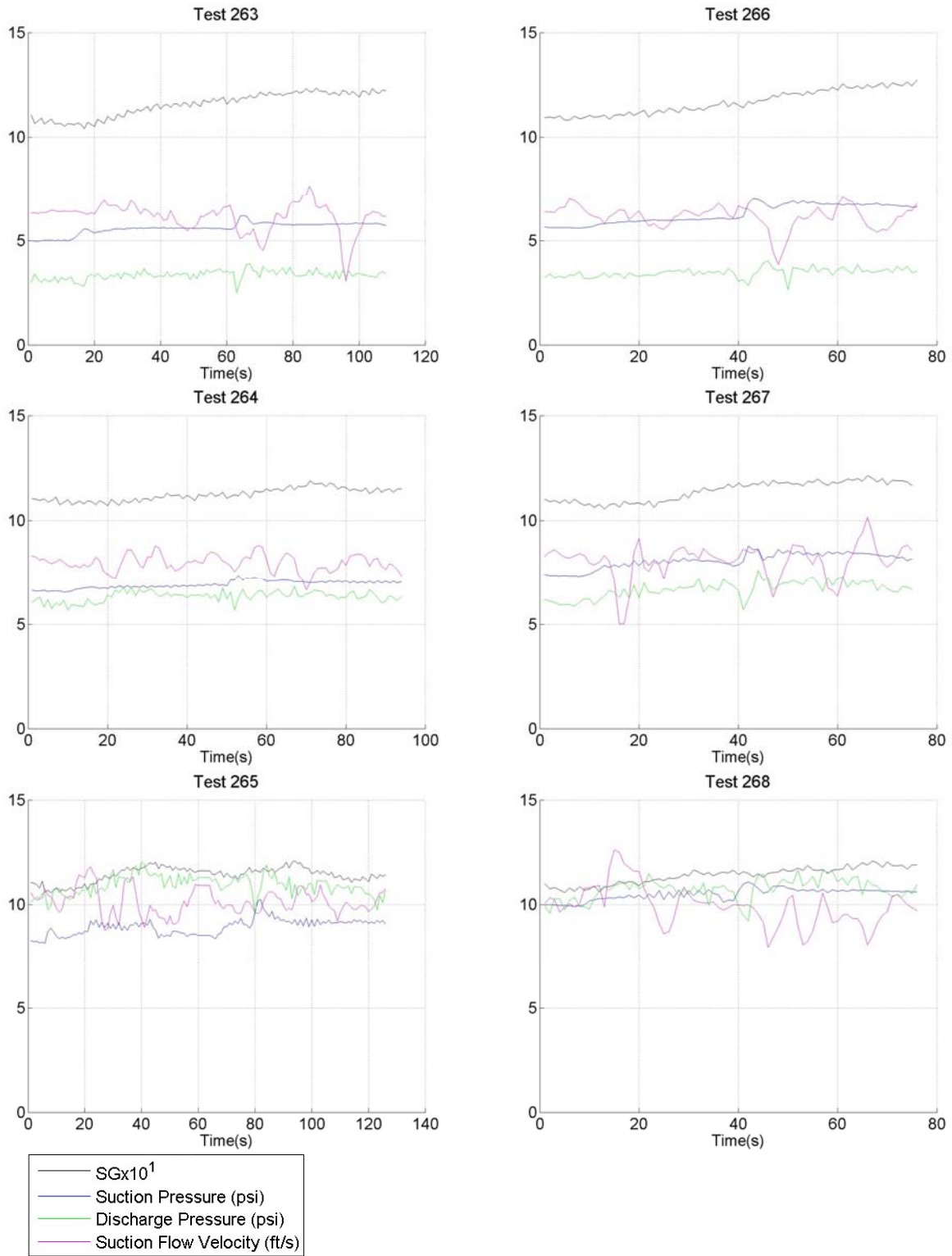


Figure B - 18: Tests 263-268.

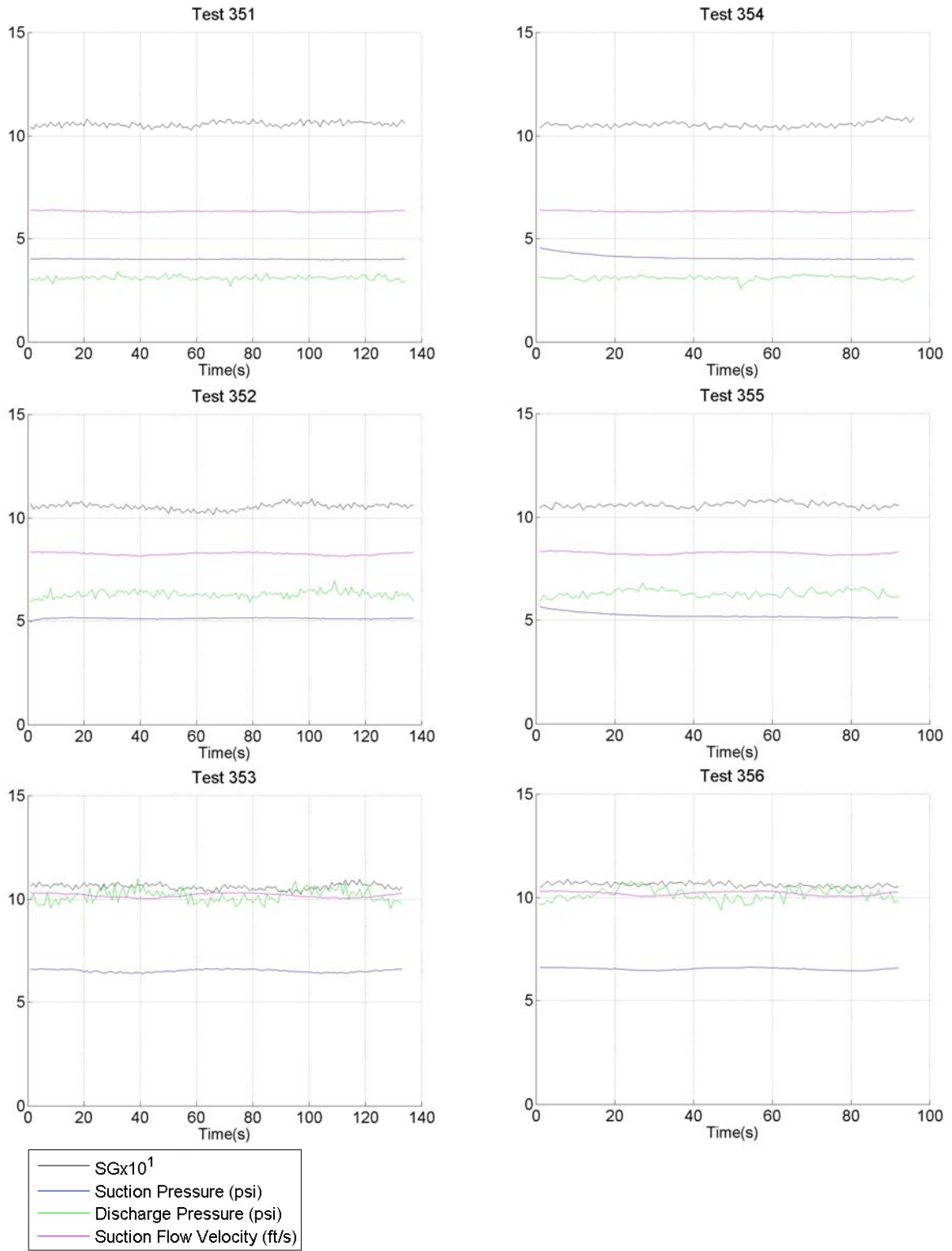


Figure B - 19: Tests 351-356.

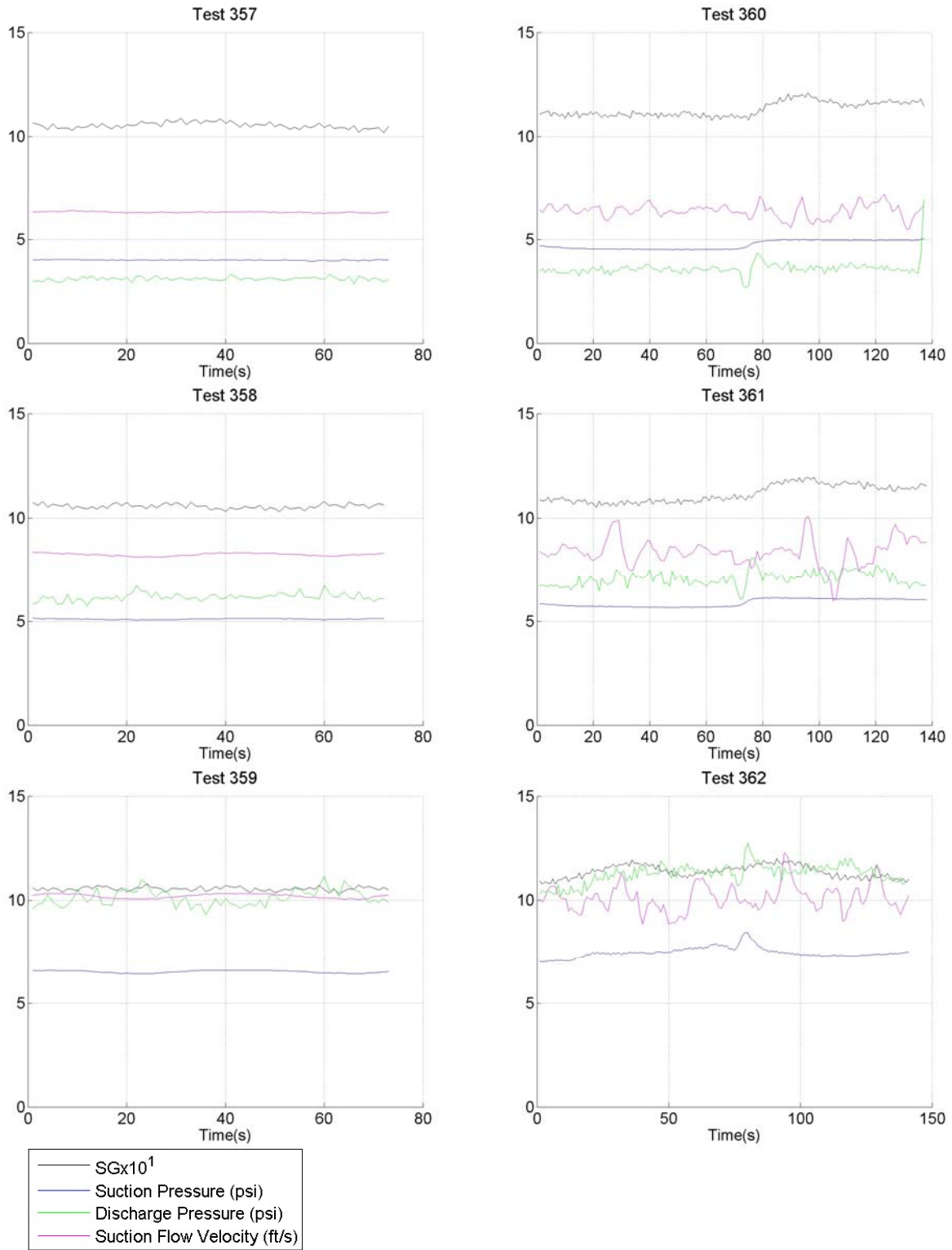


Figure B - 20: Tests 357-362.

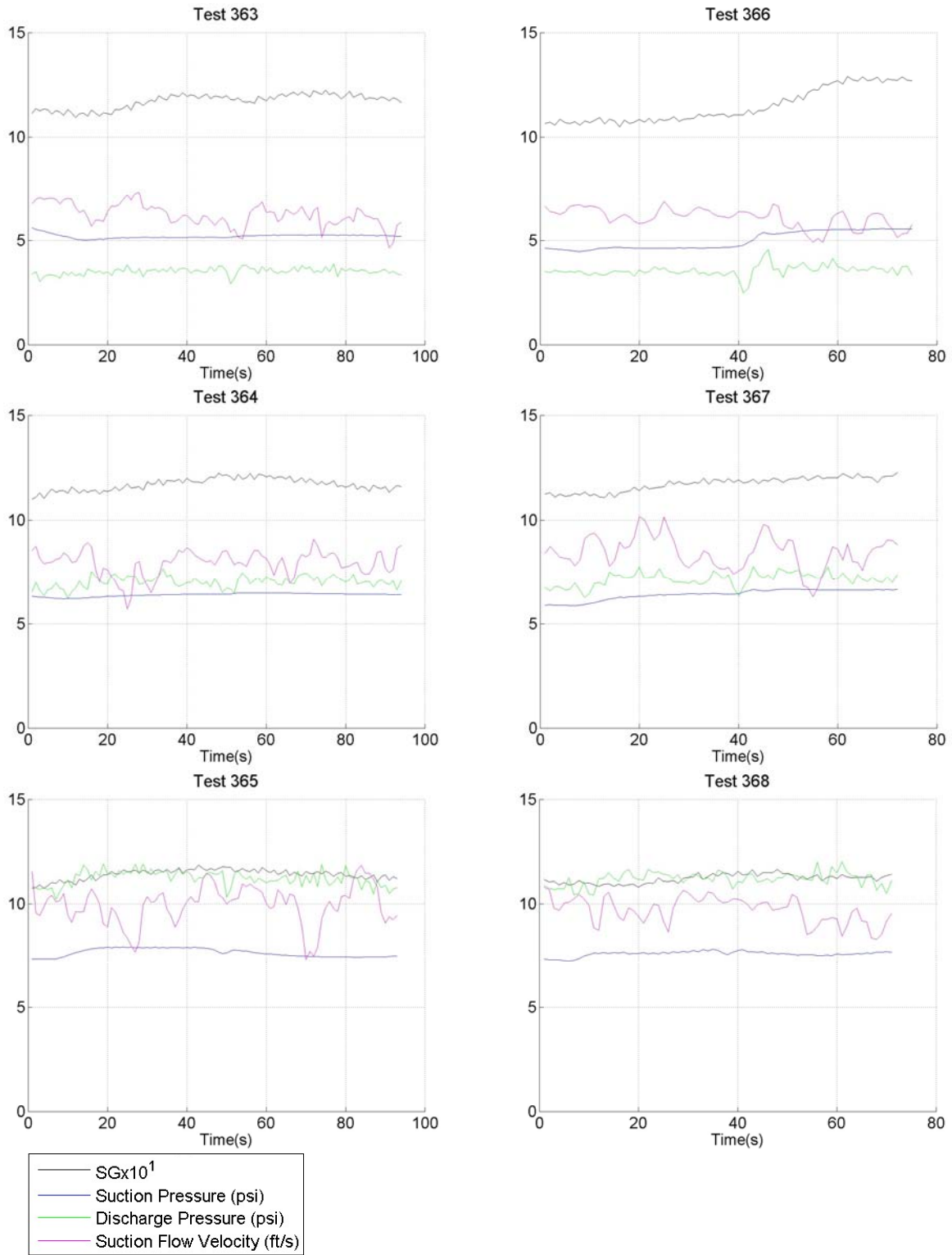


Figure B - 21: Tests 363-368.

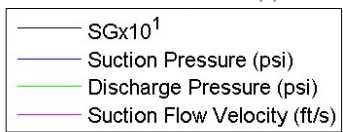
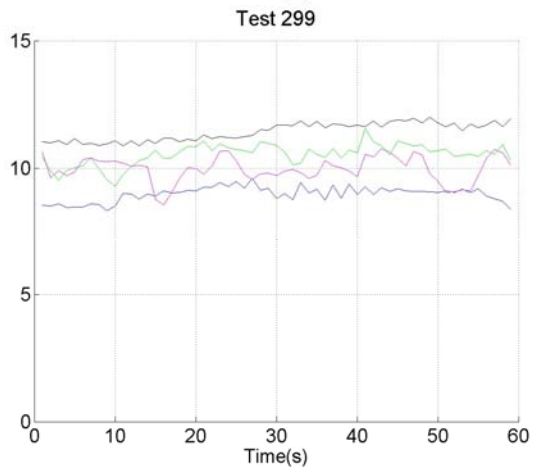
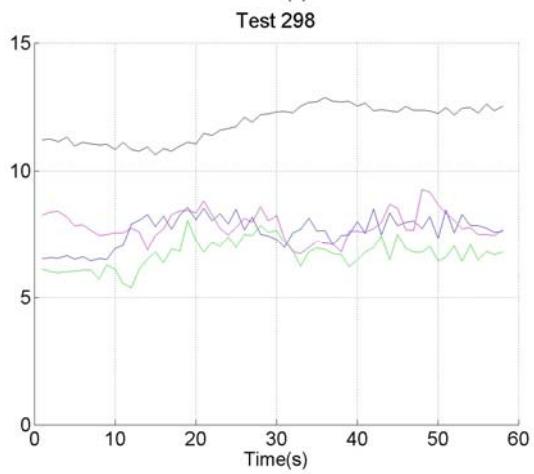
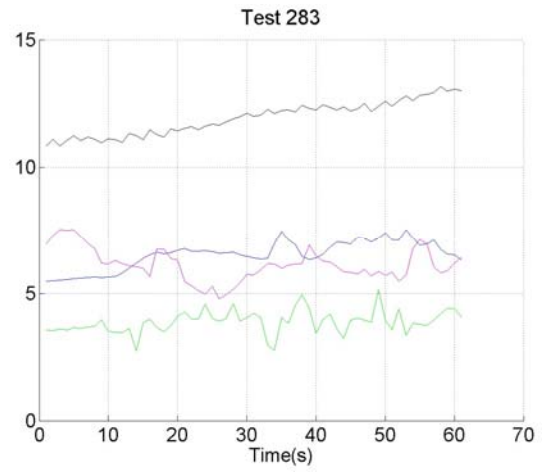
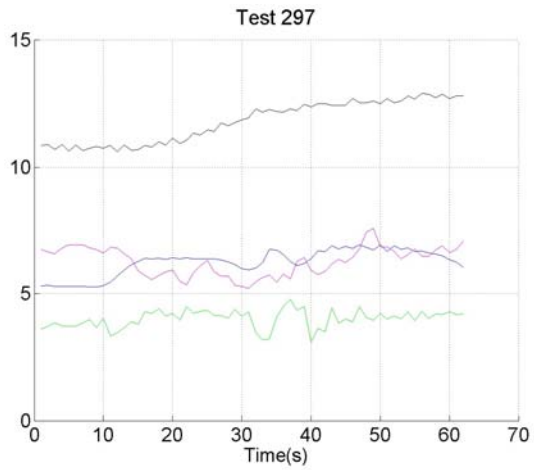


Figure B - 22: Tests 297-299 and 283.

APPENDIX C – PHOTOS



Figure C - 1: Empty hopper barge prior to testing.



Figure C - 2: Sand pit after a day of testing.

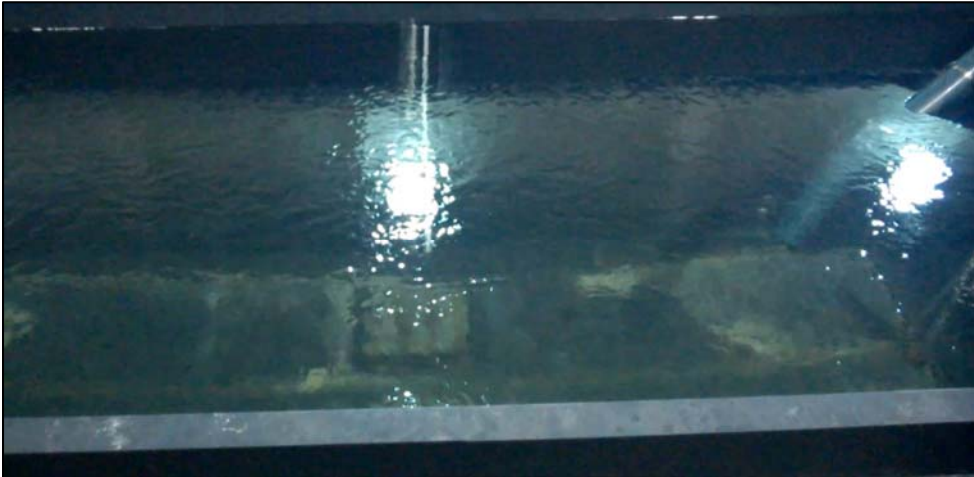


Figure C - 3: Hopper barge: empty (top); during water tests (middle); starting a sand test (bottom).



Figure C - 4: Discharge pipe and hopper barge during dredge testing.



Figure C - 5: Turning on the video camera prior to commencing sand tests (view from dredge carriage).



Figure C - 6: Turning on the video camera (view from hopper barge).



Figure C - 7: Emptying sand from hopper barge after a day's tests.



Figure C - 8: Overloaded hopper barge on day two of testing.



Figure C - 9: Failed cable on hopper barge due to overloading on day two of testing.



Figure C - 10: Plasma cutter used to construct screens.



Figure C - 11: Sheet metal from which screens were made.

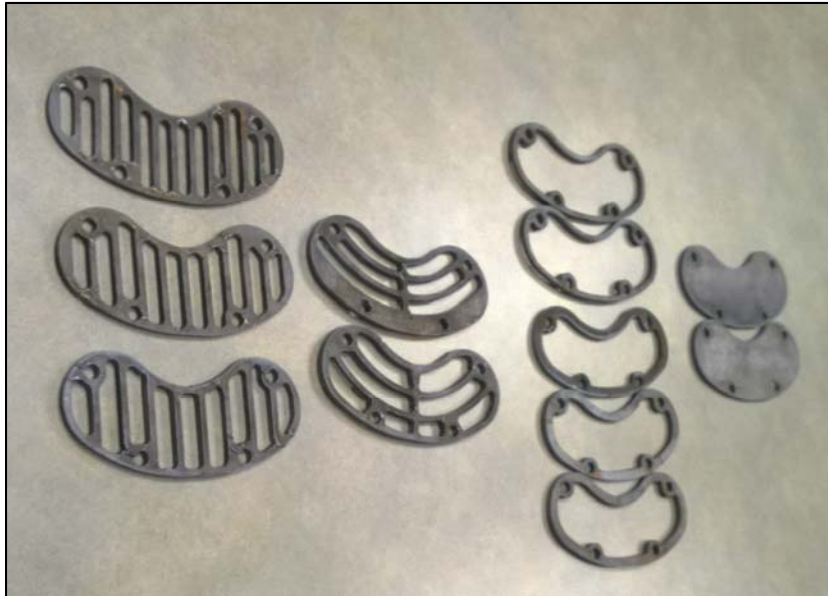


Figure C - 12: Screen options prior to commencing experiments.



Figure C - 13: Welding bolts to suction mouth.



Figure C - 14: Dredge suction mouth with bolts attached.



Figure C - 15: Video recording apparatus (top view).



Figure C - 16: Video recording apparatus (side view).



Figure C - 17: Video recording apparatus (underwater).